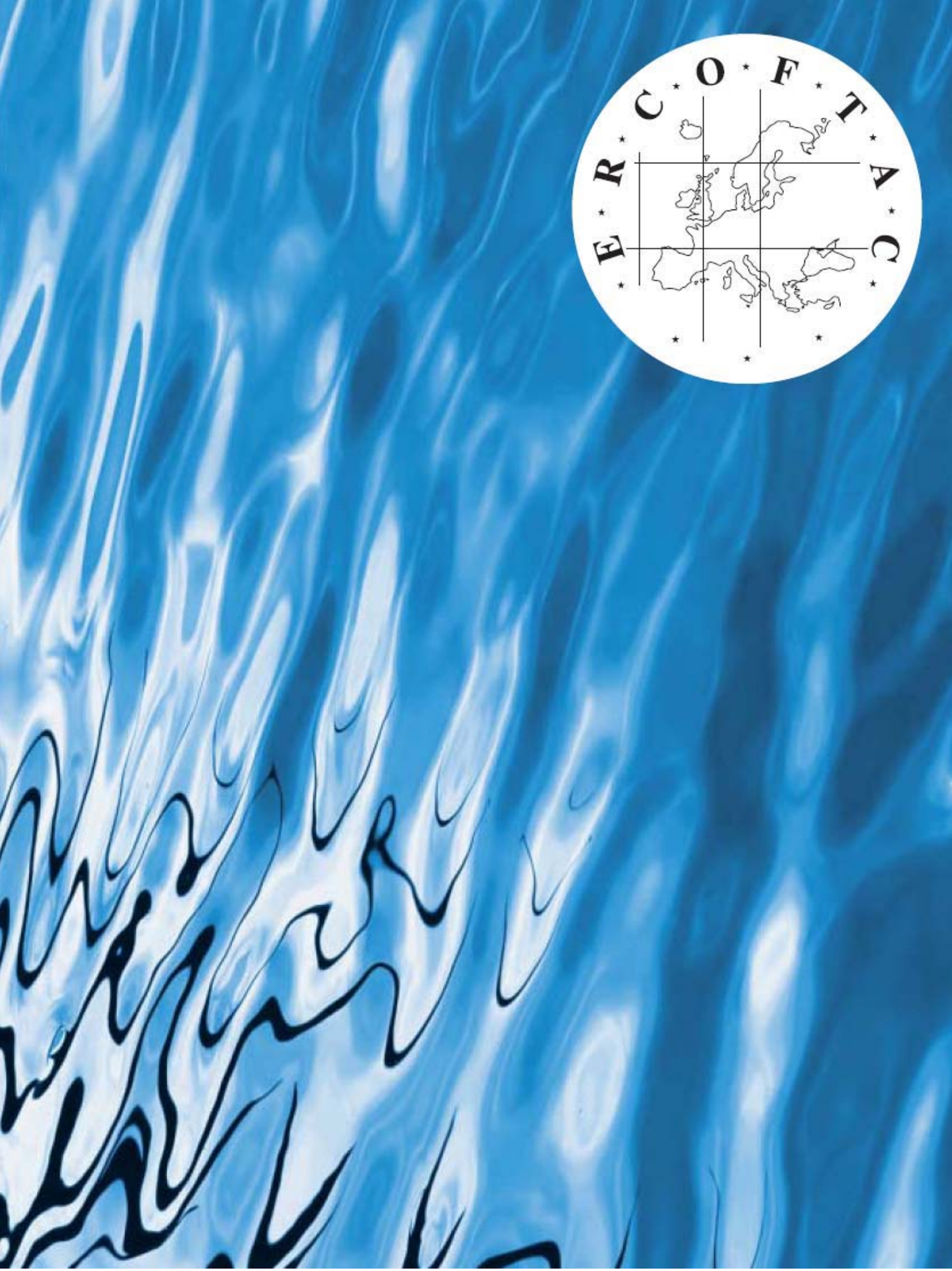
E · R · C · O · F · T · A · C

European Research Community On Flow, Turbulence and Combustion

ERCOFTAC is a leading European association of research, education and industry groups in the technology of flow, turbulence and combustion. The main objectives of *ERCOFTAC* are: To promote joint efforts of European research institutes and industries with the aim of **exchanging technical and scientific information**; to promote **Pilot Centres** for collaboration, stimulation and application of research across Europe; to stimulate, through the creation of **Special Interest Groups**, well-coordinated European-wide research efforts on specific topics; to stimulate the creation of advanced training activities; and to be influential on funding agencies, governments, the European Commission and the European Parliament.

www.ercoftac.org

ERCOFTAC Bulletin 88, September 2011

TABLE OF CONTENTS

SPECIAL THEME

Multipoint Turbulence Structure and Modelling

SUBMISSIONS

ERCOFTAC Coordination Centre
Laboratory of Heat and Mass Transfer
EPFL-STI-IGM-ERCOFTAC
ME G1 465, Station 9
CH-1015 Lausanne VD
Switzerland

Tel: +41 21 693 3503
Fax: +41 21 693 5960
Email: ercoftac@epfl.ch

HOSTED, PRINTED & DISTRIBUTED BY

ÉCOLE POLYTECHNIQUE
FÉDÉRALE DE LAUSANNE

NEXT *ERCOFTAC* EVENTS

ERCOFTAC Autumn Festival
10th October 2011
TU Darmstadt, Darmstadt, Germany.

ERCOFTAC SPC, IPC & MB-GA Meetings
11th October 2011
TU Darmstadt, Darmstadt, Germany.

The ERCOFTAC Best Practice Guidelines for Industrial Computational Fluid Dynamics

The Best Practice Guidelines (BPG) were commissioned by ERCOFTAC following an extensive consultation with European industry which revealed an urgent demand for such a document. The first edition was completed in January 2000 and constitutes generic advice on how to carry out quality CFD calculations. The BPG therefore address mesh design; construction of numerical boundary conditions where problem data is uncertain; mesh and model sensitivity checks; distinction between numerical and turbulence model inadequacy; preliminary information regarding the limitations of turbulence models etc. The aim is to encourage a common best practice by virtue of which separate analyses of the same problem, using the same model physics, should produce consistent results. Input and advice was sought from a wide cross-section of CFD specialists, eminent academics, end-users and, (particularly important) the leading commercial code vendors established in Europe. Thus, the final document can be considered to represent the consensus view of the European CFD community.

Inevitably, the Guidelines cannot cover every aspect of CFD in detail. They are intended to offer roughly those 20% of the most important general rules of advice that cover roughly 80% of the problems likely to be encountered. As such, they constitute essential information for the novice user and provide a basis for quality management and regulation of safety submissions which rely on CFD. Experience has also shown that they can often provide useful advice for the more experienced user. The technical content is limited to single-phase, compressible and incompressible, steady and unsteady, turbulent and laminar flow with and without heat transfer. Versions which are customised to other aspects of CFD (the remaining 20% of problems) are planned for the future.

The seven principle chapters of the document address numerical, convergence and round-off errors; turbulence modelling; application uncertainties; user errors; code errors; validation and sensitivity tests for CFD models and finally examples of the BPG applied in practice. In the first six of these, each of the different sources of error and uncertainty are examined and discussed, including references to important books, articles and reviews. Following the discussion sections, short simple bullet-point statements of advice are listed which provide clear guidance and are easily understandable without elaborate mathematics. As an illustrative example, an extract dealing with the use of turbulent wall functions is given below:

- Check that the correct form of the wall function is being used to take into account the wall roughness. An equivalent roughness height and a modified multiplier in the law of the wall must be used.
- Check the upper limit on $y+$. In the case of moderate Reynolds number, where the boundary layer only extends to $y+$ of 300 to 500, there is no chance of accurately resolving the boundary layer if the first integration point is placed at a location with the value of $y+$ of 100.
- Check the lower limit of $y+$. In the commonly used applications of wall functions, the meshing should be arranged so that the values of $y+$ at all the wall-adjacent integration points is only slightly above the recommended lower limit given by the code developers, typically between 20 and 30 (the form usually assumed for the wall functions is not valid much below these values). This procedure offers the best chances to resolve the turbulent portion of the boundary layer. It should be noted that this criterion is impossible to satisfy close to separation or reattachment zones unless $y+$ is based upon y^*.
- Exercise care when calculating the flow using different schemes or different codes with wall functions on the same mesh. Cell centred schemes have their integration points at different locations in a mesh cell than cell vertex schemes. Thus the $y+$ value associated with a wall-adjacent cell differs according to which scheme is being used on the mesh.
- Check the resolution of the boundary layer. If boundary layer effects are important, it is recommended that the resolution of the boundary layer is checked after the computation. This can be achieved by a plot of the ratio between the turbulent to the molecular viscosity, which is high inside the boundary layer. Adequate boundary layer resolution requires at least 8-10 points in the layer.

All such statements of advice are gathered together at the end of the document to provide a 'Best Practice Checklist'. The examples chapter provides detailed expositions of eight test cases each one calculated by a code vendor (viz FLUENT, AEA Technology, Computational Dynamics, NUMECA) or code developer (viz Electricité de France, CEA, British Energy) and each of which highlights one or more specific points of advice arising in the BPG. These test cases range from natural convection in a cavity through to flow in a low speed centrifugal compressor and in an internal combustion engine valve.

Copies of the Best Practice Guidelines can be acquired from:

ERCOFTAC ADO
Chaussée de la Hulpe 189 Terhulpsesteenweg
B-1170 Brussels
Belgium

Tel: +32 2 643 3572
Fax: +32 2 647 9398
Email: anne.laurent@ercoftac.be

The price per copy (not including postage) is:

ERCOFTAC members	
First copy	*Free*
Subsequent copies	45 Euros
Students	30 Euros
Non-ERCOFTAC academics	75 Euros
Non-ERCOFTAC industrial	150 Euros

Multipoint Turbulence Structure and Modelling

Claude Cambon[1]

[1] Laboratoire de Mécanique des Fluides et d'Acoustique, UMR 5509,

Ecole Centrale de Lyon, 69134 Ecully Cedex, France.

The SIG 35 on 'Multipoint Turbulence Structure & Modelling' (MPTSM hereinafter) was established in 2001, after a meeting reported by Godeferd, Cambon & Scott [6] on two-point closures.

Fundamental issues and challenges of turbulence theory and modelling are addressed, but we keep in mind practical modelling for engineering and environmental flows. In this sense, a significant overlap exists with the SIG 15, for instance with common interest in 'structure-based modelling' (S. Kassinos and coworkers, C. Cambon and coworkers, among others).

In addition, we continue to share an interest for a global, dynamical, statistical and structural approach to anisotropic flows, with and without rotation. From stable stratification to unstable cases, for instance, new recent elements suggest to consider, with the tools of MPTSM, buoyancy-driven flows such as thermal convection and even Rayleigh-Taylor instability with transition to turbulence. Collaboration with the CEA is particularly encouraging, from spectral approaches (RDT, nonlinear closures, supported by high resolution DNS towards LES) to engineering-oriented models, like 'two-structure–two-fluid–two-k–ε' [12]. This theme is also important for the SIG 14 (J.M. Redondo) and the SIG 4 (P. Comte).

This foreword is organised as follows. Fundamental issues and their possible applications are presented in Section 1. The closure problem is revisited, in a broad sense, in Section 2. New insights to anisotropic turbulence and interactions are given in Section 3.

1 Fundamental aspects in turbulence theory. Connections with practical modelling?

Turbulence is almost ubiquitous in fluid motions, but the recent development in related topics, especially from a bit more than a decade, is rather surprising.

On one hand, a lot of publications, in a community close to physicists, emphasize intermittency, or more precisely 'internal intermittency' at rather small scale. Space-time intermittency is a concept easy to understand intuitively by looking at a particular realization of the flow, but its impact on statistically averaged quantities is possibly complex, as well as its precise quantification from such statistics. For instance, the departure of the Kolmogorov K41 scaling laws for structure functions, via the so-called 'anomalous exponents', continue to be systematically and routinely attributed to 'internal intermittency'. This feeds an endless 'industry' of intermittency corrections. As a single example, a conjecture is emerging about a law for nth-order structure function (redefined more precisely in the next section) $S_n(r) \sim r^{n/2}$, different from the K41 scaling $S_n(r) \sim r^{n/3}$, for rotating turbulence, and intermittency is invoked, against the evidence that anisotropy and related importance of inertial wave-turbulence is probably a more physical explanation for the 'anomalous scaling'. More generally, the anomalous exponents mix in an intricate way anisotropy, finite-Reynolds number (FRN hereinafter) effect, and even inhomogeneity, not to mention intermittency.

Going back to strictly homogeneous isotropic turbulence, only for $n = 3$, the existence of the 'exact' 4/5 Kolmogorov law allows us to escape from intermittency corrections. In fact, this law

$$S_3(r) = -4/5\varepsilon r, \tag{1}$$

is an asymptotic law, which can be reached only at very high Reynolds number, as evidenced by, e.g. Antonia & Burattini (2006) [1], so that the departure of the compensated third-order structure function from the 'exact' prefactor $-4/5$ suggests that important FRN corrections be done. This also raises the question: why FRN is invoked at $n = 3$ for explaining a huge departure from K41, and not at $n \neq 3$?

On the other hand, several engineering and environmental studies, faced with the pressing need for practical modelling, and benefitting from an increasing computational power, develop a smart combination of models, often hybrid, ranging from RANS to LES. At first glance, the two communities, say 'scaling and intermittency' and 'engineering', are almost disconnected from each other.

A remarkable exception is the possible involvement of second S_2 and third-order S_3 structure functions, at a scale close to a mesh size, in refined subgrid-scale models for LES. Are there other points of contact? Is there another approach to fundamental aspects of turbulence in addition to the conventional present post-Kolmogorov *vulgate* on 'intermittency and scaling'? For instance, is there a future for models and theories ranging from linear 'Rapid Distortion Theory' (RDT) to nonlinear 'triadic' closures from the legacy of Kraichnan and Orszag? The last question is important if one considers the emphasis on homogeneous anisotropic turbulence, obtained in a recent book by Sagaut & Cambon [17] by generalizing and combining such approaches, and the lack of interest for that in the recent literature in fundamental turbulence.

We briefly review and compare very different techniques, modelling methods and theories, in connection with the following questions:

- Is Kolmogorov, K41 or K62, the ultimate recourse for—at least phenomenological—turbulence theory?
- Has the concept of 'two-point closures' radically changed in recent literature? Why 'triadic' closures, carried out in Fourier space, are almost neglected,

except in the domain of 'weak' wave-turbulence theory?

- Why the role of pressure fluctuation is almost ignored in recent literature on fundamentals? This is illustrated by the emphasis on scalar variants of the Kármán–Howarth equations, in which explicit effects of pressure can be neglected, and implicit effects are often misunderestimated.

  As an important exception, Lagrangian statistics for particle acceleration are studied, in which the pressure gradient is recognized as a leading term.

On the other hand, the correct treatment of pressure fluctuations is in the core of linear RDT as well as in nonlinear spectral triadic closures. Projection operators used in Fourier space, and/or decomposition of velocity and vorticity fields on solenoidal modes, allows the pressure fluctuation to be exactly accounted for, and therefore removed from consideration as a dependent variable. This is discussed in Section 2. Another instance of the importance of modelling pressure fluctuations, via the pressure Hessian, is given by the dynamical approach to velocity gradients, in Section 2.3. Finally, there is probably no need to recall the importance of modelling pressure strain-rate correlation tensors in the equations governing the full Reynolds stress tensor.

1.1 The legacy of Kolmogorov, K41 or K62?

Emphasis is placed on structure functions, which involve *velocity differences* between two points $\boldsymbol{x}$ and $\boldsymbol{x}+\boldsymbol{r}$, defined as

$$\delta\boldsymbol{u} = \boldsymbol{u}(\boldsymbol{x}+\boldsymbol{r},t) - \boldsymbol{u}(\boldsymbol{x},t). \tag{2}$$

Restricting our attention to pure HIT (Homogeneous Isotropic Turbulence), structure functions of nth-order are obtained by ensemble averaging products of increments, without specifying their orientation, so that

$$S_n(r) = \langle(\delta u_L)^n\rangle(r) \tag{3}$$

is for instance the nth-order structure function, related to longitudinal velocity increments—along vector r,—which does not depend on the position $\boldsymbol{x}$ (statistical homogeneity), nor on the orientation of $\boldsymbol{r}$, but only on its modulus r (statistical isotropy). The time-dependence is implicit, and only mentioned if needed.

K41 scaling amounts to a dependency only restricted to r and to the dissipation rate ε, so that dimensional analysis yields the well-known scaling

$$S_n(r) = C_n(\varepsilon r)^{n/3}, \tag{4}$$

in which C_n can be considered as a universal constant. Of course, this scaling laws are only valid in an 'inertial' range of scales, with r typically larger than the Kolmogorov scale η and smaller than the largest scales—typically an integral lengthscale,—which are affected by instabilities, boundaries or any non-universal way of injecting energy.

Following the proposal by Kolmogorov himself, or K62, a departure from these K41 scaling laws displays 'anomalous exponents' ζ_n, different from $n/3$ as follows:

$$S_n(r) \sim r^{\zeta_n}. \tag{5}$$

The search for anomalous exponents, except for $n=3$ rediscussed in the next subsection, feeds a huge litterature, centered around the concept of 'internal intermittency in the inertial range'. A non-conventional survey of this issue, especially for $n=2$ is offered by **David McComb in the present issue.**

A controversy can occur because of the lack of rigorous definition and quantification of 'internal intermittency', and because exponents are often obtained from purely empirical calculations or measurements, with huge error bars (especially at large n !). On the other hand, a real linkage of intermittency to such exponents can be suggested from the following considerations :

- Passive scalar. A strong convexity of the curve of anomalous exponents, with $\zeta_n << n/3$ at increasing n ($n > 3$), can be obtained in connection with a very different way to fill the space by the passive scalar—ramp structures?—compared to the velocity field. In addition, a strongly non-Gaussian scalar distribution can result from its transport by a purely Gaussian velocity field, as shown by Kraichnan.

- 'Burgulence' extended to 2, 3 and 4 dimensions. If the basic structures consist of shock waves, and not of tangled vortex tubes (conventional incompressible HIT), a flat distribution of anomalous exponents is found, with $\zeta_n = constant$ if $n > 3$.

- An interfacial interpretation of turbulence. More generally, if interactions of 'turbulent' structures are really organised around layers, there is a possible analogy of internal intermittency with realistic boundary intermittency. This also suggests a multifractal organisation. Such a conjecture is partly supported by the paper by **I. Eames, J.C.R. Hunt, M. Braza, C.B. Da Silva & J. Westerweel in the present issue.**

1.2 Connections with statistical theory, for second-order and third-order correlations

Starting again with pure incompressible HIT, classical Kolmogorov K41 scaling can be found at the second order, in a similar way in physical space, for $S_2(r)$ and in Fourier space, for the spherically averaged energy spectrum, $E(k)$, as

$$S_2(r) = C_2\,(\varepsilon r)^{2/3}\,,\ E(k) = K_0\varepsilon^{2/3}k^{-5/3}. \tag{6}$$

These laws are very robust, and can be found even at moderate Reynolds number. In addition, the dispersion of the Kolmogorov constant is very weak, as shown by Sreenivasan [18], suggesting an almost universal value.

Things are very different at the order 3. It is generally said that the Kolmogorov four-fifth law, with $n=3, C_3=-4/5$, in Eq. (4) is the only exact equation in turbulence theory. It is important to say in addition that this law is an asymptotic law, reached in practice at very high Reynolds number, so that a huge FRN effect has to be evaluated. The way to study the departure from this law is informative, using equations in both physical and Fourier space. The best way to model the FRN effect in physical space is to use a variant of the Kármán–Howarth equation, sometimes referred to as 'full Kolmogorov equation' [8]:

$$S_3(r,t) = -\frac{4}{5}\varepsilon r + 6\nu\frac{\partial S_2}{\partial r} - \frac{3}{r^4}\int_0^r r'^4\frac{\partial S_2}{\partial t}dr'. \tag{7}$$

The counterpart of this equation in Fourier space is the Lin equation:

$$\frac{\partial}{\partial t}E(k,t) + 2\nu k^2 E(k,t) = T(k,t), \qquad (8)$$

in which the dissipation spectrum is readily derived and the spectral transfer term $T(k)$ holds for the contribution of two-point cubic velocity correlations, as $S_3(r)$ does in Eq. (7).

2 The concept of closure and the hierarchy of theories and models

The use of variants of the Kármán–Howarth equation for more a decade, as a generalisation of Eq. (7) to anisotropic and inhomogeneous flows, can incorporate a direct modelling of generalized unsteady two-point second-order velocity correlations. In this sense, this approach can illustrate an alternative way to address two-point closures. On the other hand, techniques formerly [6] referred to as *two-point closures* or *two-point theories*, developped in Fourier space from Kraichnan's and Orszag's legacy, tackle the problem of cascade at the level of three-point third-order dynamics: it is suggested to call these approches *triadic* that rather *two-point*. We cite here the more representative among many authors, and the reader is referred to **David McComb** here, and to [14] for a broader survey.

2.1 Single-point closures and beyond: From RANS to structure-based modelling

RANS models remain very useful for complex flows of engineering and/or of environmental interest.

From the equation for the mean velocity field, it appears that the gradient of the Reynolds stress tensor (RST) $\langle u_i u_j \rangle$ is the first information to be obtained. Several models were proposed to close the equation which govern the full RST, following Launder, Lumley and many others, with the additional transport equation for the disipation rate. On the other hand, only the trace of the RST is transported in a simpler k–ε model, so that the nondimensional deviatoric part of the RSM, denoted b_{ij} here, is directly—same time, same position—linked to the mean velocity gradient $\langle A_{ij} \rangle$ via a 'turbulent effective viscosity'. The simplest 'linear' version of the k–ε model utilizes $kb_{ij} = -\nu_t \langle A_{ij} + A_{ji} \rangle$, a so-called Boussinesq approximation, whereas more complex algebraic linkage of b_{ij} to $\langle A_{ij} \rangle$ is introduced in 'nonlinear' (nonlinear with respect to A_{ij}) versions. These versions can recover a level of information comparable to EARSM (Explicitely Algebraic Stress Model.) Just recall that k–ε model remains very popular because it is robust and stabilizing for the numerical schemes, from the fact that the gradient of the RST amounts to an additional effective dissipative term, with $\nu_t \sim C_\mu k^2/\varepsilon$. In counterpart, Coriolis effects are completely missed by a 'linear' k–ε model, which, for instance cannot reproduce the asymmetry beween the 'pressure side' and the 'suction side' of a classical channel flow rotating around the spanwise direction.

More generally, and even if nonlinear k–ε and RSM models predict the abovementioned asymmetry, the rotation of the frame can question the principle of closure in any RSM. This flaw was identified by Cambon, Jacquin and Lubrano (1992, ref. in [17]), and, in a different way, by Kassinos, Reynolds and coworkers (e.g. Kassinos, Reynolds and Rogers, 2001, ref. in [17]). For instance, it was shown that the 'rapid' pressure-strain rate tensor in an homogeneous rotating shear flow contains more information than the RST itself. Additional information includes at least 'dimensionality' and 'stropholysis' tensors, whose local and intantaneous values are disconnected from the RST one. Advances in structure-based modelling are given by **Kassinos and Radhakrishnan in the present issue.**

The link from 'structure-based modelling' to linear and nonlinear approaches developped by my team in Lyon is rediscussed in Subsections 2.4 and 2.5.

2.2 Two-point approaches in physical space

This approach can be illustrated by a simple use of Eq. (7). For instance, Lindborg (1998, ref. in [20]) obtained a simple model for the FRN effect in reinjecting a conventional K41 model for $S_2(k,t)$, as in Eq. (6) in which the time-variation of ε derives from basic k–ε. This provides a satisfactory law as $C_3 = \max_r S_3(r)/(\varepsilon r) = 4/5 - 8.45 R_\lambda^{-2/3}$, at least for the largest values of $R_\lambda > 200$. Refined corrections are given in [1]. Finally, the full Kolmogorov equation, possibly generalized—but often under a scalar form—to anisotropic and inhomogeneous flows, can provide advanced subgrid-scale modelling in a channel, e.g. [4].

Assuming very large Reynolds numbers, another large part of the literature is devoted to a slight generalization of the asymptotic Kolmogorov law $C_3 = -4/5$ in various flows, with MHD, compressibility, not to mention mixed scalar-velocity third-order structure functions, following Yaglom variants of Eq. (7).

Finally, going back to studies in engineering, two-point, and even two-time, closures directly carried out in physical space, are illustrated by exponential relaxation models (e.g. studies at PPRIME, Poitiers, France). This yield a direct linkage of two-point and/or two-time second-order velocity correlations to their single-point value, using an exponential or Gaussian factor.

2.3 Transport of increments and gradients, tetrads

This is a very promising approach, in which closures and stochastic models are proposed for the full velocity gradient A_{ij}. In dedicated transport equations, is considered a coarse-grained A_{ij}, and not its Reynolds (ensemble) average precedently denoted $\langle A_{ij} \rangle$. In addition, a Lagrangian approach is performed, by **A. Naso, A. Pumir, F.S. Godeferd & C. Cambon in the present issue.** The modelling of the pressure Hessian is the main difficulty.

2.4 Recent avatars of 'Rapid Distortion Theory', from rotating shear to accretion disks

As in the recent book [17], we consider essentially homogeneous RDT, or the linear response of 'homo-

geneous' turbulence to space-uniform mean velocity—and/or density—gradients, and/or body forces consistent with statistical homogeneity for the fluctuations.

RDT is useful for improving the modelling of the 'rapid' pressure-strain rate tensor in RSM, and the development of structure-based modelling, beyond the RSM, was partly motivated by reproducing RDT. It is important to point out that the general approach which underlies RDT is more general, with implication on stability theory, as discussed below. Even if restricted to the effect of the pure plane mean shear flow, the study by Moffatt (1967) [15] included all the characteristics of modern RDT.

Technically, the starting point of the search for linear response uses a base flow with space-uniform velocity gradients, A_{ij}, possibly space-uniform density gradients (for application to density-stratified flows) and uniform external magnetic field (for MHD applications), with additional body forces, Coriolis, buoyancy, Lorentz. The base flow, in the sense of stability analysis, is the mean flow consistent with statistical homogeneity of fluctuations, and must be a particular solution of Euler equations. This condition is called 'admissibility condition' by A.C.C. Craik, and it results from the absence of feedback from the RST (the RST is space-uniform by virtue of statistical homogeneity) and absence of dissipation in the equation for the mean. The disturbance flow can be expressed in terms of advected Fourier modes with time-dependent wavevector, sometime called Kelvin modes in the community of stability analysis. Fourier space is an invaluable tool for solving the pressure disturbance, and the advection term, in addition, can be solved along characteristics lines in Fourier space, very close to base (or mean) trajectories in physical space. For instance, for a purely incompressible homogeneous velocity field subjected to the base flow given by A_{ij}, basic inviscid linear equations for both the wave vector $\boldsymbol{k}$ and the corresponding Fourier component of the velocity field, $\boldsymbol{u}(\boldsymbol{k},t)$ are

$$\dot{k}_i = -A_{ji}k_j, \quad \dot{\hat{u}}_i + \underbrace{\left(\delta_{in} - 2k_ik_n/k^2\right) A_{nj}}_{M_{ij}} \hat{u}_j = 0. \quad (9)$$

Solutions are simply obtained as

$$k_i = F^{-1}_{ji}(t,t_0)K_j, \quad (10a)$$

$$\hat{u}_i(\boldsymbol{k}(t),t) = G_{ij}(\boldsymbol{k},t,t_0)\hat{u}_j(\boldsymbol{K},t_0). \quad (10b)$$

In the previous equations, $F_{ij} = \partial x_i/\partial X_j$ is the displacement gradient, or Cauchy matrix (see also **Naso et al.** in the present issue,) which can be obtained by time-exponentiation of the gradient matrix A_{ij}, and $\boldsymbol{X}$ denotes the Lagrangian coordinates following the trajectories of the base flow. Mean trajectories are given here by

$$x_i = F_{ij}(t,t_0)X_j, \quad (11)$$

so that the characteristic curves in Fourier space correspond to a conservation of the phase $\boldsymbol{x}\cdot\boldsymbol{k} = \boldsymbol{X}\cdot\boldsymbol{K}$ of the advected Fourier mode. The linear Green's function $G_{ij}(\boldsymbol{k},t,t_0)$ generates all the information for the related linear stability analysis, but also for the statistical RDT prediction. It is deterministic, because possible randomness is only introduced by initial data in the linear initial value problem given by Eq. (9). Recent progress in RDT are illustrated by **A. Pieri, C. Cambon, F.S. Godeferd, A. Salhi, and T. Lehner in the present issue**, with comparison to full DNS.

Note that the Kassinos's 'Particle representation model' is based of equations close to (Eq. (9)), if one interprets the time-dependent wave-vector $\boldsymbol{k}(t)$ as the 'gradient vector' $\boldsymbol{N}$ in Kassinos *et al.* (2001). The term k_ik_n/k^2 in Eq. (9) reflects the contribution from fluctuating pressure, which is exactly solved.

In addition to the formal rediscovery of RDT by, e.g. Bayly and Craik, with its impact on the 'elliptical flow instability' from 1986, we can notice new developments in astrophysics, especially for rotating accretion discs. For instance, the 'shearing sheet approximation', rediscussed in **Pieri et al.** continues the analysis of the rotating pure plane shear, and yields shifting the interest of RDT and DNS from an engineering—e.g. channels in turbomachinery—context to an astrophysical one. It is also worthwhile to mention that the extension of linear RDT towards nonlinear pseudo-spectral DNS was obtained by Rogallo (1981, ref in [17]) using a comoving frame with variables denoted here $\boldsymbol{X}$ and $\boldsymbol{K}$ in eqs. (Eq. (10)) and (Eq. (11)). The same procedure, applied by Lesur [9] to the *shearing box approximation* is now used by a very large astrophysical community.

Finally, RDT operators for random flow realizations can be incorporated in KS (Kinematic Simulation), with application to Lagrangian diffusion [2]. This theme will be addressed in the next issue devoted to Synthetic Turbulence Models (SIG 42, F. Nicolleau). It is touched upon in the present issue, however, in **Naso et al.** and in **Pieri et al.**.

2.5 The legacy of Kraichnan and Orszag: Three-point, or triadic, approaches

Generalized RDT shows the interest of exactly solving the contribution of fluctuating pressure. This is linked to the fact that linear terms in the equation governing the fluctuating velocity are not divergence-free, so that the pressure gradient has to exactly balance their dilatational part. This is done in Fourier space by using algebraic projection operators, as illustrated by the matrix M_{ij} in Eq. (9): part $(\delta_{in} - k_ik_n/k^2)A_{nj}\hat{u}_j$ corresponds to the solenoidal, or divergence-free, contribution of the deformation term $A_{ij}u_j$ in physical space, whereas part $-(k_ik_n/k^2)A_{nj}\hat{u}_j$ corresponds to the contribution of the advection term $A_{jn}x_n\partial u_i/\partial x_j$. In the same way, the nonlinear advection term is not divergencefree, so that the basic Navier-Stokes equation writes

$$\left(\frac{\partial}{\partial t} + \nu k^2\right)\hat{\boldsymbol{u}}(\boldsymbol{k},t) = \mathbf{P}\widehat{\boldsymbol{\omega}\times\boldsymbol{u}}, \quad (12)$$

in which $\mathbf{P}$, $P_{ij} = \delta_{ij} - k_ik_j/k^2$, holds for the above mentioned projection operator, and the nonlinear advection term is chosen in connection with the Lamb vector, or vectoral product of vorticity by velocity. More symmetric expressions, in terms of $\widehat{u_iu_j}$, can be used as well. Of course, the Fourier transform of a product yields a convolution product, so that we have to consider the triadic nonlocal structure of $\widehat{\boldsymbol{\omega}\times\boldsymbol{u}}$, in terms of $\hat{\boldsymbol{u}}$ and $\widehat{\boldsymbol{\omega}} = \imath\boldsymbol{k}\times\boldsymbol{u}$, but the advantage of solving the pressure once for all, not to mention the algebraic counterpart of Biot-Savart equation, is essential.

2.5.1 HIT, a reminder

The most general closure approach, mainly used for HIT, deals with the hierarchy of moment equations. Because of the quadratic nonlinearity of Navier-Stokes equations, the equation that governs the second-order velocity correlations displays triple correlations, the equations for

triple correlations display fourth-order correlations, and so on. In addition, and this is less known, the pressure fluctuation is exactly solved in connection with the divergence-free property of any realization of the velocity field, only if nth-order correlations are taken at n distinct points in physical space, which give $n-1$ separation vectors when homogeneity is invoked, or a set of $n-1$ independent wave vectors in Fourier space.

At order 2, one recovers that two-point second-order velocity correlations are generated by $E(k)$, and the Lin equation (Eq. (8)) displays the spectral transfer term $T(k)$, which corresponds to the contribution of two-point third-order correlations. A similar relationship is found in physical space, as illustrated by Eq. (7) here, but integro-differential equations are needed to link different components of two-point second-order correlations, as the longitudinal and transverse self-correlations, whereas all these correlations can be expressed in terms of E by a single integral.

At order 3, the dynamical equation that governs triple correlations has to be taken at three points. A complete approach in physical space is not available, in spite of advanced equations and discussions by Batchelor, Craya (1958) and in Davidson's book. For instance, there is a direct link between the spectral transfer term $T(k)$ and the scalar function $K(r)$, defined by Batchelor, as shown by , e.g. Tchoufag *et al.* (2011) [20], and the equation for $K(r)$ is given and discussed by Davidson. On the other hand, the counterpart of the equation which governs triple correlations at three points is only given in Fourier space, under a form in which pressure contributions are exactly solved, by means of projection oprators. For instance, $T(k)$ is related to the three-point third-order spectral tensor by

$$T(k) = \iiint k_i S_{inn}(\boldsymbol{k},\boldsymbol{p}) d^3\boldsymbol{p}, \tag{13}$$

in which S_{ijk} is defined by

$$\langle \hat{u}_i(\boldsymbol{q})\hat{u}_n(\boldsymbol{k})\hat{u}_m(\boldsymbol{p})\rangle = S_{inm}(\boldsymbol{k},\boldsymbol{p})\delta^3(\boldsymbol{k}+\boldsymbol{p}+\boldsymbol{q}), \tag{14}$$

and is governed by the dynamical equation

$$\left(\frac{\partial}{\partial t} + \nu(k^2+p^2+q^2)\right) S_{inm}(\boldsymbol{k},\boldsymbol{p},t) = T^{IV}_{inm}(\boldsymbol{k},\boldsymbol{p},t), \tag{15}$$

in which $\boldsymbol{q} = -\boldsymbol{k}-\boldsymbol{p}$ and T^{IV} holds for contribution of fourth-order correlations at three points, with their exact 'corrections for pressure' terms. This level of description offers the best opportunity to introduce a robust closure, such as the EDQN one

$$T^{IV}_{inm}(\boldsymbol{k},\boldsymbol{p},t) = T^{QN}_{inm}(\boldsymbol{k},\boldsymbol{p},t) - \left(\eta(k,t)+\eta(p,t)+\eta(q,t)\right) S_{inm}(\boldsymbol{k},\boldsymbol{p},t). \tag{16}$$

The dominant term is the quasi-normal one, T^{QN}, which amounts to rewrite T^{IV} in terms of a sum of products of second-order correlation tensors, as for a normal law. The correction term, in the second line, therefore corresponds to the contribution of fourth-order *cumulants*, which are modelled as a relaxation term to reinforce the dissipative effect in Eq. (15), following heuristic arguments.

The reader is referred to specialized literature for more details on EDQNM, and more generally, on the 'tradic' approach in HIT [14]. An interesting and original insight to this approach is given by **W. Bos and R. Rubinstein in the present issue.**

We have now all the elements at hand to distinguish the two-point approach in subsection 2.2 from the 'tradic' one. In spite of the close connection between the Kármán–Howarth equation, or its variant in Eq. (7), and the Lin equation, their use is very different. Models for second-order correlations, e.g. for $S_2(r,t)$, yield immediately a model for $S_3(r,t)$ using the 'Kármán–Howarth' way. On the other hand, an elaborated closure of $T(k,t)$ in terms of $E(k',t)$ is first applied, before solving the Lin equation, and this closure is really introduced at the level of the dynamical equation for third-order correlation at three-points, such as eqs. (Eq. (15)) and (Eq. (16)) here. This difference is illustrated by Tchoufag *et al.* [20] for the search of FRN correction to the 4/5 Kolmogorov law; one can mention below two simple examples:

i) Cancellation of both dissipative and unsteady terms in Eq. (7) immediately yield the 4/5 Kolmogorov law. The same procedure applied to the Lin equation yields the unsatisfactory result $T=0$. It can be shown that the recovery of the asymptotic 4/5 law in Fourier space is found in separating the spectral domain according to the sign of the transfer term: for small ks, where the transfer is negative and corresponds to a sink of energy, the dissipation spectrum can be neglected but not the unsteadiness; integration of the inviscid Lin equation restricted to this domain yields $dk/dt = -\varepsilon_f$ (with k the kinetic energy, k is the wavenumber almost everywhere here), in which ε_f is the flux from the smallest scales (see also **McComb**); for the other domain of large k's, unsteadiness can be neglected but not the dissipation spectrum, so that $T(k) \sim 2\nu k^2 E(k)$, and integration in this domain gives the spectral balance $\varepsilon_f = \varepsilon$.

ii) Injecting Eq. (6) for $E(k,t)$ and using a k–ε model for its time-variation from $\varepsilon(t)$ gives only an evaluation of the zero of the transfer term and its behaviour close to this point but not at all a relevant model for $T(k,t)$ in a large spectral domain.

It is clear that 'triadic' closures are much more complex than 'two-point closures using the Kármán–Howarth way', but they include much more information and they are easier to extend towards anisotropic flows, generalizing both RDT and 'tradic closures for HIT'. On the other hand, we have mentioned that 'two-point closures' in physical space are simpler, more flexible and can easily relax a too strict assumption of statistical homogeneity: This is rediscussed in subsection 3.2.

2.5.2 Principle for easy generalisation to anisotropic turbulence

It is clear that *the fully tensorial, with full wavevectors* relationship in Eq. (16) is valid for arbitrary anisotropic turbulence. This is particularly true for the quasi-normal term, or S^{QN}_{inm}, which is exactly expressed in terms of the second order spectral tensor $\hat{R}_{ij}(\boldsymbol{k}',t)$; isotropy is used in basic EDQNM for HIT for deriving the final closure for $T(k,t)$, derived from S_{imn}, in terms of $E(k',t)$, derived from the second order spectral tensor $\hat{R}_{ij}$. Even if an anisotropic form of the fourth-order cumulant relaxation term is possible, it is better to firstly incorporate in the closure method the 'true' linear term responsible for the anisotropisation, such as the matrix M_{ij} in Eq. (9).

We have developed for a long time an original procedure for inverting the anisotropic 'true' linear operators in equations for cubic moments. This allows us to base the closure on a zeroth-order Kraichnan's response function, which is actually the RDT exact linear Green's function,

as in Eq. (10). In this sense, we generalize EDQNM, but also we incorporate more general concepts coming from DIA, but in byppassing the strenuous procedure of coupled equations for the response tensor and the two-time second-order spectral tensor. Note that our procedure can easily incorporate the RDT for cubic correlations, as well as the asymptotic limit of 'weak' wave-turbulence theory, when three-wave resonance is permitted by the dispersion law.

Before presenting more dedicated studies, for rotating, stratified and/or MHD anisotropic flows, one can say a few words about the fully anisotropic form of the second-order spectral tensor, and use of generalized Lin equations.

The divergence-free condition is an algebraic one in Fourier space, or $\boldsymbol{k}\cdot\hat{\boldsymbol{u}} = 0$. Accordingly, the Fourier component has only two components in a local, right-handed and orthonormal, frame of reference attached to the wave vector $\boldsymbol{k}$, often called Craya-Herring frame in the turbulence community, so that

$$\hat{\boldsymbol{u}} = \underbrace{u^{(1)}\boldsymbol{e}^{(1)}(\boldsymbol{k}) + u^{(2)}\boldsymbol{e}^{(2)}(\boldsymbol{k})}_{\text{solenoidal}} + \underbrace{u^{(3)}}_{\text{dil.}=0}\frac{\boldsymbol{k}}{k}.$$

This frame of reference $(\boldsymbol{e}^{(1)}(\boldsymbol{k}), \boldsymbol{e}^{(2)}(\boldsymbol{k}), \boldsymbol{k}/k)$ is the classical parallel / meridional /radial frame in a system of polar-spherical coordinates for $\boldsymbol{k}$. In the latter equation, the first two terms correspond to a toroidal-poloidal decomposition in physical space, both giving the solenoidal (divergence-free) part of the velocity field in the Helmholtz decomposition (see details and definition of $\boldsymbol{e}^{(1)}, \boldsymbol{e}^{(2)}$ in [17].)

Note that a similar decomposition (e.g. Yi Li, private) can be applied in physical space, for instance for the fluctuating velocity increment, using the same frame of reference with respect to the separating vector $\boldsymbol{r}$, or

$$\delta\boldsymbol{u} = \underbrace{(\delta u)_1\boldsymbol{e}^{(1)}(\boldsymbol{r}) + (\delta u)_2\boldsymbol{e}^{(2)}(\boldsymbol{r})}_{(\delta\boldsymbol{u})_T} + (\delta u)_L\frac{\boldsymbol{r}}{r},$$

displaying *transverse* (subscript 'T') and *longitudinal* (subscript 'L') increments. A similar decomposition in terms of cylindrical coordinates (Lindborg 1996) is much less convenient. The difference is that the Fourier component is really two-component in Fourier space for arbitrary anisotropy, whereas a similar claim by Lindborg that the velocity increment is 'dyadic' in structure functions, is simply wrong, even for axisymmetric turbulence.

The two-component character of the velocity Fourier vector yields drastic simplifications for statistical spectral tensors. The second-order spectral tensor $\hat{R}_{ij}$, which is given by correlating $\hat{u}_i(\boldsymbol{k},t)$ and the conjugate of $\hat{u}_j(\boldsymbol{k},t)$ at the same wavevector, can be expressed in terms of four pseudo-scalar terms for arbitrary anisotropy. This can be seen from a classical trace-deviator decomposition, but restricted to the plane normal to $\boldsymbol{k}$, or

$$\hat{R}_{ij} = e(\boldsymbol{k},t)P_{ij} + \hat{R}_{ij}^{(pol)} + \hat{R}_{ij}^{(hel)},$$

with $e = (1/2)\hat{R}_{nn}$. The deviatoric part, or $\hat{R}_{ij} - (1/2)\hat{R}_{nn}P_{ij}$, is exactly split into a real part, which is generated by a complex valued scalar Z, related to the polarization of the spectral energy, and a purely imaginary part, which is generated by the helicity spectrum $\mathcal{H}(\boldsymbol{k},t)$. Note that all generating scalars, e, Z and $\mathcal{H}$ can depend on the full wavevector $\boldsymbol{k}$, even if simplified forms exist for axisymetric turbulence, with and without mirror symmetry. As a consequence, the fully 3D energy spectrum $e(\boldsymbol{k})$ does not coincide in general with its spherically averaged part $E(k)/(4\pi k^2)$, the difference describing a 'directional' anisotropy, which is reflected, as the first nontrivial spherical harmonic, by the dimensionality tensor. Finally, the real part of the second-order spectral tensor is split into three terms

$$\hat{R}_{ij} = \underbrace{\frac{E(k,t)}{4\pi k^2}P_{ij}}_{(iso)} + \underbrace{\left(e(\boldsymbol{k},t) - \frac{E(k,t)}{4\pi k^2}\right)P_{ij}}_{(dir)} + \hat{R}_{ij}^{(pol)},$$

which characterize successively a purely isotropic part (iso), a contribution (dir) from directional anisotropy, and a contribution (pol) from polarization anisotropy. It has been shown (e.g. in [17]) that all structure tensors introduced by Kassinos and Reynolds are a byproduct of this decomposition, so that for instance $b_{ij} = b_{ij}^{(dir)} + b_{ij}^{(pol)}$, $d_{ij} = -2b_{ij}^{(dir)}$, $f_{ij} = b_{ij}^{(dir)} - b_{ij}^{(pol)}$ in **Kassinos and Radhakrishnan**.

From a dynamical viewpoint, general equations for $\hat{R}_{ij}$, obtained by combining the linear 'RDT' part in (Eq. (9)) and the nonlinear and viscous part in eq(Eq. (12)) are equivalent to coupled Lin equations in terms of e, Z, and $\mathcal{H}$. Exact equations in the case of homogeneous turbulence subjected to mean velocity gradient A_{ij} and in a rotating frame are given in Salhi *et al.* [16] and Cambon *et al.* [3], whereas the case of purely rotating, stratified, and quasi-static MHD, is detailed in this issue by **Godeferd et al.**

3 New insights to turbulence, essentially anisotropic, and interactions

3.1 Studies in collaboration within the ANISO ANR project

Anisotropy is a very important characteristic of turbulent flows, but often its statistical description is restricted to the RST anisotropy, with for instance an intensive use of the Lumley's invariant map. It is clear that more information is needed, for instance about the dimensionality, either using the structure-based modelling or the systematic splitting of anisotropy descriptors in terms of 'directional anisotropy' and 'polarisation anisotropy'. The general approach in Fourier space presented here allows us to recover such a structure-based modelling, and give a deeper scale-to-scale and even angle-to-angle analysis of anisotropic flow structure. A systematic description of anisotropy is proposed for structure functions, based on the SO(3) symmetry group (e.g. Arad *et al.*, Biferale, Proccaccia and coworkers), but this results in identifying only the first angular harmonics in practice, and this is disconnected from dynamical equations. A systematic comparison of anisotropic description is in progress, both in physical space and in Fourier space, supported by a contract (ANR, Agence Nationale de la Recherche), and a Summer School, also supported by ERCOFTAC, just took place on this topic (Morphology and dynamics of anisotropic flows, Cargese, Corsica, July 18-29 2011). The approach directly carried out in physical space, especially in the CORIA, is based on an axisymmetric and inhomogeneous generalization of Eq. (7), with various application to jets and wakes.

3.2 Dynamics of interfaces

Interfaces separate turbulent and laminar areas at the edge of jets, plumes and wakes, and they largely control the global features of these flows, such as entrainment. To what extent are similar mechanisms—acting in the periphery of vortices and between fluid volumes of different properties—reflected in global aspects of turbulence? New insights on this topic are given by **Eames et al.**, using new diagnostic tools and suggesting new modelling methods. We have already mentioned the possibility to revisit the concept of 'internal intermittency' in closer connection with such dynamics of interfaces. This introduces the multifractal approach as well. At first glance, the general emphasis on quasi-homogeneous turbulence given in my present survey is almost disconnected from a very local analysis including intermittency. On the other hand, the study of turbulence driven by buoyancy and started with Rayleigh-Taylor instability, gives a very good opportunity to reconcile the different viewpoints, as said in the very beginning of this paper.

3.3 Turbulence and coupled fields with and without rotation

This topic is illustrated by **R.P.J. Kunnen, H.J.H. Clercx and B. Geurts in the present issue, with 'Turbulent rotating convection: desktop geophysics.'** Thermal convection induces a buoyancy-driven energy production, and the flow is reorganized in columnar structures by dominant rotation.

Emphasis on flows with Coriolis force and/or with buoyancy force, is also considered in 'cases without production'. The simple scheme inherited from Kolmogorov is that energy, injected at large scale, and dissipated at small scale, has just a constant flux in an extended inertial range. It is assumed in addition that the inertial range can be described by HIT, even if energy is injected in an anisotropic and even inhomogeneous way. This scheme can be radically questionned for turbulence subjected to anisotropic body forces, in which there is no direct injection of energy, so that one can consider such flows as 'without production'. The first example is rotating turbulence, in which the Coriolis force produces no energy, but deeply alters the cascade via its impact on cubic velocity correlations. Anisotropy can penetrate deeply in the inertial range, and even can affect more the inertial scales than the largest scales, as confirmed very recently by experimental results [11]. Another example is the stably-stratified turbulence, if one considers that there is no production of total, kinetic + potential energy. MHD turbulence gives a third example, considering kinetic + magnetic energy. The specificity of our studies, with respect to existing litterature, is summarized in **F.S. Godeferd, C. Cambon, B. Favier and A. Delache in this issue**, for these three cases. All these studies combine pseudo-spectral DNS, with an original post-processing dedicated to a refined scale-to-scale and angle-to-angle description of anisotropy, and a recourse to axisymmetric EDQNM, for Reynolds numbers far beyond the DNS limits, with a detailed cross-comparison EDQNM/DNS at moderate Reynolds number. Promising applications deal with plasmas and superfluids (see, e.g. Tchoufag & Sagaut, 2010 [19], for an application of EDQNM to the latter topic).

4 Conclusions

Eight articles will follow in the present issue:

- Kolmogorov's theory: K41 or K62, by W.D. McComb,
- Interfaces in turbulence and implications for advanced modeling methods, by I. Eames *et al.*,
- Advances in structure-based modeling, by S.C. Kassinos & H. Radhakrishnan,
- Modelling approach to velocity and scalar gradients and increments, by A. Naso *et al.*,
- Advances in RDT and DNS for coupled effects of shear, rotation and stratification, by A. Pieri *et al.*,
- Statistical theories of turbulence: Non-gaussianity and coherence, by W.J.T. Bos & R. Rubinstein,
- Turbulent rotating convection: desktop geophysics, by R.P.J. Kunnen *et al.*,
- Axisymmetric theory and DNS in rotating, stratified, and MHD turbulence, by F.S. Godeferd *et al.*.

We have not surveyed important issues in Lagrangian turbulent diffusion, nor in high speed compressible flows, which are in the domain of our SIG, in addition to SIG 42 and SIG 4. Finally, investigation of the infrared limit has important consequences for practical turbulence models (e.g. [13]), and this merits to be generalized towards anisotropic turbulence with interactions, in the future activities of our SIG. Finally, promising applications of 'Crayalets' [5] will be investigated as an extension of the domain of wavelets to the general toroidal / poloidal (or Craya in Fourier space) decomposition extensively used here.

Careful rereading of this foreword by Antoine LLor and Ian Eames is gratefully acknowledged.

References

[1] R.A. Antonia and P. Burattini (2006), 'Approach to the 4/5 law in homogeneous isotropic turbulence,' *J. Fluid Mech.* **550**, 175-184.

[2] C. Cambon, F.S. Godeferd, F.C.G.A. Nicolleau & J.C. Vassilicos (2004), 'Turbulent diffusion in rapidly rotating flows with and without stable stratification,' *J. Fluid Mech.* **499**, 231–255.

[3] C. Cambon, L. Danaila, F.S. Godeferd and J. Scott (2011) 'Impact of third-order statistics in the dynamical approach to strongly anisotropic turbulence,' *J. Fluid Mech.* to be submitted

[4] A. Cimarelli and E. De Angelis (2011), 'Analysis of the Kolmogorov equation for filtered wall-turbulent flows,' *J. Fluid Mech.* **676**, 376-395.

[5] E. Deriaz, M. Farge & K. Schneider (2010), 'Craya decomposition using compactly supported biorthogonal wavelets', *Appl. Comput. Harm. Anal.*, **28**, 267-284.

[6] F.S. Godeferd, C. Cambon & J.F. Scott (2001), 'Two-point closures and their applications: report on a workshop,' *J. Fluid Mech.* **436**, 393–407.

[7] B.-J. Gréa, J. Griffond & O. Soulard, 2010, 'One point structure tensors and spectral structure of Rayleigh - Taylor turbulence: From self-similar to rapidly distorted regimes,' *12th IWPCTM Conference*, Moscow.

[8] L.D. Landau and E.M. Lifschitz (1987), *Fluid Mechanics,* 2nd. Ed., Pergamon, New York.

[9] G. Lesur (2007), PhD on accretion discs, Université de Grenoble.

[10] T. von Kármán and C.C. Lin (1949), 'On the concept of similarity in the theory of isotropic turbulence,' *Rev. Mod. Phys.* **21** (3) 516–519.

[11] C. Lamriben, P.P. Cortet, F. Moisy, (2011), 'Direct measurements of anisotropic energy transfers in a rotating turbulence experiment', *Phys. Rev. Lett.*, **107**, 2.

[12] A. Llor and P. Bailly, (2003), 'A new turbulent two-field concept for modelling Rayleigh–Taylor, Richtmeyer–Meshkov and Kelvin–Helmholtz mixing layers,' *Laser and particle beams* **21**, 311–315.

[13] A. Llor, (2011), 'Langevin equation of big structure dynamics in turbulence: Landau's invariant in the decay of homogeneous isotropic turbulence,' *European Journal of Mechanics – B/Fluids* **30**, 480–504.

[14] W.D. McComb, (1990), *The Physcics of Fluid Turbulence*, Oxford University Press.

[15] H.K. Moffatt, (1967), 'The interaction of turbulence with strong wind shear,' *Colloquium on Armospheric Turbulence and Radio Wave Propagation*, Ed. A.M. Yaglom and V.I. Tatarsky, Nauka, Moscow, **139**.

[16] A. Salhi, F. Jakobitz, K. Schneider and C. Cambon (2011), 'Comparison of spectral theory and DNS for rotating sheared turbulence: Anisotropy and multiscale approach,' *Phys. Fluids*, to be submitted.

[17] P. Sagaut & C. Cambon, *Homogeneous Turbulence Dynamics*, 2008, Camb. U. Press, New York.

[18] K.R. Sreenivasan, 'On the universality of the Kolmogorov constant,' *Phys. Fluids* **7**, 2778 (1995).

[19] J. Tchoufag and P. Sagaut, 2010, 'Eddy Damped quasinormal Markovian simulations of superfluid turbulence in helium II,' *Phys. Fluids* **22**, 125103.

[20] J. Tchoufag, P. Sagaut, and C. Cambon (2011), 'Spectral approach to finite Reynolds number effects on Kolomogorov's 4/5 law in isotropic turbulence,' *Phys. Fluids*, submitted.

Kolmogorov's Theory: K41 or K62?

W David McComb

SUPA, School of Physics and Astronomy,

University of Edinburgh, EDINBURGH EH9 3JZ, UK.

Email:wdm@ph.ed.ac.uk

Abstract

From a critical review of the subject, we infer that concerns about the effect on the K41 picture of *internal intermittency*, *problems with averages*, *anomalous exponents*, and *vortex stretching*, may be without foundation. Furthermore, research by various workers over the last two decades strongly suggests that deviations of S_2 (or $E(k)$) from the K41 result are due to the effects of finite viscosity. We conclude that K41 is probably correct, but that this matter will ultimately be settled by direct numerical simulation. We conjecture that the K41 picture works better in wavenumber space, rather than scale space, due to the large number of degrees of freedom, random phase effects and, not least, the presence of a cascade.

1 Introduction

In this article we restrict our attention to homogeneous, isotropic turbulence (HIT). In this way, we rule out effects due to mean shear, system rotation, density stratification, and so on. This leaves us with a stark choice: deviations from Kolmogorov's predictions for the energy spectrum (or second-order structure function) must be due either to the Reynolds number being finite (K41 is based on an assumption of very large Reynolds numbers) or to the effects of internal intermittency, as was suggested later on, by Kolmogorov, in 1962.

Over the last few decades a veritable industry has grown up, based on the search for so-called *intermittency corrections*. Currently it is dominated by multi-scale or multifractal models of turbulence. This activity finds a sympathetic audience, because many people seem to see the K41 picture as being counter-intuitive, when one considers aspects of turbulence such as *vortex-stretching*, *localness*, *intermittency* and the taking of *averages*.

Running counter to this belief in 'intermittency corrections' (or, increasingly, 'anomalous exponents') which has been dominant in recent times, there is a growing view [1]- [7] that K41 is an asymptotic theory, valid in the limit of infinite Reynolds number. In this school of thought, any deviations from K41 are due to finite viscosity.

As a result, opinion in the turbulence community is deeply divided on this fundamental issue.

Here we will begin by considering the various criticisms of, or sources of unease about, K41. This is followed by a discussion of the various theories which advocate finite-viscosity effects in explaining deviations from K41. We conclude with a brief discussion of the situation.

2 Criticism of Kolmogorov's 1941 theory

As is well known, in 1941, Kolmogorov [8, 9] gave two different derivations of his now-famous result for the second-order structure function:

$$S_2 = C\varepsilon^{2/3} r^{2/3}, \tag{1}$$

for $L > r > l$, where l is a measure of the scale at which viscous effects begin to dominate (i.e. the internal scale), L is a measure of the large scales of the system (i.e. the external scale) and the prefactor takes the value $C \simeq 2$. As is equally well known, the corresponding result for the energy spectrum in wavenumber is

$$E(k) = \alpha\varepsilon^{2/3} k^{-5/3}, \tag{2}$$

where the prefactor α is widely known as the *Kolmogorov constant* and takes a value of about $\alpha = 1.6$.

Shortly after this work was published, it was criticised by Landau (see the footnote on page 126 of [10]). Kolmogorov [11] interpreted this criticism as a need to treat the dissipation rate as a variable; and, working with its average taken over a sphere of radius r, concluded that the right hand side of Eq. (1) should be multiplied by a factor $(L/r)^\mu$, where μ is often referred to nowadays as an *intermittency correction*.

That development gave rise to further attempts by other workers to obtain a value for μ. As a result, for many years K41 has had a question mark hanging over its status as a theory of inertial-range turbulence. We will find it convenient to classify criticisms of the Kolmogorov (1941) theory under four main headings, thus: the effect of internal intermittency; problems with averages; anomalous exponents; and the difficulty of interpreting vortex stretching as a local cascade. As we discuss these in turn, it will be apparent, these groupings are by no means mutually exclusive.

2.1 The effect of internal intermittency

We do not intend to examine the relationship between the Kolmogorov-Obukkov proposal of [11] and the famous footnote in the book by Landau and Lifshitz [10]. This is a well known conundrum and, apart from pointing out that Landau and Lifshitz inconsistently use the symbol ε to denote both a mean dissipation (main part of the page) and an instantaneous dissipation (in the footnote), we shall leave this matter alone. The important fact is that Kolmogorov [11] amended his original theory to take account of the spatial intermittency[1] of the

1. Although the word 'intermittency' does not actually appear in his paper.

instantaneous dissipation rate $\hat{\varepsilon}$.

The intermittency concerned was first pointed out by Batchelor and Townsend [12], and used to be referred to as 'fine-scale' or 'small-scale intermittency'. Nowadays it seems to be more usual to call it 'internal intermittency'. In any case, it should be distinguished from the intermittency associated with a free edge of unconfined shear flows or with the 'bursting process' in duct flows. In both these cases, intermittency is associated with *structure*, which exists in some average sense. Due to the restrictive symmetries, it is impossible for structure to exist in HIT in anything other than an instantaneous sense.

There seem to be two crucial difficulties with the idea that the existence of spatial intermittency implies the need for some corrections to the Kolmogorov (1941) theory. These are as follows:

1. The dissipation rate is not the relevant quantity for K41A. The relevant quatity is the inertial flux of energy. The use of the same symbol ε (and even the same terminology!) for both these quantities may have caused some confusion. It is for this reason that we have introduced ε_T for flux and ε_D for dissipation rate [7].

2. Internal intermittency is a phenomenon associated with a single realization. it must necessarily 'average out'; or, in other words, disappear, under any global averaging operation. It is not immediately obvious that its existence it will affect relationships between globally-averaged quantities. In the case of K41B, Kolmogorov's starting point was the Karman-Howarth equation and of course this equation is ensemble-averaged and contains the mean rate of dissipation. This fact was recognised in K62, where it was stated that the '4/5' law for $S_3(r)$ was unaffected by the process of locally averaging the instantaneous dissipation rate $\hat{\varepsilon}$ over a sphere of radius r. The significant new element in that work was the introduction of an *ad hoc* expression for the skewness and the abandonment of the assumption of constant skewness, as made in K41B.

However, despite the lack of any obvious causal factor, the use of the term 'intermittency corrections' became quite widespread. By 1990, the exponent μ was widely referred to as the *intermittency exponent*: see [13]. And evidently this usage persisted: see, for example, the review by Sreenivasan [14]. More recently the term *anomalous exponents* has become popular.

2.2 Cascade or vortex stretching?

The idea of a cascade, as believed to underpin the Kolmogorov picture, is often seen to be incompatible with the vortex-stretching behaviour of turbulence (e.g. see [15], [16]). In order to examine this proposition, we need to understand the meaning of both these terms and indeed how they relate to the Kolmogorov theories.

The term 'cascade' is used to describe a process in which energy is transferred from large scales to small scales. However, there is no cascade in real space. This is because there is no inertial flux: the Karman-Howarth equation is a *local* energy balance[2], taken at a position $\mathbf{x}$ or a scale r. Of course, in shear flows, the inhomogeneity leads to a flux of energy from where it is produced to where it is dissipated. But in HIT no such flux exists. Good discussions of this topic may be found in the books by Tsinober [17] and that of Sagaut and Cambon [18] (who cite the first edition of Tsinober's book).

How then does all this affect K41A and K41B, both of which were formulated in real space? Taking them in reverse order, K41B does not rely on a cascade. It relies on the vanishing of the viscous term in the Karman-Howarth equation when one takes the limit of infinite Reynolds numbers at constant dissipation rate. Also, bearing in mind the local nature of the Karman-Howarth equation, one may also apply a suitably chosen stirring force, such that its effects are confined to scales greater than some input scale r_I. Then the energy balance applies to an *inertial range of scales* where the detailed effects of dissipation and forcing are not felt. This separation of input (or energy-containing) scales from viscous dissipation scales offers a sort of intuitive basis for K41A, which is actually no more than a dimensional analysis. Or, K41A could be based on some intuitive decomposition of scales which may be thought of as a conjugate to the Fourier representation. Further discussion of scale-space formulations, as analogous to wave-number space formulations, may be found in the book by Davidson [19]. And for some comments on the effect of decomposition on scale-space behaviour, see p133 in [17].

It is generally understood that turbulence is characterised by various processes involving vortical structures, in which the vorticity increases with time in ways that we tend to associate with vortex stretching. One can think of a vortex tube being stretched by a velocity gradient, and in the process, conservation of angular momentum ensuring that the associated kinetic energy is concentrated in ever-smaller regions of space.

In the past, various models have been proposed to describe this process and these include arrays of tubes, plane vortex sheets,and so on. Naturally in each case, analytical tractability is a prime consideration in choosing the model. A brief introduction to such methods may be found in [13]. However, in recent years it has become clear, from numerical simulations of HIT, that surfaces of constant vorticity tend to take the form of randomly-coiling worm-like structures.

When we seek to confront the cascade picture with the vortex-stretching picture, the difficulty in so doing is twofold. First, the cascade is in wavenumber space, whereas the vortex structures are in real space. Second, the cascade is an ensemble-averaged process, whereas the vortex structure is an instantaneous phenomenon. It is characteristic of a single realization and may be eliminated by averaging. Nevertheless, it is still possible, in very general terms, to identify some apparent inconsistency between the two pictures, as follows.

Granted that the cascade describes the transfer of energy from small wavenumbers to large; and intuitively associating the corresponding 'scales' with the reciprocal of the wavenumbers, one can see two difficulties in reconciling the two processes [15], [16]. These are:

1. When a vortex tube is drawn out in space, the length scale of the extensional field may be expected to be much larger than the diameter of the extended tube. This is not immmediately compatible with the idea of localness of a cascade.

2. When a vortex tube, or any comparable vortical

2. This is not the case for the Navier-Stokes equation, where the pressure term is known to be non-local in real space. But the NSE describes momentum transfer in a single realization, not ensemble-averaged energy transfer.

structure, is stretched, at least one dimension of the structure remains large (when compared to the cross-section) and thus does not appear to support the idea of transfer to a larger wavenumber (i.e. smaller scales).

We can offer counter arguments to both these points. But before doing so, let us enter a caveat. This to the effect that we should not rely too heavily on intuition which might just cope with Fourier transforms applied to some very simple problem such as waves in linear electric circuits or physical optics. Fluid turbulence is not only a highly nonlinear phenomenon but also involves random amplitudes and phases. In some many-body problems, the approximate cancellation of phases justifies a *random phase approximation*; and in other cases the phases are known to cancel exactly. Indeed, when we form the energy spectrum in turbulence, the phases cancel exactly by construction. But this does not alter the fact that making intuitive connections between phenomena in x-space and those in k-space is likely to prove a rather fraught procedure. Having said that, let us now take the two points in order.

The idea of localness is crucial to the cascade. When we consider the Fourier-transformed NSE, the first thing we learn is that nonlinear mixing couples each Fourier mode to every other mode. So it would be helpful if we had something like a 'nearest neighbour' assumption for interactions, (e.g. as in the Ising model for ferromagnetism). This situation is made worse by the fact that the interactions between modes of the NSE are triadic. So the concept of 'nearest neighbour' is not available to us and has to be replaced by some idea of 'strongly interacting triads' and 'weakly interacting triads'. This topic has been the subject of numerical investigations. For example, see [20], and [21]. The latter investigation is particularly interesting in our present context as it considers concurrent real-space and wavenumber-space views. However, interesting although these matters are, we do not need to rely on them in order to justify Kolmogorov's picture. It was recognised by Batchelor [22], at least as early as the 1950s, that the key was not the transfer spectrum but the flux through mode k. It follows rigorously from the symmetry of the NSE, that the *local flux* through mode k is determined by a sum over all contributions j such that $j \leq k$. This is the only concept of localness that K41 needs. And as the Reynolds number increases, and the energy-containing and dissipation ranges move apart, the inertial range becomes that range of wavenumbers where the flux is approximately constant and equal to the dissipation.

As regards the second point, one must be aware of identifying a vortical structure, such as a vortex tube, with a particular Fourier mode. If a given vortex tube contributes to $u_1^2(k)$ and $u_2^2(k)$, where k is large; but not to the corresponding $u_3^2(k)$, then some other vortex tube must make up the deficit. At the end of the day, the combined effects of ensemble-averaging and isotropy will ensure that this is so. We would reiterate that the Kolmogorov spectral picture involves only average quantities and reasoning from some speculation about a single realization is likely to prove tenuous at best.

2.3 Problems with averages

The idea that K41 had some problem the way that averages were taken has its origins in the famous footnote on page 126 of the book by Landau and Lifshitz [10]. This footnote is notoriously difficult to understand; not least because it is meaningless unless its discussion of the 'dissipation rate ε' refers to the *instantaneous* dissipation rate. Yet ε is clearly defined in the text above (see the equation immediately before their (33.8)) as being the *mean* dissipation rate. Nevertheless, the footnote ends with the sentence 'The result of the averaging therefore cannot be universal'. As their preceding discussion in the footnote makes clear, this lack of universality refers to 'different flows': presumably wakes, jets, duct flows, and so on.

As we have already observed, Kolmogorov interpreted this criticism as referring to the small-scale intermittency of the instantaneous dissipation rate. His response was to adopt Obukhov's proposal to introduce a dissipation rate which had been averaged over a sphere of radius r. This procedure runs into an immediate fundamental objection. In K41A, (or its wavenumber- space equivalent) the relevant inertial-range quantity for the dimensional analysis is the local (in wavenumber) energy transfer. This is of course equal to the mean dissipation rate by the global conservation of energy[3]. However, there is no such simple relationship between locally-averaged energy transfer and locally-averaged dissipation [16].

Another point worth reiterating at this stage is that the derivation of the '4/5' law is completely unaffected by the 'refinements' of K62. This is really rather obvious. The Karman-Howarth equation involves only ensemble-averaged quantities and the derivation of the '4/5' law requires only the vanishing of the viscous term. This fact was noted by Kolmogorov [11].

The averaging process in K62 has been discussed in some detail by Monin and Yaglom [23]. A more extensive discussion (complete with helpful diagrams) can be found in the book by Davidson [19]. We will only make one particular point here, which arises from an observation by Kraichnan [16], and which does not actually depend on the *nature* of the averaging process. In fact Kraichnan worked with the energy spectrum, rather than the structure function, and interpreted Landau's criticism of K41 as applying to

$$E(k) = \alpha \varepsilon^{2/3} k^{-5/3}. \tag{3}$$

His interpretation of Landau was that the prefactor α may not be a universal constant because the left-hand side of Eq. (3) is, an average, while the right-hand side is the 2/3 power of an average. He then went on to discuss this in terms of the partial averaging procedure of K62.

However, as we have mentioned above, this relationship could be a problem for any averaging procedure. Any average involves the taking of a limit. Suppose we consider a time average, then we have

$$E(k) = \lim_{T \to \infty} \frac{1}{T} \int_0^T \widehat{E}(k,t) dt, \tag{4}$$

where as usual the 'hat' denotes an instantaneous value. Clearly the statement

$$E(k) = \text{a constant}; \tag{5}$$

or equally the statement,

$$E(k) = f \equiv \langle \hat{f} \rangle, \tag{6}$$

3. It is a potent source of confusion that these theories are almost always discussed in terms of dissipation when the proper inertial-range quantity is the nonlinear transfer of energy.

for some suitable f, presents no problem. It is the '2/3' power on the right-hand side of Eq. (3) which means that we are apparently equating the operation of taking a limit to the 2/3 power of taking a limit. However, it has recently been shown [7] that this issue is resolved by noting that the pre-factor α itself involves an average over the phases of the system.

2.4 Anomalous exponents

The term *anomalous exponents* is used to refer to the case where the power-law exponents ζ_n of structure functions $S_n(r)$ differ from the Kolmogorov values $n/3$. The rise in interest in this topic has (unsurprisingly) gone hand in hand with the trend in recent years away from measurements of spectra to measurements of moments and structure functions in real space. Typically an experimental plot of exponents ζ_n against n yields a curve in which the difference between ζ_n and $n/3$ increases with increasing n.

The idea of *anomalous exponents* seems to have arisen by analogy with the concept of *anomalous dimension* in the statistical field theory of equilibrium critical phenomena. However, such analogies should be interpreted with caution. In equilibrium, critical exponents determined by renormalization group methods differ from those obtained by dimensional analysis. The central role of the dimension of space in these theories leads to a natural interpretation in terms of anomalous dimension. But this situation arises because dimensional analysis is a very weak method in equilibrium problems and requires the introduction of densities in order to introduce dimensional considerations. In contrast, non-equilibrium systems are characterised by a symmetry-breaking current or flux. In the case of turbulence, this is the inertial transfer flux; and, combined with conservation of energy, this provides a strong constraint on dimensional analysis. A simple introduction to these ideas can be found in the book [24].

Our use of inverted commas with the term 'Kolmogorov values' is an implicit recognition of the fact that the $S_n(r)$, for $n > 3$, are not actually part of the Kolmogorov (1941) theory, which is (in both K41A and K41B forms) a theory of S_2 and S_3. There are three points which we would like to emphasise here. These are as follows:

1. The structure functions $S_2(r)$ and $S_3(r)$ are connected together by the principle of conservation of energy. This takes the form of the Karman-Howarth equation; or, if we are using spectral forms, the Lin equation. It is with reference to these equations that we can define the energy-containing (or input); inertial; and dissipation ranges of wavenumbers.

2. For structure functions $S_n(r)$, with $n \geq 4$; these wavenumber ranges are undefined.

3. Any systematic trend in the dependence of ζ_n on n, with increasing n, may be a systematic error due to the increasing importance of rare events with order n.

These points are often glossed over or ignored; particularly in the search for the so-called *intermittency corrections*.

The association of internal intermittency with anomalous exponents has developed strongly over the last few decades. Originally fractal models were popular (for an introductory discussion, see [13]) but later on multifractal models replaced them in popularity: for a recent review, see [25]. Over the same time, there has been a growing body of work supporting the obvious explanation for the deviation of exponents from the Kolmogorov (1941) values: namely that the conditions imposed by the theory are not fully satisfied at finite Reynolds numbers.

This disagreement is capable of being resolved, as follows.

1. If intermittency effects are dominant, then these are expected to increase with increasing Reynolds number and

$$E(k) \to k^{-5/3+\mu} \quad \text{as} \quad R \to \infty.$$

2. Conversely, if finite-Reynolds-number effects are dominant, then

$$E(k) \to k^{-5/3} \quad \text{as} \quad R \to \infty.$$

As direct numerical simulations increase in size and resolution, an examination of the dependence of μ on Reynolds number should settle this question.

However we may conclude this part of our discussion with a salutary quotation, taken from Kraichnan's 1974 discussion of Kolmogorov's theories [16]. If (1) above is correct, and $E(k) \sim k^{-5/3+\mu}$ is aysmptotically valid, then it follow that

> '... the value of μ depends on the details of the nonlinear interaction embodied in the Navier-Stokes equation and cannot be deduced from overall symmetrels, invariance and dimensionality.'

In other words, perceived intermittency is an aspect of the solution of the Navier-Stokes equation.

3 Kolmogorov (1941) revisited

In this section we give a brief discussion of six different investigations which, individually and collectively, offer considerable support to K41 rather than K62. Among the earliest in this category is the work by Effinger and Grossmann on the second-order structure function for the velocity field [26], which was later extended to structure functions of the temperature field in passive convection [27].

These authors studied the second-order structure function, by introducing a spatial smoothing operation in which they averaged the fluid velocity field $u_\alpha(\mathbf{x}, t)$ over a sphere of radius r, thus:

$$u_\alpha^{(r)}(\mathbf{x}, t) = \langle u_\alpha(\mathbf{x}, t) \rangle^{(r)} , \tag{7}$$

where $u_\alpha^{(r)}$ is referred to as the *super-scale* velocity field and the superscript on the angle-brackets indicates that the spatial average is taken over a sphere of radius r. The corresponding *sub-scale* velocity field $\tilde{u}_\alpha^{(r)}$ was then obtained by subtraction, thus:

$$\tilde{u}_\alpha^{(r)}(\mathbf{x}, t) = u_\alpha(\mathbf{x}, t) - u_\alpha^{(r)}(\mathbf{x}, t). \tag{8}$$

The authors drew an analogy between their approach, and that of Reynolds, in which they operate on the NSE

with Eq. (7) in order to derive separate equations of motion for the super-scale and sub-scale velocity fields. In principle, then, their strategy is to solve the equation for the sub-scale field and substitute the result into the equation for the super-scale field. In order to do this, they make a number of approximations, predominantly of the type used in renormalization group theory, which their method to some extent resembles. But, although approximate, their result for S_2 agrees well with experimental results and its asymptotic behaviour supports K41 with viscous corrections.

For completeness we should mention that Effinger and Grossmann [27] extended this method to the problem of passive scalar convection. Later this group presented an analysis of data from DNS which supported the idea that there are no intermittency corrections to energy spectra, when their results are extended to very high Reynolds numbers [28]; and more recently they have argued that the use of nonperturbative renormalization group methods enforces the K41 spectrum for HIT [3].

Chronologically, our next approach is due to Qian, who has published a series of papers dealing with aspects of the scaling properties of HIT; and, in particular, on deciding whether the second-order exponent ζ_2 corresponds to normal Kolmogorov scaling ($\zeta_2 = 2/3$) or anomalous scaling ($\zeta_2 > 2/3$). Here we shall concentrate on just three of these, that is [4], and the two papers leading up to it, [29, 30]. We may begin by noting that his method is different from all the other theoretical approaches, in that it is really a sophisticated form of data analysis, and is based on the use of exact relationships, combined with well-established data correlations, in order to extract as much information as possible from experimental results. Where assumptions are made, careful testing of the effect of varying these assumptions shows that they are innocuous.

We will give only a brief impression of this work and concentrate on his analysis of extended spectral similarity or ESS. Qian shows that a log-log plot of S_2 versus S_3 produces the expected straight line. But when he plots the local gradient of that line against r/η, instead of being constant as one would expect, it shows a prominent peak, only becoming constant at large values of the scale. This in itself appears to question the validity of ESS. However, extending this work to higher-order structure functions, Qian demonstrates that the results from ESS actually support K41 rather than K62.

We cannot do justice to Qian's analysis here. The interested reader should consult the original papers which, although hard work, are rewarding. We now turn to the work of Barenblatt and Chorin, who also have published extensively on the theory of turbulence, particularly with reference to scaling and similarity, over a period of years. A good starting point is their two papers in 1988 [2, 31], which summarise their approach and which cite many earlier references. Their main emphasis is on the so-called 'law of the wall' in wall-bounded shear flows. However, they also deal with the inertial-range spectrum and conclude that the classical, unmodified K41 theory gives '.. an adequate description of the local features of developed turbulent flows'. It is, of course, this latter aspect which concerns us here.

Essentially, Barenblatt and Chorin discuss the nature of scaling theory in turbulence. At the point where most people follow K62, and introduce the external length-scale to fill the gap in the dimensional analysis, these authors give arguments to support the use of the dissipation length-scale for this purpose. As a result they conclude that both the prefactor and the exponent in K41 are subject to corrections which are dependent on the Reynolds number. Overall, they conclude that ' ... there are no intermittency corrections to the Kolmogorov '5/3' spectral exponent'.

Next, we consider the first of two asymptotic matching theories: in this case for the energy spectrum. The work of Gamard and George [5] was motivated by the experimental study of Mydlarski and Warhaft [32], which reported finite Reynolds number effects in inertial-range spectra. As with other investigations discussed here, the paper cited is the outcome of a programme of work over some years and gives a number of references to previous work by George and co-workers.

Their starting point is the recognition that the energy spectrum can be scaled both on Karman-Howarth variables (which gives a better collapse of data at low wavenumbers) and also on Kolmogorov variables (which gives a better collapse of data at high wavenumbers). Accordingly they introduced the dimensionless functions f_L for low wavenumbers, and f_H for high wavenumbers. Recognising that f_L must asymptote to an inertial-range form for high wavenumbers and f_H must asymptote to an inertial-range form for low wavenumbers, Gamard and George set out to establish their functional form in a common region such that this form exists in the limit of infinite Reynolds numbers. This required an extensive analysis. Extension of this to finite Reynolds numbers involved some approximations, but these were checked by experimental comparisons at crucial stages. In a convincing analysis, they showed that the intermittency exponent μ vanishes as the Reynolds number increases, in agreement with experiment.

Our second asymptotic analysis is the theory of Lundgren [6], who adopted a similar strategy to that of Gamard and George, but who worked in real space with the structure functions. Like them, he employed both Karman-Howarth and Kolmogorov variables to scale the structure functions, and then matched asymptotic high-Reynolds expansions to obtain the Kolmogorov '2/3' law. However, where Gamard and George *demonstrate* the point, Lundgren *proves analytically* that the KH scaling (at large scales) and the Kolmogorov scaling (at small scales) are both asymptotically valid, as the Reynolds number tends to infinity. Matching asymptotic expansions, Lundgren concluded that, in the limit of infinite Reynolds numbers, $S_2 \sim r^{2/3}$ and $S_3 \sim r$, in accordance with K41. In later work, Lundgren examined the dependence on Reynolds number in a more general way [33].

Gamard and George on the one hand, and Lundgren on the other, leave very little room for doubt. Their identical conclusions are to the effect that the predictions of K41 for $S_2(r)$ or $E(k)$ are subject to corrections due to finite viscosity and are asymptotically valid in the limit of infinite Reynolds number. Both can point to experimental support for their theoretical conclusions.

We close this discussion with the observation that K41b relies on a *de facto* closure of the Karman-Howarth equation as the viscosity tends to zero. The same idea can be employed in wavenumber space with the Lin equation [7], but here the effect of the phases can be taken into account explicitly. It transpires that the spectral prefactor arises from an integral over the phases and that the presence of this average resolves the problem of dependence on an average to the '2/3' power, as noted earlier.

4 Conclusion

It has to be conceded that K41A is not a completely satisfactory theory. There is no cascade in real space and the dimensional analysis seems to rely on some sort of intuitive appeal to what is going on behind the scenes, as it were, in wavenumber space. There we have the concept of flux of energy from *all* lower wavenumbers to the wavenumber of interest. This is a property of the equations of motion. The necessary additional concept of scale invariance (which defines the inertial range) arises inevitably as the Reynolds number increases and the dissipation is pushed to ever-higher wavenumbers. This also is a property of the NSE. Perhaps it is better, therefore, to carry out the analysis in wavenumber space and recover the inertial-range form of $S_2(r)$ by Fourier transformation.

In contrast, K41B, as a prediction of the inertial-range form of the third-order structure function, is incontrovertible. The analyis is asymptotically exact and the Kolmogorov form must apply at infinite Reynolds numbers. From this, two points arise as a corollary. They are, as follows:

1. Any theory or procedure which relies on the assumption that the scaling exponent of S_3 is exactly $n = 1$ at finite Reynolds numbers is already subject to error, however small.

2. The fact that S_3 is subject to finite-viscosity corrections sets a precedent for S_2 which is rigorously connected to it by conservation of energy. However, higher structure functions are not part of K41.

Overall, our conclusion is that K41 is basically correct and that, in particular, the work of Gamard and George [5] and of Lundgren [6], when taken together, leave little room for doubt on this matter. In both wavenumber and physical space, K41 is asymptotically exact at large Reynolds numbers and otherwise subject to finite-viscosity corrections. As pointed out by Kraichnan [16] and by Qian [4], K62 is not a 'refinement' of K41, but rather represents quite a different physical picture of turbulence. It is important to settle this matter and in time the development of DNS should lead to a resolution (for example, see the review [34]). However, it should be borne in mind that our present discussion is limited to homogeneous, isotropic turbulence and the conclusions may have to be modified for any more general situation. The necessity for this type of examination for other classes of flow must be borne in mind. Further, and more detailed, examination of the issues discussed in this article will appear later in the book [35], which is now in preparation.

References

[1] John C Bowman. On inertial-range scaling laws. *J. Fluid Mech.*, 306:167–181, 1996.

[2] G.I. Barenblatt and A. J. Chorin. New perspectives in turbulence: scaling laws, asymptotics and intermittency. *SIAM Rev.*, 40:265–291, 1998.

[3] A. Esser and S. Grossmann. Nonperturbative renormalisation group approach to turbulence. *Eur. Phys. J. B*, 7:467–482, 1999.

[4] J. Qian. Closure Approach to High-Order Structure Functions of Turbulence. *Physical Review Letters*, 84(4):646–649, 2000.

[5] S. Gamard and W. K. George. Reynolds number dependence of energy spectra in the overlap region of isotropic turbulence. *Flow, turbulence and combustion*, 63:443 – 477, 1999.

[6] Thomas S. Lundgren. Kolmogorov two-thirds law by matched asymptotic expansion. *Phys. Fluids*, 14:638, 2002.

[7] David McComb. Scale-invariance and the inertial-range spectrum in three-dimensional stationary, isotropic turbulence. *J. Phys. A: Math. Theor.*, 42:125501, 2009.

[8] A. N. Kolmogorov. The local structure of turbulence in incompressible viscous fluid for very large Reynolds numbers. *C. R. Acad. Sci. URSS*, 30:301, 1941.

[9] A. N. Kolmogorov. Dissipation of energy in locally isotropic turbulence. *C. R. Acad. Sci. URSS*, 32:16, 1941.

[10] L. D. Landau and E. M. Lifshitz. *Fluid Mechanics*. Pergamon Press, London, English edition, 1959.

[11] A. N. Kolmogorov. A refinement of previous hypotheses concerning the local structure of turbulence in a viscous incompressible fluid at high Reynolds number. *J. Fluid Mech.*, 13:82–85, 1962.

[12] G.K. Batchelor and A. A. Townsend. The nature of turbulent motion at large wavenumbers. *Proc. R. Soc Lond. A*, 199:238, 1949.

[13] W. D. McComb. *The Physics of Fluid Turbulence*. Oxford University Press, 1990.

[14] K. R. Sreenivasan. Fluid turbulence. *Rev. Mod. Phys.*, 71:S383, 1999.

[15] P. G. Saffman. Lectures on homogeneous turbulence. In N. Zabusky, editor, *Topics in nonlinear physics*, pages 485–614. Springer-Verlag, 1968.

[16] R. H. Kraichnan. On Kolmogorov's inertial-range theories. *J. Fluid Mech.*, 62:305, 1974.

[17] A. Tsinober. *An Informal Conceptual Introduction to Turbulence*. Springer, Dordrecht, 2nd edition, 2009.

[18] P. Sagaut and C. Cambon. *Homogeneous Turbulence Dynamics*. Cambridge University Press, Cambridge, 2008.

[19] P. A. Davidson. *Turbulence*. Oxford University Press, 2004.

[20] J. A. Domaradzki and R. S. Rogallo. Local energy transfer and nonlocal interactions in homogeneous isotropic turbulence. *Phys, Fluids A*, 2:413, 1990.

[21] P. K. Yeung, J. G. Brasseur, and Qunzhen Wang. Dynamics of direct large-scale couplings in coherently forced turbulence: concurrent physical- and fourier-space views. *J. Fluid Mech.*, 283:43–95, 1995.

[22] G.K. Batchelor. *The theory of homogeneous turbulence*. Cambridge University Press, Cambridge, 2nd edition, 1971.

[23] A. S. Monin and A. M. Yaglom. *Statistical Fluid Mechanics*. MIT Press, 1975.

[24] W.D. McComb. *Renormalisation Methods*. Oxford University Press, 2004.

[25] G Boffetta, A Mazzino, and A Vulpiani. Twenty-five years of multifractals in fully developed turbulence: a tribute to Giovanni Paladin. *J. Phys. A: Math. Theor.*, 41:363001, 2008.

[26] H. Effinger and S. Grossmann. Static Structure Function of Turbulent Flow from the Navier-Stokes Equations. *Z. Phys. B*, 66:289–304, 1987.

[27] H. Effinger and S. Grossmann. Prandtl number dependence of turbulent temperature structure functions: A unified theory. *Phys. Fluids A*, 1:1021 – 1026, 1989.

[28] S. Grossmann and D. Lohse. Universality in fully developed turbulence. *Phys. Rev. E*, 50:2784, 1994.

[29] J. Qian. Scaling exponents ofthe second-order structure function of turbulence. *J. Phys. A: Math. Gen.*, 31:3193–3204, 1998.

[30] J. Qian. Normal and anomalous scaling of turbulence. *Physical Review E*, 58(6):7325–7329, 1998.

[31] G.I. Barenblatt and A. J. Chorin. Turbulence: an old challenge and new perspectives. *Meccanica*, 33:445–468, 1998.

[32] L. Mydlarski and Z. Warhaft. On the onset of high-Reynolds-number grid-generated wind tunnel turbulence. *J. Fluid Mech.*, 320:331–368, 1996.

[33] Thomas S. Lundren. Turbulent scaling. *Phys. Fluids*, 20:031301, 2008.

[34] T. Ishihara, T. Gotoh, and Y. Kaneda. Study of high-Reynolds number isotropic turbulence by direct numerical simulation. *Ann. Rev. Fluid Mech.*, 41:165, 2008.

[35] W. David McComb. *Homogeneous, isotropic turbulence: the nature of the problem*. Oxford University Press: in preparation, 2012.

Interfaces in Turbulence and Implications for Advanced Modeling Methods

I. Eames[1], J.C.R. Hunt[1,2,3], M. Braza[4], C.B. da Silva[5], and J. Westerweel[2]

[1] University College London, Torrington Place, London, WC1E 7JE, UK
[2] Delft University of Technology, Mekelweg 2, 2628 CD Delft, The Netherlands
[3] Trinity College, Cambridge
[4] Institut de Mécanique des Fluides de Toulouse-IMFT-UMR CNRS 550, France
[5] IST/Technical University of Lisbon, Avenida Rovisco Pais, 1049-001 Lisbon, Portugal

Abstract

The interfaces that define significant changes in turbulence statistics, vorticity and the concentration of a scalar, at the edges of jets, plumes, vortices and between bodies of fluids with different properties (in the presence of body forces) largely control the gross features of these flows, such as entrainment. New diagnostics tools have been developed within the fluids community to analyse, classify and understand the influence of these interfaces. In turn, this is leading to new modeling strategies that can be applied to describe these processes. This survey brings together broad elements across fluids mechanics to highlight the importance of reduced modeling approaches for interfaces in turbulence.

1 Introduction

Thin, approximately continuous layers, and even thinner interfaces that bound these layers, are a characteristic feature of turbulent flows separating regions of high and low fluctuations of kinetic energy. They also delineate at the same time and place, regions of high and low concentration of other scalar and vector fields. These layers are observed at the edges of boundary layers (see Figure (1)(a,b)), clouds, exhaust jets from vehicles, flames or, at very high Reynolds number, within turbulent flows (see Figure (1)(c)). Interfaces between regions of high and low concentration of a scalar are also often associated with jumps in the mean velocity (measured relative to the interface) as occurs at the edges of chimney plumes. Recent research has shown that these layers are significant dynamically because their internal small scale motions control the mean motion outwards of regions of turbulence-the 'nibbling effect'. They also directly block and distort large scale eddies, a process which can keep the interfaces sharp. But very energetic larger scale motions can break up the interface [1]. In other words these interfaces are not merely passive markers as previously considered.

New methods to measure conditionally sampled velocity fields within and around these interfaces have been achieved in experiments [2, 5, 6] and very high resolution computations at high Reynolds numbers [4]. New theoretical models of the turbulent velocity fields across interfaces [1] and simulations [3, 7], show similar types of layered flows, with similar dynamics and statistics in different types of homogeneous and inhomogeneous turbulent flows.

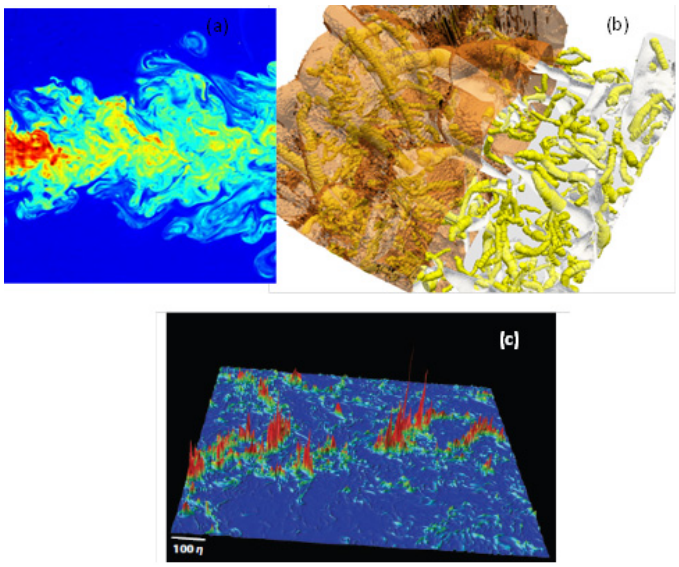

Figure 1: (a) Experimental concentration field in a thin slice through a turbulent jet at $Re \sim 2000$ (from [2]). (b) The vortices near (under) a T/NT interface (from [3]). (c) Thin layers containing high intensity micro-scale vortices in homogeneous turbulence at $Re \sim 1000$ (simulations of Ishihara *et al* [4]).

Interfaces with similar properties of sharp gradients in velocity occur in many other kinds of flows, such as geophysical flows, free surface flows and magnetohydrodynamics [8]. We review the diagnostic tools being applied to analyse these turbulent flow features, understand the physics and the modelling techniques that are able to capture their salient features. This survey is topical and current, following on from a recent Euromech 517 meeting at UCL (June 2010) and a themed volume with the Royal Society on Dynamical Barriers and Interfaces in Turbulent Flows [9].

2 Diagnostic tools

A variety of diagnostic tools have been developed to interrogate data fields derived from experimental and computational studies of turbulence and to analyse the interfaces within such flows. When the fluctuation of the interfaces are small compared to the integral scale, L, the characteristic features can be studied using an Eulerian-Galilean frame of reference. For instance, in the presence

of strong stratification (low Fr), the interfaces exist as step-stratified horizontal layers. When the fluctuations of the interface are not small compared to the integral scale, the flow properties must then be studied using a Lagrangian or conditionally averaged framework. In this new frame of reference the physics is common between different types of turbulent flows and can be used to explain measurements made in the Eulerian frame. Here we introduce some of the diagnostic tools used to analyse interfaces.

2.1 Interface identification and position

Interfaces at $Y(x,t)$ in a two-dimensional flow – occur where there is intense turbulence in the region where $y < Y$. They are usually identified by rapid changes in a scalar quantity or its gradient. For instance, where the magnitude of the mean (or one component) of vorticity is above a threshold value Ω, e.g.

$$Y(x,t) = \{y; |\bar{\omega}(x,Y,t)| > \Omega\} \tag{1}$$

where the average value is defined along the interface and within the thin interface layer. The interface position can be identified as the mean of the points within the interface i.e. $Y_I(x,t) = \bar{Y}(x,t)$, where the average is over the points at fixed x. A measure of the interface lengthscale l_{mx} is defined by $|\bar{\omega}(Y_I < y < Y_I + l_{mx})| < \Omega$. In some cases $max(|\bar{\omega}|)$ occurs near the centre of the layer in which case the interface thickness is $l \sim 2l_{mx}$. At the edges of jets and wakes and in high Re turbulence has a thickness comparable to $LRe^{-1/2}$ [7, 10]. Within the layer there may be intense fluctuations for a scalar concentration field, C, a similar criterion can be applied The RMS fluctuation of the interface position can be defined as

$$\sigma_Y = \sqrt{\overline{(Y - \bar{Y})^2}}. \tag{2}$$

Since the interfaces are thin and difficult to capture experimentally, some authors have used the temperature fluctuation (for heated jets, wakes) or a dye contour as a marker for the edge of the interface [2]. In this case, $Y(x,t) = \{y; C(x,Y,t) < C_m\}$. This definition of the interface position is relatively insensitive to the choice of the threshold values for scalars because generally the jump in concentration tends to be about 10 times the threshold value, as seen in Figure (1)(a).

2.2 Conditional averages based on relative distance

Once the position, in time, of the interface has been identified, the average properties relative to the flow can then be determined. For instance, the conditionally average horizontal velocity in the vicinity of the interface, expressed in terms of a coordinate n outwards from the interface, is

$$\tilde{U}(n) = \frac{1}{T}\int_0^T u(x, Y_I(x,t) + n)\mathrm{d}t, \tag{3}$$

where the average is over time. Similar definitions can be applied, for instance, for the Reynolds stress etc.

2.3 Bulk parameters in relation to the interface

The outward speed of the interface position, E_I,

$$E_I = \left\langle \frac{\mathrm{d}Y_I}{\mathrm{d}t} \right\rangle \tag{4}$$

is determined by the turbulence and mean flow in the shear layer. For some shear flows the interface speed is related to the mean entrainment coefficient through $\alpha = E_I\langle U\rangle$ [11]. For jets or plumes where the volume flux increases, the entrainment velocity E_v is negative (towards the interface). The value of α_I is related to the bulk entrainment coefficient $\alpha_E = E_v|\langle U\rangle|$ which depends on the geometry and nature of the forcing. For instance, normalizing $|E_I|$, $|E_v|$ on $\langle U\rangle$, gives $|\alpha_I| = 2|\alpha_E|$ (axisymmetric jet), $|\alpha_I| = |\alpha_E|$ (two-dimensional jet), for an axisymmetric plume. The reduction in α_I from a jet to a plume caused the momentum flux increasing with distance. For turbulent wakes, the mean velocity is a perturbation on the background velocity $U_\infty (U = U_\infty - \Delta U)$ and the bulk momentum and volume flux are both proportional to $Q = \int_{-\infty}^{\infty} \Delta U dy \sim \Delta U Y_W$, and therefore to E_I. In wakes, E_V is small and not dynamically significant. When these shear flows are perturbed by external forces (eg combustion or by external turbulence) (ie $u_E > \Delta U$) then E_I can be increased and E_V decreased, as the interface breaks up [1].

3 Deriving mean flow profiles

The interface statistics are linked to the gross-characteristics of the ambient flow. For instance, for jets, plumes and wakes, adjacent to the interface, the mean momentum flux across the interface is linked to the conditional mean jump in velocity [2, 5],

$$E_I \Delta U_C \cong \Delta\tau, \tag{5}$$

where $\Delta\tau$ is difference between the Reynolds stress within the vortical region and the negligible stress outside the interface. $\Delta\tau$ can be estimated in terms of the conditional mean flow

$$\Delta\tau_c(n) \cong -\nu_e \frac{\partial\langle U_c\rangle}{\partial n} \qquad (n > 0), \tag{6}$$

where ν_e is the approximately constant eddy viscosity inside the interface. The conditionally averaged vorticity field $\partial\tilde{U}/\partial n$ varies sharply and is similar to a vortex sheet where the vorticity is a delta function, plus a step function. The conditionally averaged velocity is therefore characterized by a jump and a gradient:

$$\tilde{U}(n) \cong H(n)\Delta U + nH(n)\frac{\partial\langle U\rangle}{\partial n}. \tag{7}$$

Considering the convolution of conditionally averaged velocity field with the p.d.f. of the interface (Y_I) position provides a direct link with the mean velocity field near an interface, $U(y)$. For a single interface, the mean Eulerian profile gives a Gaussian fluctuation of the interface (with variance σ_I), is

$$U(y) \cong \frac{1}{2}\Delta U\left\{1 + erf\left(\frac{y - Y_I}{\sigma_I\sqrt{2}}\right)\right\}. \tag{8}$$

This accords with jet experiments by Westerweel *et al.* [2], who note that constant eddy viscosity (in a fixed frame) - as hypothesized by Prandtl [12] - accounts for this kind of profile without any numerical problems near the outer edge .This is the model used in some industries. Thus in general models for σ_I, and the implications for other flow variables, are needed for Eulerian CFD models to account for the effects of the unsteady interface on the mean flow and turbulence [2]. A related problem concerns the role of the turbulent eddies in the dynamics and characteristics of the interface and the nature of the 'nibbling' eddy motions near its surface [3, 5, 7, 13].

4 Implications for advanced modeling techniques

The interface at the edge of a turbulent boundary layer is too thin to be resolved at Reynolds numbers typical of practical engineering problems. One modeling approach is to calculate explicitly the unsteady interface in (continuum) turbulence models and then calculate the turbulence characteristics on either side of it. The second is based on a fresh re-evaluation of the traditional models of flows where interfaces occur.

4.1 Continuum models

Large eddy simulation (LES) models are available to represent flows and eddy motions down to the filter scale Δ (which should be significantly smaller than 1/10 of the integral scale L). Accurate prediction of the detailed turbulent flow characteristics near thin T/NT interfaces raises new challenges for LES. Arguably LES is not a practical method for calculating the flow over an aircraft wing or in geophysical flows where the integral scale of the turbulence is much less than the overall scale of the flow. Consequently, hybrid simulation methods (e.g. detached or organised eddy simulations - OES) are used where the large scale eddy motions are computed explicitly and the small scales are modelled statistically as a Reynolds stress acting on the large scales [14]. A new approach is being developed to represent the high gradients and anisotropic characteristics of turbulence near boundary interfaces and to capture the thin shear layers in high-Reynolds separated turbulent flows. This is necessary for the correct prediction of the unsteady aerodynamic coefficients and especially of the pressure fluctuations in the near, intermediate and far wake regions, in respect of aeroacoustics.

The aim of the present study, still in progress, is to enhance the accuracy of OES, using grid sizes larger than the interface layer thickness l. Stochastic forcing of a series of inhomogeneous large scale random Fourier modes [15], in the region adjacent to the interfaces. This forcing, which is modified by the blocking effect towards the interface, is introduced into the dynamical equations at each iterative step. This keeps the interface thin [10], and modifies the shear stress model. This mechanism overcomes the limitation of standard statistical approaches that are not able to capture inhomogeneous upscale process in turbulence modelling; they simulate downscale energy transfer and eddy diffusion that causes thickening of the interfaces. The process is iterative as the interface position, large scale modes, and Reynolds stress calculations interact with each other.

To illustrate this method, the flow past a flat strut with an incident angle of 10 degrees was considered and the results are shown in Figure (2)(a,b). Two-dimensional OES simulations were performed using a NSMB (Navier-Stokes Multi-Block) code, which consisted of solving a 'phase-averaged' Navier-Stokes equation with a finite-volume implicit formulation. The 2D structured mesh consists in 3×10^5 nodes. The chord Reynolds number is equal to 4×10^6. This unsteady flow separates at leading edge and develops a von Karman street interacting with Kelvin-Helmholtz instability at trailing edge. The capture of these irrotational/rotational interfaces is essential to define correctly the domain where stochastic perturbation must be added and where the shear stress model is changed. The iso-contours of turbulent kinetic energy (Figure (2)(a)) and vorticity (Figure (2)(b)) are shown, where the black line corresponds to the computed interface.

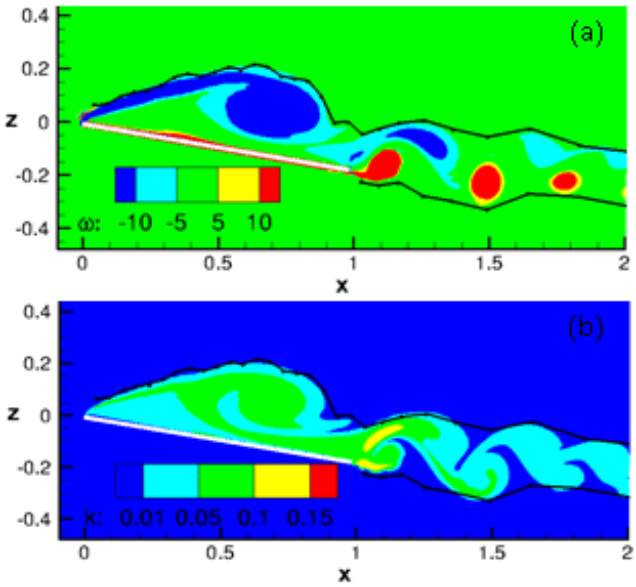

Figure 2: Simulations of OES showing contours of (a) turbulent kinetic energy and (b) vorticity.

4.2 Discrete top hat models

Two types of approximate analytical models, in Eulerian frames, for describing laminar and turbulent jets/plumes/wakes, with some initial scale D, are based on different assumptions about the form of the mean velocity distribution $U(x, y)$ (i) a characteristic profile, e.g. $U(y)/U(y_{REF})$, or (ii) a selfpreserving form as the scale $l(x)$ changes, i.e $U(x/l(x))$. This may also be self-similar as the length scale change, e.g. if $l(x)$ varies as a power law $l(x) \sim ((x - x_0)/D)^p$ where x_0 is the origin position and p is a constant in the flow direction [16].

For turbulent jets / plumes, Morton *et al* [17] and others assumed 'top-hat' profiles defined by the average across the section $\langle U\rangle(x)$ and the radius $l(x)$; the resulting analytical models compared well with experiments. But this model does not account for the significant observed difference between the instantaneous (Figure (3)(a)) and time (or ensemble) averaged profiles (Figure (3)(b)). The time-averaged concentration field of a jet has a nearly Gaussian profile, although the instantaneous view shows a significant variation in the cross-stream concentration field, the conditional average relative to the fluctuating outer interface is rather flat [2]. This is why the interface move outwards largely by 'nibbling' at the interface,

until external turbulence dominates (which is excluded from the MTT model). Self-preserving and self-similar

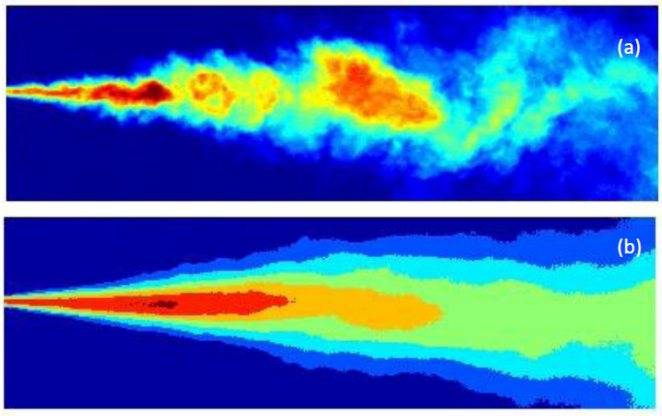

Figure 3: Comparison between experimental measurements of the instantaneous and time average concentration field in a jet (from [18]).

wake/jet solutions become valid at a distance when the form of the initial profile become small-though the influence of the initial large eddy structure is significant along the entire flow [19]. But, for three-dimensional flows, the Reynolds number of a turbulent wake $l\Delta U/v$ decreases with distance, so that the flow eventually becomes laminar (over many hundreds of diameters). Then the wake deficit similarity solution changes and becomes an exact solution of the Navier-Stokes equation. For two and three-dimensional wakes where they are turbulent the self- preserving forms of the deficit profiles $\Delta U(x, y)$ agree with turbulence closure models. In complex bodies (e.g. with porosity) the flow near the body needs to be specified.

It is useful to combine the concept of randomly moving sharp interfaces, developed in Section 3, with the approximation of a top-hat form for the ensemble mean velocity profile within the interface. Take for example the turbulent wake downstream of a cylinder (diameter, D). The conditionally averaged velocity u, in a uniform flow U_∞, is approximately

$$u = U_\infty - \Delta U[H(y - Y_I) - H(y - Y_2)], \qquad (9)$$

where y-coordinates of the fluctuating wake interfaces are at Y_1 and Y_2, and the velocity deficit is ΔU, which also fluctuates. Coupled with the conservation of momentum flux requires the mean drag on the cylinder to be

$$F = \int_{-\infty}^{\infty} \rho u(u - U_\infty)\mathrm{d}y = \rho\langle\Delta U\rangle(U_\infty - \langle\Delta U\rangle)(Y_2 - Y_1). \qquad (10)$$

The self-preserving form of cylinder wakes only begins to occur several diameters downwind when the vorticity from one side of the wake diffuse into the other side [20]. In the near wake the vertical interfaces Y_1, Y_2 meander as a results of the alternate shedding of vortices into the ambient flow. The dominant frequency of the wake interface fluctuations is SU_∞/D (where $S \sim 0.2$). Downwind of the near wake the mean width of the wake is $\langle Y_W\rangle = \langle|Y_1 - Y_2|\rangle$, where

$$\langle Y_W\rangle = \frac{C_D U_\infty^2 D}{2\langle\Delta U\rangle(U_\infty - \langle\Delta U\rangle)}. \qquad (11)$$

The jump in the Reynolds stress at the edge of the interface is given by Eq. (5). For a two-dimensional flow,

$$\overline{u'\nu'} = -|E_I|\Delta U_c \frac{\left\langle y - \frac{1}{2}(Y_1 + Y_2)\right\rangle}{\langle Y_W\rangle} \qquad (12)$$

The solution for $\langle\Delta U\rangle$, $\langle Y_W\rangle$ derived from Eq. (9) and Eq. (11) is self-similar far downstream when $\langle\Delta U\rangle << U_\infty$ (eg $\langle Y_W\rangle \sim (x/D)^{\frac{1}{2}}$). But in the near field, where $\langle Y_W\rangle(x)$ and the mean flow profile $\langle U\rangle(y)$ are determined by the p.d.f. of the wake position, their variations with x are also self-similar ($\sim ((x - x_0)/D)^{\frac{1}{2}}$). But note there is a transition in the 'false' origin of the self-similar solutions between the near and far wake. There is a further transition far downwind if the flow becomes laminar.

Thus Gaussian-like wake profiles which are measured behind rigid bodies in turbulent flows are all self-preserving and have self-similar rates of decay over certain ranges. The profiles result from the combined effects of the fluctuations of the interfaces and the dynamics across the interface, which is mostly small scale, and within the wake. The former is greatest near the body and the latter further downwind. In some flows with high external turbulence the vorticity in the wake is advected randomly like a scalar, and the local wake dynamics are not significant. But if the external turbulence is weak, there may be three ranges of self-similarity: near (self-induced vortex shedding), far (wake dynamics), far-field (dominated by external turbulence). If there is no external turbulence and the wake is three-dimensional, there may be a very farÂŰfield wake flow that is laminar and again self-similar. These differences in the dynamics lead to transitions between self-similar rates of decay, which may have different exponents or false origin positions x_0/D. More complex unsteady Reynolds stress models or simulations are necessary to describe these processes.

5 Conclusions

Where fluid particle displacements are larger than the characteristic distance over which there are large changes in velocity, such as turbulence near external and internal interfaces, or atmospheric eddies disturbing wakes and plumes, the statistical analysis of turbulent flows based wholely on Eulerian-Galilean frames of reference give wrong results. This is why, for example, engineering-based CFD models are not used for many external environmental applications. Conditional analysis based on Lagrangian, randomly moving frames of reference become necessary. But the analysis of the intermediate/smaller scales of motion in this frame can benefit from the standard approximations of Reynolds averaged modeling [2].

Local analysis of the flow near moving interfaces shows that turbulent kinetic energy and mean shear keep the interface sharp. But in a fixed frame, the mean effect of a fluctuating interface produces a smooth profile of the mean flow variables. This explains why a finite value of eddy viscosity exists at the other outer region of the jet, despite the fact that the turbulence varies here. The outward movement of the boundary is determined by small-scale turbulent eddies 'nibbling' at the interface, rather than by engulfing motions of large eddies because these only extend a limited distance, there is very little unmixed external fluid in the interior of the turbulence.

The conclusion from this work is that the time averaged

results can be synthesized from the conditionally averaged metrics, providing additional measures are taken regarding the statistics of the interface position and the physics of the flow near the interface. In this paper we have highlighted some of the new advanced modelling techniques which are coming into the place to understand, analyse and predict their movement.

References

[1] J. C. R. Hunt, I. Eames, and J. Westerweel. Mechanics of inhomogeneous turbulence and interfacial layers. *Journal of Fluid Mechanics*, 554:499–523, 2006.

[2] J. Westerweel, C. Fukushima, J.M. Pedersen, and J.C.R. Hunt. Momentum and scalar transport at the turbulent/non-turbulent interface of a jet. *Journal of Fluid Mechanics*, 631:199–230, 2009.

[3] C.B. da Silva and R.J.N. dos Reis. The role of coherent vortices near the turbulent/non-turbulent interface in a planar jet. *Philosophical Transactions of the Royal Society A*, 369:738–753, 2011.

[4] T. Ishihara, T. Gotoh, and Y. Kaneda. Study of high reynolds number isotropic turbulence by direct numerical simulation. *Annual Review of Fluid Mechanics*, 41:165, 2009.

[5] J. Westerweel, C. Fukushima, J.M. Pedersen, and J.C.R. Hunt. Mechanics of the turbulent/nonturbulent interface of a jet. *Physical Review Letters*, 95:174501, 2005.

[6] N. A. Worth and T. B. Nickels. Some characteristics of thin shear layers in homogeneous turbulent flow. *Philosophical Transactions of the Royal Society A*, 369:709–722, 2011.

[7] C.B. da Silva and R. Taveira. The thickness of the t/nt interface is equal to the radius of the large vorticity structures near the edge of the shear layer. *Physics of Fluids*, 22:121702, 2010.

[8] M. Davey and J.C.R. Hunt. The importance of thin models -a workshop on critical regions in geophysical flows. *Mathematics Today*, pages 53–57, 2007.

[9] I. Eames and J.B. Flor. New developments in understanding interfacial processes in turbulent flows. *Philosophical Transactions of the Royal Society A*, 369:702–705, 2011.

[10] J.C.R. Hunt, I. Eames, J. Westerweel, P. A. Davidson, S. Voropayev, J. Fernando, and M. Braza. Thin shear layers the key to turbulence structure? In *IAHR-APD*, 2010.

[11] J.C.R. Hunt, D.D. Stretch, and R.E. Britter. Length scales in stably stratified turbulent flows and their use in turbulence models. In *Proc. I.M.A. Conf. on Stably Stratified Flow and Dense Gas Dispersion (Ed. J.S. Puttock), Clarendon Press*, 1988.

[12] L. Prandtl. *Essentials of fluid dynamics*. New York, 1952.

[13] J. C. R. Hunt, I. Eames, and J. Westerweel. Vortical interactions with interfacial shear layers. In *IUTAM Conference on Computational Physics and New Perspectives in Turbulence*, 2008.

[14] R. Bourguet, M. Braza, G. Harran, and R. El Akoury. Anisotropic organised eddy simulation for the prediction of non-equilibrium turbulent flows around bodies. *Journal of Fluids and Structures*, 24:1240–1251, 2008.

[15] C. Turfus and J.C.R. Hunt. A stochastic analysis of the displacements of fluid elements in inhomogeneous turbulence using kraichnanâĂŹs method of random modes. In *Proceedings of the First European Turbulence Conference, Ecully, France*, 1987.

[16] A.A. Townsend. *The structure of turbulent shear flow*. Cambridge University Press, 1976.

[17] B.R. Morton, G.I. Taylor, and J.S. Turner. Turbulent gravitational convection from maintained and instantaneous sources. *Proceedings of the Royal Society A*, 234:1–23, 1956.

[18] H. Ulpre, I. Eames, J. Eames, and A Greig. Acidic jets/plumes injected into an alkaline environment. *Journal of Fluid Mechanics*, 2011.

[19] P.M. Bevilaqua and P.S. Lykoudis. Turbulence memory in self-preserving wakes. *Journal of Fluid Mechanics*, 89:589606, 1978.

[20] J.C.R. Hunt and I. Eames. The disappearance of viscous and laminar wakes in complex flows. *Journal of Fluid Mechanics*, 457:111–132, 2002.

Advances in Structure-based Modelling

Stavros C. Kassinos[1], Hari Radhakrishnan[1]

[1] Computational Science Laboratory, University of Cyprus, Cyprus.

Email:kassinos@ucy.ac.cy

Abstract

Introduced in the mid-1990's, Structure-Based turbulence Models (SBMs) provide today one of the few promising routes for improved turbulence closures. In this paper, we provide a brief historical account of the approach, the main types of SBMs, and focus in greater technical detail on the Algebraic Structure-based Model (ASBM). We then study an example application of the ASBM, and finally conclude with a discussion of the future directions for structure-based modeling.

1 Introduction

In a paper dealing with rapidly rotated flows, Reynolds [1] was the first to recognize that traditional RANS approaches suffer from a fundamental limitation. The limitation stems from the fact that traditional turbulence models, not just eddy-viscosity type models but also algebraic and differential models, contain information about the componentality of the turbulence, but not about its structure dimensionality [1, 2]. This limits the performance of these models in complex non-equilibrium flows, where the fluid can locally be exposed to strong mean deformation or rotation. Here, "structure dimensionality" refers to the morphology of the dynamically important energy-containing structures in the turbulence field. Large-scale energy-containing eddies tend to organize spatially the fluctuating motion in their vicinity. In doing so, they eliminate gradients of fluctuation fields in some directions (those in which the spatial extent of the structure is significant) and enhance gradients in other directions (those in which the extent of the structure is small). Thus, associated with each eddy are local axes of dependence and independence that determine the dimensionality of the local turbulence. In the case of vector fluctuation fields, e.g. the turbulent velocity, dimensionality determines the spatial variation of the fluctuations, but not the orientation of the fluctuating vector in space, which is the componentality information contained in the turbulent stresses. In equilibrium flows, the principal axes of the turbulent stresses can be assumed to roughly track those of the local mean stain rate tensor. Therefore, the turbulent stress anisotropy can be approximated without reference to the dimensionality of the underlying turbulence structure. However, in non-equilibrium flows (strong rotation, separation and reattachment, etc.), the dimensionality of the turbulence structure dictates how the turbulence will respond to external deformation, and the turbulence exhibits a viscoelastic-like response. The alignment of the principal axes of the turbulent stresses, i.e. the componentality of the turbulence, is to a large extent determined by the dimensionality of the local turbulent structure, i.e. by the morphology of the local turbulence eddies. This realization led to the development of the structure-based approach to turbulence modeling. In Kassinos and Reynolds [2–4] this approach was placed on a rigorous mathematical foundation.

The initial development of the Structure-Based approach was carried out at Stanford University. In the late 1990's, a Structure-Based Model [3, 5, 6] was developed and shown to perform better than standard Reynolds Stress Transport (RST) models in many complex flows, such as flows with strong mean or frame rotation. In Structure-Based Models (SBM), the Reynolds stress tensor is expressed as a function of the one-point turbulence structure tensors that sensitize the model not only to the anisotropy of the turbulence componentality, but also to structural anisotropy [2, 3]. Kassinos and Reynolds [3, 4] constructed a differential structure-based model (SBM) that made use of the model transport equation for the eddy axis. By introducing hypothetical turbulence eddies with carefully selected properties, and by averaging over an ensemble of such eddies, they were able to relate the eddy-axis transport equation to the exact transport equations of the structure tensors. A schematic representation of the eddy-axis and structure tensors associated with an idealized "eddy" field is shown in Fig. 1. Later [6, 7], a differential structure-based model making direct use of the exact transport equations of the structure tensors was also proposed and successfully applied to a number of basic benchmark flows.

Closely related to one-point structure-based models is the Particle Representation Model (PRM) and the Interactive Particle Representation Model (IPRM). The PRM is essentially a reduced Fourier representation retaining the minimum information beyond one-point that allows an exact closure of the Rapid Distortion Theory (RDT) governing equations without using a model. Form a different point of view, the PRM formalism can be thought of as a real space Monte Carlo type of approach, and this duality offers a valuable framework for developing one-point structure-based closures. The IPRM, or Interactive Particle Representation Model, is an extension of the PRM method for flows with weak deformation rates. The IPRM has been successfully applied to all standard benchmark cases for homogeneous turbulence. What makes the IPRM particularly interesting is the concept of *Effective Gradients*. In the IPRM, it is postulated that the nonlinear turbulence-turbulence interactions can be represented by an effective deformation rate, which acts on each eddy or particle in addition to the mean gradients as a result of the deformation caused by the sea of all other eddies (particles). What is impressive is that the IPRM transport equations retain the same form as the RDT (PRM) equations, with just the mean velocity gradient tensor replaced by the sum of the mean and effective gradient tensors. The effective gradient tensors are modeled in terms of the one-point structure tensors

thus providing the route for closure even at the one-point level.

Although the performance of the original SBM was considered quite satisfactory [3, 5–7], it was computationally expensive. For this reason, it was deemed necessary to simplify the approach into an algebraic two-equation model for engineering use. An effort was initiated in 2001, again at Stanford University, to develop a simplified two-equation algebraic structure-based model (ASBM). In the ASBM, the eddy axis concept [3] is used again, but in an algebraic formulation relating it to the mean deformation field and the scales of the turbulence without a transport equation for the structure. Also, in ASBM the eddy axis concept has been improved by allowing for flattening of the turbulence eddies in the presence of mean rotation or shear [8–10].

With the passing of Prof. Reynolds in 2003, and the relocation of the first author to the University of Cyprus, the ASBM development effort was transferred to Europe [11–16]. The development of the ASBM was supported by a several European grants, while a close collaboration has been maintained between the University of Cyprus, ONERA, other European collaborators and the Center of Turbulence Research at Stanford-NASA/Ames. One of the key conclusions of a large-scale European project (WALLTURB) was that the ASBM is one of a very few new advanced turbulence models that have the potential to lead to significant improvements in the performance of CFD codes used in aerospace design [16].

In a series of recent studies [14, 16–18], the ASBM has been shown to offer promising performance in flows with system rotation (e.g. rotated channel flow), separation (e.g. backward facing step, atmospheric flow over complex terrain), adverse pressure gradients (e.g. asymmetric diffuser flow), and shock-induced flow separation over the RAE2822 transonic airfoil [19]. In these flows, the ASBM captures correctly the characteristics of the separated region and reattachment, including the components of the Reynolds stress tensor.

2 Algebraic Structure Based Model

In a RANS model, the flow is governed by the following equations:

$$\frac{\partial U_i}{\partial t} + U_j \frac{\partial U_i}{\partial x_j} = -\frac{1}{\rho}\frac{\partial p}{\partial x_i} + \frac{\partial}{\partial x_j}\left(\nu \frac{\partial U_i}{\partial x_j}\right) - \frac{\partial \left\langle u_i' u_j' \right\rangle}{\partial x_j} \tag{1}$$

$$\frac{\partial U_i}{\partial x_i} = 0, \tag{2}$$

where U_i is the i$^{\text{th}}$ component of the mean velocity field, and the $\left\langle u_i' u_j' \right\rangle$ are the components of the Reynolds stress tensor. In most RANS models, the Reynolds stress tensor components are derived from gradients of the mean velocity field using the eddy-viscosity concept. In the ASBM, they are calculated from the statistics of a hypothetical eddy field.

2.1 Structure Tensors

The turbulence structure tensors, as defined in [3] and [2], are the Reynolds stresses, R_{ij}, the dimensionality, D_{ij}, and the circulicity, F_{ij}. D_{ij} and F_{ij} contain information about the large-scale, energy-bearing structures that is not conveyed by the componentality information in R_{ij}.

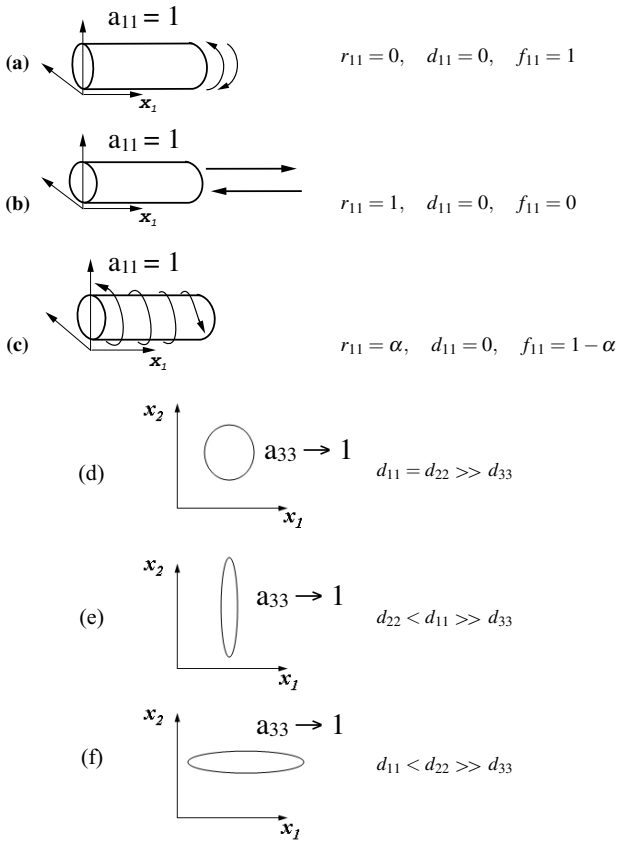

Figure 1: Idealized "eddy" fields and the associated eddy-axis and structure tensors. In (a)-(c) the field is assumed to consist of axisymmetric eddies aligned with the x_1-axis and in (d)-(e) the field consists of flattened eddies aligned with the x_3-axis. Case (a) corresponds to a vortical eddy, (b) to a jetal eddy and (c) to a helical eddy.

In the case of homogeneous turbulence, the contractions of the structure tensors are all twice the turbulent kinetic energy, i.e. $R_{ii} = D_{ii} = F_{ii} = q^2 = 2k$. Thus, one can define normalized structure tensors as

$$r_{ij} \equiv R_{ij}/q^2, \quad d_{ij} \equiv D_{ij}/q^2, \quad f_{ij} \equiv F_{ij}/q^2\,. \tag{3}$$

The constitutive relation

$$r_{ij} + d_{ij} + f_{ij} = \delta_{ij} \tag{4}$$

shows that in homogeneous turbulence only two are linearly independent.

2.2 Linking the Stresses to the Structure

The eddy-axis concept [3] is used to relate the Reynolds stress and structure tensors to parameters of a hypothetical turbulent eddy field. Each eddy represents a two-dimensional turbulence field, and is characterized by a unit eddy-axis vector a_i. The turbulent motion associated with the eddy can be decomposed into a jetal component along the eddy axis, and a vortical component perpendicular to the eddy axis (see Fig. 1). Averaging over an ensemble of such eddies allows one to relate

the normalized Reynolds stresses, r_{ij}, and the one-point turbulence structure tensors to the statistics of the eddy ensemble,

$$r_{ij} = \frac{\overline{u_i' u_j'}}{2k} = (1-\phi)\frac{1}{2}(\delta_{ij} - a_{ij}) + \phi a_{ij} + (1-\phi)\chi[\frac{1}{2}(1 - a_{nm}b_{mn})\delta_{ij} - \frac{1}{2}(1 + a_{nm}b_{mn})a_{ij} - b_{ij} + a_{in}b_{nj} + a_{jn}b_{ni}] - \frac{\gamma\Omega_k^T}{\Omega^T}(\epsilon_{ipr}a_{pj} + \epsilon_{jpr}a_{pi}) \{\frac{1}{2}[1 - \chi(1 - a + nmb_{mn})]\delta_{kr} + \chi b_{kr} - \chi a_{kn}b_{nr}\}, \quad (5)$$

$$d_{ij} = \frac{1}{2}(\delta_{ij} - a_{ij}) + \chi[-\frac{1}{2}(1 - a_{nm}b_{mn})\delta_{ij} + \frac{1}{2}(1 + a_{nm}b_{mn})a_{ij} + b_{ij} - (a_{in}b_{nj} + a_{jn}b_{ni})], \quad (6)$$

$$f_{ij} = \delta_{ij} - r_{ij} - d_{ij}, \quad (7)$$

where the eddy-axis tensor, $a_{ij} = \langle V^2 a_i a_j\rangle / \langle V^2\rangle$, represents the *energy-weighted* average direction cosine of the eddy-axis vector. ϕ and χ are scalar parameters that determine the allocation of energy between the jetal and vortical modes and the flattening of the eddy cross sections respectively. The helical parameter, γ , is representative of the correlation between the jetal and the vortical modes. Under irrotational RDT $\gamma = 0$, but it becomes energized under the influence of rotation or weak deformation. Similarly, rotation can "flatten" the eddies, so that their cross section becomes non-axisymmetric. The flattening tensor is

$$b_{ij} = \frac{(\Omega_i + C_b\Omega_i^f)(\Omega_j + C_b\Omega_j^f)}{(\Omega_k + C_b\Omega_k^f)(\Omega_k + C_b\Omega_k^f)}, C_b = -1.0, \quad (8)$$

where Ω_i is the mean rotation vector, and Ω_i^f is the frame rotation rate vector. A point of departure from the original SBM approach is that we avoid the direct use of the eddy-axis transport equation [3] for the sake of computational efficiency. Instead, in the ASBM we use an algebraic formulation (which is nevertheless based on the transport equation), to obtain the eddy-axis tensor. Thus, the homogeneous eddy-axis tensor is obtained by applying a rotation transformation to the strained eddy-axis tensor a_{ij}^*

$$a_{ij} = H_{ik}H_{jl}a_{kl}^*, H_{ij} = \delta_{ij} + h_i\frac{\Omega_{ij}}{\sqrt{\Omega_{pp}^2}} + h_2\frac{\Omega_{ik}\Omega_{kj}}{\Omega_{pp}^2} \quad (9)$$

where $\Omega_{pp}^2 = \Omega_{pq}\Omega_{pq}$, and Ω_{pq} is the mean rotation rate tensor. The orthonormality conditions $H_{ki}H_{kj} = \delta_{ij}$ require

$$h_1 = \sqrt{2h_2 - h_2^2/2}. \quad (10)$$

h_2 is obtained through RDT for combined homogeneous plane strain and rotation [8, 20],

$$h_2 = \begin{cases} 2 - 2\sqrt{\frac{1}{2}(1+\sqrt{1-r})} & \text{if } r \le 1 \\ 2 - 2\sqrt{\frac{1}{2}(1-\sqrt{1-1/r})} & \text{if } r \ge 1 \end{cases}, \quad (11)$$

where $r = (a_{pq}\Omega_{qr}S_{rp}^*)/(S_{kn}^*S_{nm}^*a_{mk})$. The strained a_{ij}^* is given by

$$a_{ij}^* = \frac{1}{3}\delta_{ij} + \frac{(S_{ik}^*a_{kj}^* + S_{jk}^*a_{ki}^* - \frac{2}{3}S_{mn}^*a_{nm}^*\delta_{ij})\tau}{a_0 + 2\sqrt{a_1^2 + \tau^2 S_{kp}^*S_{kq}^*a_{pq}^*}} \quad (12)$$

where $S_{ij}^* = S_{ij} - S_{kk}\delta_{ij}/3$ is the traceless strain-rate tensor with $S_{ij} = \frac{1}{2}(\partial u_i/\partial x_j + \partial u_j/\partial x_i)$, τ is a time scale of the turbulence, and a_0 is a "slow" constant, chosen here to be 1.6. This choice gives realizable states for the eddy-axis tensor.

2.3 Wall Blocking

Near the wall, as the flow approaches the no-slip boundary condition, the flow velocity becomes zero by the action of viscous forces. The wall normal component of the velocity falls faster than the tangential components because of wall blocking which acts at scales larger than the viscous scales. This makes the velocities near the wall lie in planes parallel to the wall. In the ASBM, the eddies close to the wall are postulated to also be parallel to the wall. This is achieved by introducing a blockage tensor B_{ij} which reorients the eddies to be parallel to the wall by defining a wall blocking tensor whose components are given by

$$B_{ij} = \frac{\phi_{,i}\phi_{,j}}{\phi_{,k}\phi_{,k}}\phi \quad \text{if} \quad \phi_{,k}\phi_{,k} > 0 \quad (13)$$

where ϕ is the solution of the modified Helmholtz equation:

$$L^2\frac{\partial^2\phi}{\partial x_k \partial x_k} = \phi \quad (14)$$

$L = C_L\max\left(\frac{k^{3/2}}{\epsilon}, C_\nu\sqrt[4]{\frac{\nu^3}{\epsilon}}\right)$ and $\phi_{,i} \equiv \partial\phi/\partial x_i$. In this work, C_L was chosen to be 0.17 and C_ν was chosen to be 80. At solid walls, $\phi = 1$, and its derivative along the wall-normal direction $\phi_{,n} = 0$ where x_n is the wall-normal direction.

3 Example Application

The ASBM was coupled with a Navier-Stokes solver based on the unstructured-grid finite-volume method. The solver was used to compute flow over a backward-facing step.

The incompressible RANS equations are solved using an implicit predictor-corrector method. The computations are initialized using a converged v^2–f solution. The steady-state solutions using the ASBM are then obtained by time-marching the solver till convergence is achieved. A deferred correction approach was used for the ASBM to ensure stability. Computational results were compared with previously reported experimental results [21], DNS results [22] and results from the v^2–f [23] and k-ω SST [24] models implemented in the same solver.

3.1 Computational Domain

The computational domain for the backward-facing step consists of an inlet section of length $3h$ and height $5h$ prior to the sudden expansion, where h is the step height. After the expansion, the computational domain has an

outlet section of length $40h$ and height $6h$. The effective expansion ratio is 1.20. The computational domain has a width of $0.5h$ in the spanwise direction, but the present computations are formally two-dimensional because only one grid cell was used in the spanwise direction. In the streamwise direction, the grid consists of 150 cells in total with a compressed grid spacing in the vicinity of the step. There are 118 cells along the vertical direction of which 68 are placed within the step ($y < h$). The grid was compressed along the vertical direction at the step and towards the lower wall to ensure $y+ < 1.0$.

3.2 Boundary Conditions

A profile obtained from a v^2–f solution for a fully developed channel flow was applied at the inlet of each computational domain. The values of the flow velocity, and the turbulence scalars, k, ϵ, and v^2, were read from an input file as a function of inlet height, and the flux of f and ϕ were taken to be zero at the inlet. A penalty boundary condition was applied at the outlet to ensure global mass conservation within the computational domain. For the backward facing step, the step-height Reynolds number $Re_h \equiv U_0 h/\nu \approx 5000$, where U_0 is the mean inlet velocity, h is the step height, and ν is the viscosity.

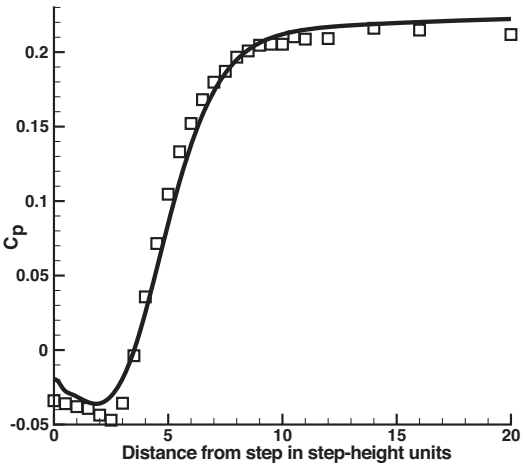

Figure 2: Wall static pressure coefficient along the bottom wall: ASBM (—) vs. experiments of [21].

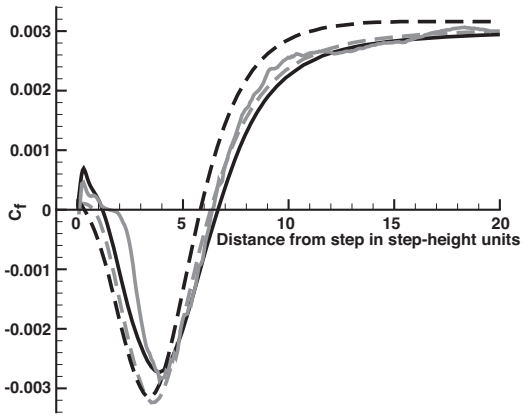

Figure 3: Skin-friction coefficient on the bottom wall: DNS (solid gray line), ASBM (solid black line), v^2–f (dashed gray line), & k-ω SST (dashed black line)

4 Results and Discussion

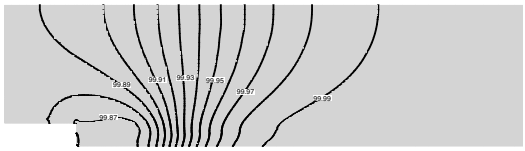

(a) k-ω SST model

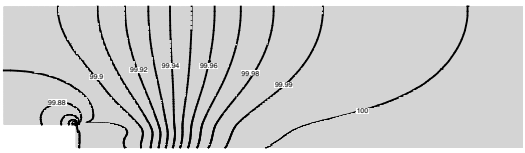

(b) v^2–f model

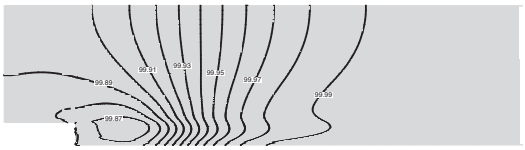

(c) ASBM

Figure 4: Mean pressure in the channel predicted by the different RANS models. Only the ASBM results show the same profile as the DNS results of [22].

Figure (4) shows the pressure contours within the channel as calculated by the k–ω shear-stress transport (SST) model [24], the v^2–f model [23], and the ASBM model. Negative values of the pressure just before the expansion indicate the presence of a favourable pressure gradient.

Figure (5) shows recirculation regions predicted by the k–ω SST model, v^2–f model, and the ASBM model. Only the ASBM model is able to correctly predict the size of the secondary recirculation bubble at the foot of the step. Figure (2) shows the wall static-pressure coefficient $C_p \equiv (p - p_0)/\frac{1}{2}\rho U_0^2$ along the bottom wall predicted by the ASBM and the experimental results of [21]. The ASBM results show good agreement with the experimental values over the entire distance. Figure (3) shows the skin friction coefficient $C_f \equiv \tau_w/\frac{1}{2}\rho U_0^2$ along the bottom wall where τ_w is the shear stress measured at the wall. Predictions from the three different RANS models are plotted with the DNS results of [22]. Only the ASBM is able to predict the rise in the skin friction due to the secondary bubble also seen in the DNS results. Past the recirculation region, both the ASBM and the v^2–f model show good agreement with the DNS results. The reattachment length predicted by DNS is $X_r = 6.39$ in step-height units. The v^2–f model's prediction of $X_r = 6.31$ is the closest to the DNS results compared to the ASBM ($X_r = 6.66$) and the k-ω SST ($X_r = 5.82$) results.

Figure (6) compares the ASBM computational results with the experimental results of [21] for streamwise velocity (Figure (6)(a)) and the Reynolds stresses $\langle u'u' \rangle$, $\langle u'v' \rangle$, and $\langle v'v' \rangle$ (Figure (6)(b) – (d)) at different stations along the flow direction. The ASBM results for the velocity correspond very well with the experimental values. The ASBM is also predicts the initial rise and subsequent fall in the turbulent stresses as seen experimentally.

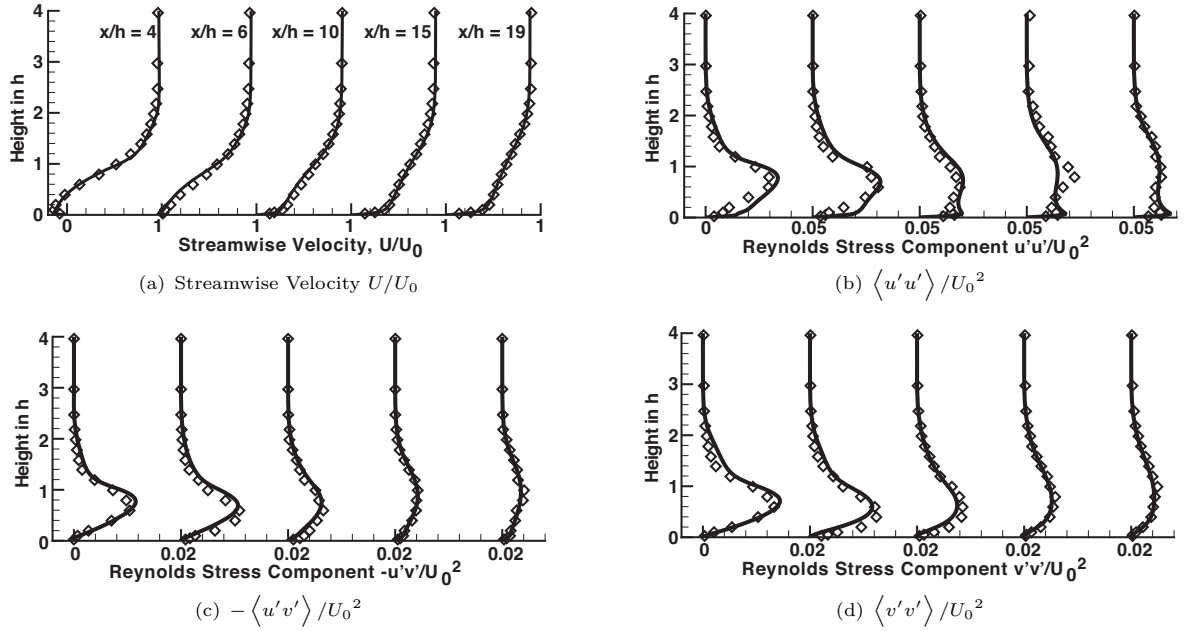

(a) Streamwise Velocity U/U_0

(b) $\left\langle u'u' \right\rangle / {U_0}^2$

(c) $-\left\langle u'v' \right\rangle / {U_0}^2$

(d) $\left\langle v'v' \right\rangle / {U_0}^2$

Figure 6: ASBM predictions(—) vs. the experiments of [21] for flow over a backward-facing step.

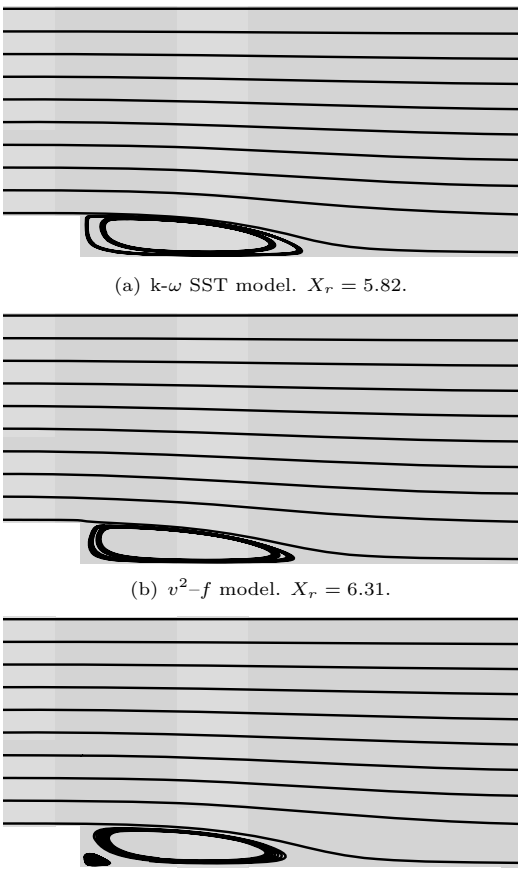

(a) k-ω SST model. $X_r = 5.82$.

(b) v^2–f model. $X_r = 6.31$.

(c) ASBM. $X_r = 6.66$.

Figure 5: Isopleths of the mean stream function φ. Only the ASBM model predicts the presence of the secondary recirculation bubble.

5 Current Developments and Future Directions

Recently, the structure dimensionality concept has been extended for dispersed phase through the introduction of the Dispersed Phase Structure Dimensionality (DPSD) tensor,

$$D^{\theta}_{ij} =< \Phi_{z,i}\Phi_{z,j} > , \tag{15}$$

where,

$$\nabla^2 \mathbf{\Phi} \ = \nabla\theta', \tag{16}$$

and θ' is the turbulent fluctuation of the dispersed scalar. In a series of studies it has been shown that the Dispersed Phase Structure Dimensionality (DPSD) tensor accurately describes the large-scale structures in a turbulent dispersed phase. An example is shown in Figure (7) for the case of irrotational axisymmetric expansion where the mean velocity gradient is given by $S_{22} = S_{33} = -S_{11}/2 = S$. The initial turbulence field is isotropic with zero scalar fluctuations and a uniform mean scalar gradient $d\Theta/dx_2 = \Gamma$. The DPSD tensor shows that at large total strain ($C \approx 10$), the scalar fluctuation field is organized in pancake like structures that are thin in the axial direction ($d^{\theta}_{11} \rightarrow 1$) and long in the lateral directions ($d^{\theta}_{22} \approx^{\theta}_{33} \rightarrow 0$). An effort is currently under development at the University of Cyprus to use these ideas for the construction of an ASBM that will include such effects, with the aim of using the extended model in heat transfer and dispersion modeling.

The University of Cyprus is collaborating with various groups around the world that are interested in the further development of the structure-based approach. In collaboration with ONERA it was shown that the ASBM can be coupled with the k-ω scale equations of the widespread BSL model in the process proving a much more complete description of the turbulence. The coupling requires minimal modifications to the standard BSL scale equations, thus providing an easy route to incorporating the ASBM technology in current engineering codes. In collaboration with the Center for Turbulence Research (CTR), it was similarly shown that the ASBM structure module can be successfully coupled with the v^2-f scale equations. While hybrid versions of the model are not the end objective, they might provide an easy implementation path for engineers wishing to quickly test the basic model performance before investing the time to implement the full ASBM description.

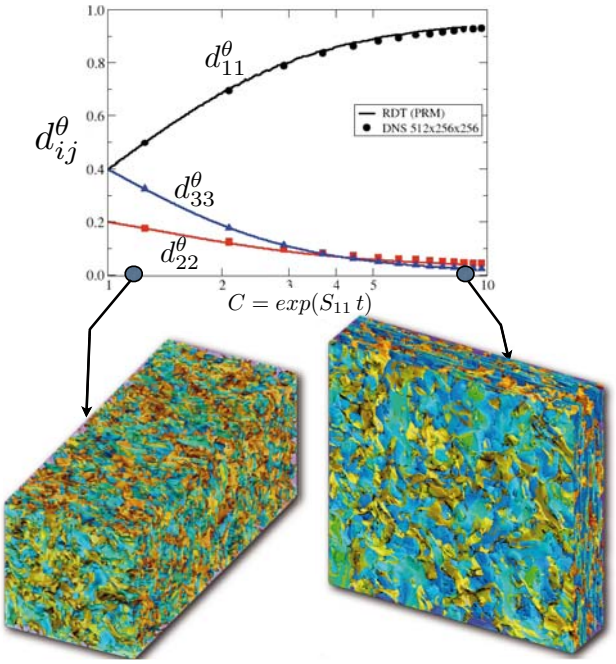

Figure 7: The DPSD for passive scalar fluctuations in rapid (RDT) irrotational axisymmetric expansion and the corresponding magnitude iso-contours. Lines represent exact RDT predictions via the PRM and symbols results from 512x256x256 DNS.

Recently, the model has been tested with excellent results in benchmark cases for flow over complex terrain [18]. Furthermore, the group in New Zealand has successfully coupled the ASBM with wall-functions and computed very high Reynolds number atmospheric flows.

Clearly, there is still more testing that has to be done, in strongly three-dimensional and unsteady aerodynamic flows in particular, but the outlook is promising. Computational efficiency and stability are also being continuously improved as the model is tested in increasingly more demanding flows.

References

[1] Reynolds, W. C. 1989 Effects of rotation on homogeneous turbulence, in *Proceedings of the 10th Australasian Fluid Mechanics Conference*, University of Melbourne: Melbourne, Australia.

[2] Kassinos, S. C., Reynolds, W. C. & Rogers, M. M. 2001 One-point turbulence structure tensors. *J. Fluid Mech.* **428**, 213–248.

[3] Kassinos, S. C. & Reynolds, W. C. 1994 A structure-based model for the rapid distortion of homogeneous turbulence. *Tech. Rep.* TF-61. Mechanical Engineering Department, Stanford University.

[4] Reynolds, W. C. & Kassinos, S. C. 1995 One-point modelling of rapidly deformed homogeneous turbulence. *Proceedings of the Royal Society: Mathematical and Physical Sciences (1990-1995)*, **451** (1941), 87–104.

[5] Kassinos, S. C. & Reynolds, W. C. 1998 A structure-based model with stropholysis effects. *Annual Research Briefs 1998*, Center for Turbulence, Stanford/NASA Ames.

[6] Kassinos, S. C., Langer, C. A., Haire, S. L. & Reynolds, W. C. 2000 Structure-based turbulence modeling for wall-bounded flows. *International Journal of Heat and Fluid Flow* **21**, 599–605.

[7] Poroseva, S. V., Kassinos, S. C., Langer, C. A. & Reynolds, W. C. 2002 Structure-based turbulence model: Application to a rotating pipe flow. *Physics of Fluids* **14** (4), 1523–1532.

[8] Langer, C. A. & Reynolds, W. C. 2003 An algebraic structure-based turbulence model for rotating wall-bounded flows, *Technical Report* TF-85, Mechanical Engineering Department, Stanford University.

[9] Haire, S. L. & Reynolds, W. C. 2003 Toward an affordable two-equation structure-based turbulence model. *Technical Report* TF-84. Mechanical Engineering Department, Stanford University.

[10] Reynolds, W. C.,Langer, C. A. & Kassinos, S. C., 2002 Structure and scales in turbulence modeling. *Physics of Fluids*, **14(7)**, 2485–2492.

[11] Langer, C. A., Kassinos, S. C., & Haire, S. 2005 Application of a new structure- based model to rotating flows, in *Proceedings of the 6th Int. ERCOFTAC Symp. on Eng. Turb. Modelling and Measurements (ETMM6)*, Sardinia, Italy.

[12] Kassinos, S. C. & Langer C. A. 2005 A new algebraic structure-based model with proper handling of strong rotation, in *Proceedings of the 5th GRACM Int. Congress on Computational Mechanics*, Limassol, Cyprus.

[13] Kassinos, S. C., Langer, C. A., Kalitzin, G. & Iaccarino, G. 2006 A simplified structure-based model using standard turbulence scale equations: computation of rotating wall-bounded flows. *International Journal of Heat and Fluid Flow* **27** (4), 653–660.

[14] Radhakrishnan, H., Pecnik, R., Iaccarino, G., & Kassinos, S. C. 2008 Computation of separated turbulent flows using the ASBM model, in *Proceedings of the 2008 Center for Turbulence Research Summer Program*, 365–376.

[15] Aupoix, B., Kassinos, S. C. & Langer, C. A. 2009 ASBM-BSL: An easy access to the structure based model technology. in *Proceedings of 6th International Symposium on Turbulence and Shear Flow Phenomena* Seoul, South Korea.

[16] Benton, J. J. 2010 Evaluation of v2-f and ASBM turbulence models for transonic aerofoil RAE2822, in *Progress in Wall Turbulence: Understanding and Modeling*, ERCOFTAC Series Vol. 14, Stanislas, M.; Jimenez, Javier; Marusic, Ivan (Eds.)

[17] Radhakrishnan, H., Pecnik, R., Iaccarino, G., & Kassinos, S. C. 2008 Computation of turbulent flow for some benchmark cases using the ASBM RANS model, in *Proceedings of the 8th International ERCOFTAC Symposium on Engineering Turbulence Modeling and Measurements (ETMM8)*, Marseille, France.

[18] O'Sullivan, J. P., Pecnik, R., & Iaccarino, G. 2008 Investigating turbulence in wind flow over complex terrain, in *Proceedings of the 2010 Center for Turbulence Research Summer Program*, 129–139.

[19] Cook, P. H., McDonald, M. A., & Firmin, M. C. P. 1979 Aerofoil RAE 2822 - Pressure Distributions, and Boundary Layer and Wake Measurements, in *Experimental Data Base for Computer Program Assessment*, AGARD Report AR-138.

[20] Kassinos, S. C., Akylas, E. & Langer, C. A. 2007 Rapidly sheared homogeneous stratified turbulence in a rotating frame. *Physics of Fluids* **19**, 02170, DOI: 10.1063/1.2710291.

[21] Jovic, S. & Driver, D. M. 1994 Backward-facing step measurements at low Reynolds number, $Re_h =$ 5000. *NASA Technical Memorandum* 108807.

[22] Le, H., Moin, P. & Kim, J. 1997 Direct numerical simulation of turbulent flow over a backward-facing step. *J. Fluid Mech.* **330**, 349–374.

[23] Durbin, P. A. 1995 Separated flow computations with the k-ϵ-v^2 model. *AIAA Journal* **33** (4).

[24] Menter, F. R. 1992 Improved two-equation k–ω turbulence models for aerodynamic flows. *NASA Technical Memorandum* 103975.

Modelling Approach to Velocity and Scalar Gradients and Increments

Aurore Naso[1], Alain Pumir[2], Claude Cambon[1], Fabien Godeferd[1]

[1] Laboratoire de Mécanique des Fluides et d'Acoustique, UMR 5509,

Ecole Centrale de Lyon, 69134 Ecully Cedex, France.

[2] Laboratoire de Physique, Ecole Normale Supérieure de Lyon and CNRS (UMR 5672),

46, allée d'Italie, 69364 Lyon Cedex 07, France.

1 Introduction

A wide number of studies in fluid turbulence can be related either to the modelling of engineering and environmental flows ("turbulent fluid mechanics") or to specialists of intermittency and scaling (say "physics for intermittency"). The overlapping is small, except when looking at interscale energy transfer applicable to sub-grid scale modelling in LES. Can SIG 35 try to reconcile these almost disconnected approaches?

A very interesting starting point is to model the transport of velocity gradients. In particular, modeling the **coarse-grained** velocity gradient tensor is very useful in LES. The subject has attracted some theoretical and numerical attention lately, as shown in the recent review [1]. These developments, such as those by Chertkov *et al.* 1999 [2], can now even be tested in the laboratory [3].

2 Modeling the velocity gradient tensor dynamics in turbulence

2.1 Transport equation

Our starting point is the transport equation for the (fluctuating) velocity gradient tensor

$$A_{ij} = \frac{\partial u_i}{\partial x_j}. \tag{1}$$

A generic transport equation, describing the time evolution of $\mathbf{A}$ following fluid particles, can be derived by taking the gradient of the Navier-Stokes equation. For an incompressible flow, this equation can be written as

$$\begin{aligned} \frac{dA_{ij}}{dt} = & - \left(A_{ik}A_{kj} - \frac{1}{3}Tr(\mathbf{A}^2)\delta_{ij} \right) \\ & + H_{ij}^{(p)} + H_{ij}^{(v)} + \frac{\partial f_i}{\partial x_j}, \end{aligned} \tag{2}$$

where d/dt is the Lagrangian derivative, f_i is a possible additional body force (namely Coriolis, buoyancy or Lorentz),

$$H_{ij}^{(p)} = -\left(\frac{\partial^2 p}{\partial x_i \partial x_j} - \frac{1}{3}\frac{\partial^2 p}{\partial x_k \partial x_k}\delta_{ij} \right) \tag{3}$$

is the anisotropic, traceless part of the presure Hessian, and

$$H_{ij}^{(v)} = \nu \frac{\partial^2 A_{ij}}{\partial x_k \partial x_k} \tag{4}$$

is the viscous term.

Eq. (2) is a set of nine coupled ordinary differential equations, in which the terms $H_{ij}^{(p)}$ and $H_{ij}^{(v)}$ need to be modeled. Various closures, listed in the subsection 2.3, have been proposed in the last decades. For a recent review of these models, the reader can refer to [1].

2.2 Gradients & increments, Lagrangian approach, preliminary remarks

As stressed in the foreword of this special issue, many studies start with the velocity increment, for instance to look at statistical structure functions, or

$$\delta \boldsymbol{u} = \boldsymbol{u}(\boldsymbol{x} + \boldsymbol{r}) - \boldsymbol{u}(\boldsymbol{x}). \tag{5}$$

For a small separation vector $\boldsymbol{r}$ and assuming smoothness of the velocity field, the velocity gradient is easily found as the Taylor's limit, or $\delta \boldsymbol{u} = \boldsymbol{A} d\boldsymbol{r}$, so that a model for the velocity gradient tensor derives from a model for the velocity increment. Of course, this relationship is not consistent with the K41 scaling $\delta u \sim r^{1/3}$ at significant r values, so that special care is needed depending on the scale of the velocity increment. For instance, the "Deltavee" models can be used for this purpose of recovering some properties of the velocity gradient tensor, but they do not include in general all the components of the velocity increment, only a transverse one and a longitudinal one.

It is perhaps useful to recall some useful Lagrangian or semi-Lagrangian relationships before discussing the models for transport equations. The mapping of Eulerian $\boldsymbol{x}$ to Lagrangian coordinates $\boldsymbol{X}$ is given by the flow trajectories. Assuming smoothness, it is possible to differentiate the trajectory equation, as

$$dx_i = u_i dt + F_{ij} dX_j,$$

so that the important semi-Lagrangian tensor (often called gradient of displacement tensor, or Cauchy matrix in [18]), is found as

$$F_{ij}(\boldsymbol{X}, t) = \frac{\partial x_i}{\partial X_j}. \tag{6}$$

The Lagrangian time-derivative of $\boldsymbol{F}$ gives

$$dF_{ij}/dt = A_{in}F_{nj}, \tag{7}$$

indicating that $\boldsymbol{F}$ is a time- accumulated deformation tensor following the trajectories, or $\mathbf{F} = \exp(\int^t \boldsymbol{A}dt)$. Of course, it follows that

$$\boldsymbol{A} = \frac{d\boldsymbol{F}}{dt}\cdot\boldsymbol{F}^{-1},$$

so that the velocity gradient tensor simply derives from the Cauchy matrix.

Decomposition of A_{ij} into a symmetric part S_{ij} and an antisymmetric one reintroduces the vorticity vector $\boldsymbol{\omega}$, as

$$A_{ij} = S_{ij} + (1/2)\epsilon_{inj}\omega_n, \quad \omega_i = \epsilon_{inj}A_{jn}.$$

It is obvious that the antisymmetric part of Eq. (2) gives the classical Helmholtz equation for the vorticity vector, with no contribution from the pressure Hessian because it is a symmetric tensor. On the other hand, the 6 components of S_{ij} are directly affected by the pressure Hessian, whose only the trace, or pressure Laplacian, is given in terms of A_{ij} (classical Poisson equation $\nabla^2 p = -\boldsymbol{A}^2$). Looking at the Cauchy matrix, satisfying $Det\boldsymbol{F} = 1$ from the incompressibility constraint, a multiplicative decomposition is suggested as

$$\boldsymbol{F} = \mathbf{DQ}, \tag{8}$$

in term of a product of a symmetric matrix (accumulated strain) by an orthogonal one (accumulated rotation), the first one being identified by forming the Cauchy-Green tensor as $\mathbf{C} = \boldsymbol{F}\boldsymbol{F}^t = \mathbf{D}^2$.

2.3 Models

The simplest approach of the closure of Eq. (2) consists in neglecting the terms Eq. (3) and Eq. (4). The resulting system, in which the time evolution of $\mathbf{A}$ is fully determined by its initial condition, has been first studied by Vieillefosse [4,5]. Unfortunately, it can be shown that the solution A_{ij} of this so-called Restricted Euler dynamics exhibits a finite-time singularity for almost any initial condition. However, this solution also shows encouraging features as the singularity is approached. In particular, the predicted structure of the velocity gradient tensor shows a tendency:

- to create disk-like structures, in the sense that a small, initially spherical fluid element moving with the flow extends in two dimensions and contracts in the third one. This is reflected by the fact that the strain tensor $\mathbf{S}$ (symmetric part of $\mathbf{A}$) has two positive eigenvalues and a negative one (the sum of these eigenvalues must be equal to zero to satisfy the incompressibility condition);
- to align the vorticity vector $\boldsymbol{\omega}$ (antisymmetric part of $\mathbf{A}$) with the eigenvector of $\mathbf{S}$ associated to its (positive) intermediate eigenvalue.

These two tendencies are characteristic trends of 3D turbulence that have been observed in many experiments and numerical simulations [6–9].

To go further than this crude approximation of Eq. (2), more accurate closures have been proposed. One can mention in particular:

- a linear damping model [10], in which

$$H_{ij}^{(p)} + H_{ij}^{(v)} = -A_{ij}/\tau_0, \tag{9}$$

  where τ_0 is a relaxation timescale;
- a stochastic diffusion model with prescribed log-normal dissipation [11], in which $H_{ij}^{(p)}+H_{ij}^{(v)}$ is modeled as the sum of a drift term meant to model parts of the deviatoric part of the pressure Hessian, and of a stochastic term;
- a Lagrangian linear diffusion model [12], focusing on the viscous term Eq. (4) and modeling it as a function of the Cauchy-Green tensor

$$\mathbf{C} = \mathbf{F}\mathbf{F}^t, \tag{10}$$

  where F_{ij} has been precedently introduced;
- the recent fluid deformation approximation [13], in which $H_{ij}^{(p)} + H_{ij}^{(v)}$ is modeled as the sum of three terms: two of them are deterministic functions of the "recent Cauchy-Green tensor" $\mathbf{C}_{\tau K}$, whereas the third one is analogous to the stochastic term of the Lagrangian linear diffusion model [12]. The tensor $\mathbf{C}_{\tau_K}$ is expressed in terms of simple matrix exponentials:

$$\mathbf{C}_{\tau_K} = e^{\tau_K \mathbf{A}} e^{\tau_K \mathbf{A}^t}, \tag{11}$$

  from Eq. (7)

Recourse to the Cauchy-Green tensor, with possibly a truncated time-memory, asks the questions: Why the pressure Hessian is "more spherical" in Lagrangian coordinates, or $\partial^2 p/(\partial X_i \partial X_j)$, than in Eulerian coordinates? why the orthogonal matrix in Eq. (8) is not involved in the closure model?

3 Modeling the coarse-grained velocity gradient tensor dynamics in turbulence

Another quantity of interest in turbulence modeling is the **coarse-grained** velocity gradient tensor, defined as:

$$M_{ij} = \frac{1}{V}\int_\Omega d^3x \, \frac{\partial u_i}{\partial x_j}, \tag{12}$$

where V is the volume of the domain Ω.

A model for the Lagrangian dynamics of $\mathbf{M}$ has been proposed by Chertkov, Pumir and Shraiman [2]. This so-called "tetrad model" is based on a particle representation of the velocity of four fluid particles. The model is formulated in terms of two coupled stochastic differential equations, modeling the evolution of $\mathbf{M}$, the coarse-grained velocity gradient tensor, along with the three vectors $\boldsymbol{\rho}^i$ $(i = 1, 2, 3)$, which describe the shape of the tetrad with respect to its center of mass,

$$\frac{dM_{ab}}{dt} + (1-\alpha)\left(M_{ab}^2 - \Pi_{ab}Tr(\mathbf{M}^2)\right) = \eta_{ab}, \tag{13}$$

$$\frac{d\rho_a^i}{dt} + \rho_b^i . M_{ba} = u_a^i, \tag{14}$$

$$\Pi_{ab} = k_a^i k_b^i / Tr(\mathbf{k}\mathbf{k}^t), \tag{15}$$

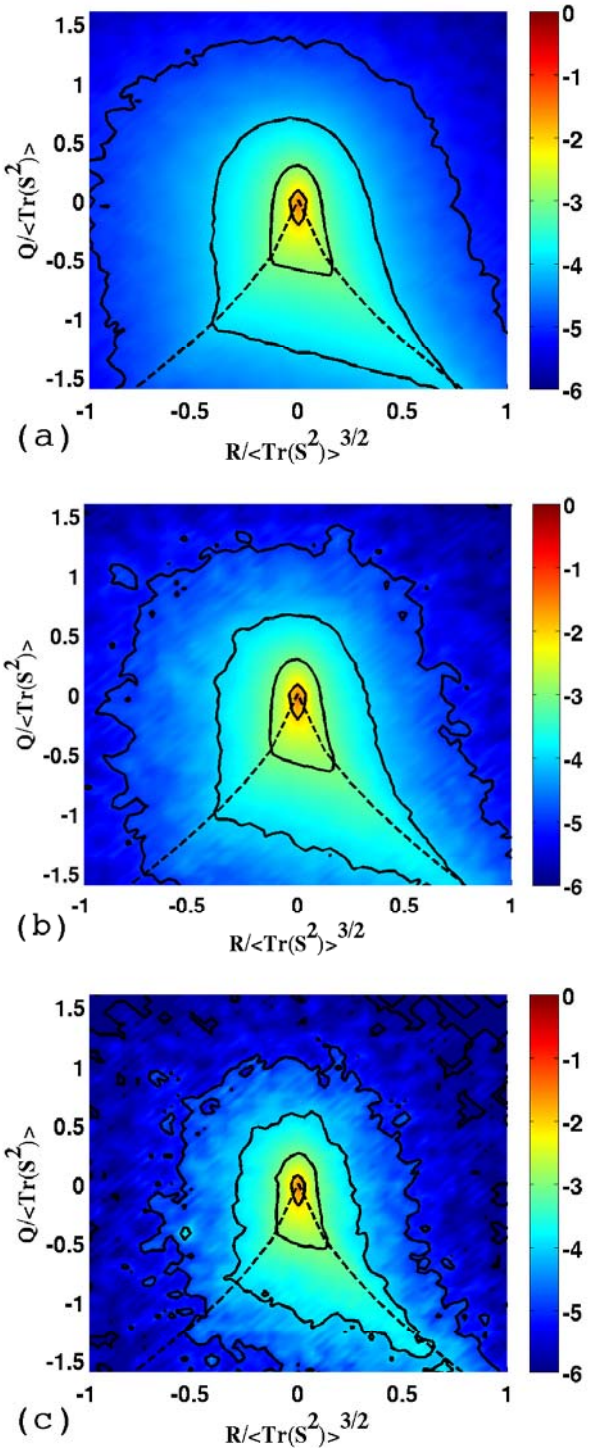

Figure 1: Scale dependence of the joint PDF of the normalized R and Q invariants, solutions of the tetrad model: $Q = -\frac{1}{2}Tr(M^2)$, $R = -\frac{1}{3}Tr(M^3)$. The solutions corresponding to $\alpha = 0.3$, $C_u = 0.15$ and $C_\eta = 1$ are represented at scale (a) $|\rho| = L/2$, (b) $|\rho| = L/4$ and (c) $|\rho| = L/16$. The evolution of the shape of the PDF is very limited over the range of scales studied here. The isoprobability lines shown on the graphs correspond to probability levels 10^{-n}, where n is an integer ($n \leq 6$).

where the matrix $\mathbf{k}$ is the inverse of $\boldsymbol{\rho}$. In the notation used here, the lower indices a, b,... refer to the space dimension and the upper indices i, j,... specify one among the three vectors describing the shape of the tetrad. The deterministic terms on the left-hand side of Eq. (13) and Eq. (14) represent the effect of the dynamics induced by scales of order $|\rho|$. The matrix $\mathbf{\Pi}$, defined by Eq. (15), is symmetric with a trace 1; it provides a coupling of the geometry with the dynamics of $\mathbf{M}$. Lastly, the stochastic terms in Eq. (13) and Eq. (14), $\boldsymbol{\eta}$ and $\mathbf{u}$, represent the random effect of the small scales of motion. They are represented by Gaussian, white in time noise terms, with a scale dependence prescribed by dimensional considerations, consistent with the Kolmogorov scaling,

$$\langle \eta_{ab}(0)\eta_{cd}(t)\rangle = C_\eta \delta(t)\frac{\varepsilon}{\rho^2}\left(\delta_{ac}\delta_{bd} - \frac{1}{3}\delta_{ab}\delta_{cd}\right), \quad (16)$$

$$\langle u_a^i(0)u_b^j(t)\rangle = C_u \delta(t)\sqrt{Tr(\mathbf{M}\mathbf{M}^t)}(\delta_{ab}\rho^2\delta^{ij} - \rho_a^i\rho_b^j), \quad (17)$$

where $\rho^2 = Tr(\boldsymbol{\rho}\boldsymbol{\rho}^t)$. The noise term acting on $\boldsymbol{\rho}$, $\mathbf{u}$, is assumed here to act only in the direction transverse to the nine-dimensional vector $\boldsymbol{\rho}$, which is not expected to be a significant restriction. $\alpha \in]0;1[$, $C_\eta > 0$ and $C_u > 0$ are dimensionless parameters.

Although the solution of this stochastic model, written as a set of 14 coupled ODEs, can be formally expressed in terms of path integrals, its numerical determination in terms of the Monte-Carlo method is very challenging, as very few configurations contribute effectively to the statistical weight. For this reason the model was first solved in the semiclassical approximation [14, 15]. These results allowed to design more accurate methods of resolution [16]. More recently, a full Monte-Carlo simulation of the tetrad model was carried out [17], by using an algorithm based on the importance sampling method, which consists of identifying and sampling preferentially the configurations that are likely to correspond to a large statistical weight, and selectively rejecting configurations with a small statistical weight. The algorithm led to an efficient numerical determination of the solutions of the model and allowed to determine their qualitative behaviour as a function of scale (see *e.g.* Figure (1)).

By using this numerical method, Pumir and Naso found that the moments of order $n \leq 4$ of the solutions of the tetrad model scale with the coarse-graining scale and that the scaling exponents are very close to the predictions of the Kolmogorov theory. The model qualitatively reproduces quite well the statistics concerning the local structure of the flow. However, they also found that the model generally tends to predict an excess of strain compared to vorticity. Thus, their results show that while some physical aspects are not fully captured by the model, the latter leads to a very good description of several important qualitative properties of real turbulent flows.

4 Perspectives

This global approach can be generalized to anisotropic flows, first in the presence of body forces, then in the presence of coupled fields (buoyancy scalar, magnetic field). In addition to the basic isotropic case, three cases of increasing complexity will be addressed:

- Rotating turbulence. Attempts by Yi Li to generalize the "isotropic" delta-vee model are not completely satisfactory. Long experience of Claude Cambon's team in both inertial wave turbulence and anisotropic two-point closures is expected to improve the synergy [18, 19].

- Turbulence with buoyancy in a stably stratified fluid, rotating or not. In addition to the effect of the buoyancy force, as a body force involved in modified Navier-Stokes equations, the transport equation must be considered for the gradient of the *active* buoyancy scalar.

- Turbulence with coupled MHD effects, with and without rotation. Applications will concern turbulent liquid metal in engineering and for geodynamo. In this case, the additional body force involved in Navier-Stokes equations is the Lorentz force; the coupled field is the fluctuating magnetic field: this is an *active* vector, because of its feedback via the Lorentz force.

It is worth mentioning that two steps have already been made in this direction. Naso, Chertkov and Pumir investigated the statistics of the coarse-grained velocity gradient tensor $\mathbf{M}$ predicted by the tetrad model in the presence of a large-scale shear [20]. Li investigated the statistics of the velocity gradient tensor $\mathbf{A}$ in a rotating frame [21] predicted by the recent fluid deformation approximation from Chevillard and Meneveau [13].

Briefs comments in subsection 2.2 suggest to study the tensor $\boldsymbol{F}$ prior to the velocity gradient tensor. Studies by Koji Ohkitani, including DNS, are encouraging for this way of research, as well as Lagrangian relationship for Euler equations reminded in [18]. Finally, both tensors $\mathbf{A}$ and $\boldsymbol{F}$ are crucially involved in Rapid Distortion Theory, as recalled in the foreword. These quantities are related to an ideal, too simple, base flow, in "homogeneous" RDT, but recourse to a localized form, as WKB RDT, can be informative.

We do not discuss here some counterparts of this analysis for a scalar gradient, even firstly for the gradient of a passive scalar, which could be re-investigated before, or in the same time, as the "active" buoyancy scalar in stratified turbulence.

About synthetic models of turbulence, one can mention that KS (Kinematic Simulation) is remarkably consistent with DNS and esperimental results, from A. Pumir and Tabeling, for triangles and tetrahedrons of fluid particles [22]. These KS studies were extended to particles with inertia and effect of gravity [23].

References

[1] C. Meneveau, Lagrangian Dynamics and Models of the Velocity Gradient Tensor in Turbulent Flows, *Annu. Rev. Fluid Mech.*, **43**, 219, 2011

[2] M. Chertkov, A. Pumir & B. I. Shraiman, Lagrangian tetrad dynamics and the phenomenology of turbulence, *Phys. Fluids*, **11**, 2394, 1999

[3] H.T. Xu, A. Pumir & E. Bodenschatz, The pirouette effect in turbulent flows, *Nat. Phys.*, **7**, 709, 2011

[4] P. Vieillefosse, Local interaction between vorticity and shear in a perfect incompressible fluid, *J. Phys. (Paris)*, **43**, 837, 1982

[5] P. Vieillefosse, Internal motion of a small element of fluid in an inviscid flow, *Phys. A*, **125**, 150, 1984

[6] W.T. Ashurst, A.R. Kerstein, R.M. Kerr & C.H. Gibson, Alignment of vorticity and scalar gradient with the strain rate in simulated Navier-Stokes turbulence, *Phys. Fluids*, **30**, 2343, 1987

[7] R.M. Kerr, Histograms of helicity and strain in numerical turbulence, *Phys. Rev. Lett.*, **59**, 783, 1987

[8] A. Tsinober, E. Kit & T. Dracos, Experimental investigation of the field of velocity gradients in turbulent flows, *J. Fluid Mech.*, **242**, 169, 1992

[9] G. Gulitski, M. Kholmyansky, W. Kinzelbach, B. Luthi, A. Tsinober & Y. Yorish, Velocity and temperature derivatives in high-Reynolds-number turbulent flows in the atmospheric surface layer. Part 1. Facilities, methods and some general results, *J. Fluid Mech.*, **589**, 57, 2007

[10] J. Martin, C. Dopazo & L. Valino, Dynamics of velocity gradient invariants in turbulence: restricted Euler and linear diffusion models, *Phys. Fluids*, **10**, 2012, 1998

[11] S.S. Girimaji & S.B. Pope, A diffusion model for velocity gradients in turbulence, *Phys. Fluids A*, **2**, 242, 1990

[12] E. Jeong & S.S. Girimaji, Velocity-gradient dynamics in turbulence: effect of viscosity and forcing, *Theoret. Comput. Fluid Dyn.*, **16**, 421, 2003

[13] L. Chevillard & C. Meneveau, Lagrangian dynamics and statistical geometric structure of turbulence, *Phys. Rev. Lett.*, **97**, 174501, 2006

[14] A. Naso & A. Pumir, Scale dependence of the coarse-grained velocity derivative tensor structure in turbulence, *Phys. Rev. E*, **72**, 056318, 2005

[15] A. Naso, Intermittence en Turbulence pleinement développée et en Dynamique non linéaire, PhD thesis, Université de Nice-Sophia Antipolis, 2005

[16] A. Naso, A. Pumir & M. Chertkov, Statistical geometry in homogeneous and isotropic turbulence, *J. Turbul.*, **8**, 39, 2007

[17] A. Pumir & A. Naso, Statistical properties of the coarse-grained velocity gradient tensor in turbulence: Monte-Carlo simulations of the tetrad model, *New J. Phys.*, **12**, 123024, 2010

[18] P. Sagaut & C. Cambon, Homogeneous Turbulence Dynamics, 2008, *Camb. U. Press* (monograph, 463 p.)

[19] L. van Bokhoven, C. Cambon, L. Liechtenstein, F. S. Godeferd & H. J. H. Clercx, Refined vorticity statistics of decaying rotating three-dimensional turbulence, *J. of Turbulence*, **9**, 1

[20] A. Naso, M. Chertkov & A. Pumir, Scale dependence of the coarse-grained velocity derivative tensor: influence of large-scale shear on small-scale turbulence, *J. Turbul.*, **7**, 41, 2006

[21] Y. Li, Lagrangian evolution of velocity increments in rotating turbulence: The effects of rotation on non-Gaussian statistics, *Physica D*, **239**, 1948, 2010

[22] F. Nicolleau and A. ElMaihy (2006), Effect of the Reynolds number on three- and four-particle diffusion in three-dimensional turbulence using Kinematic Simulations, *Phys. Rev. E*, **74**, 046302.

[23] A. Abou El-Azm Aly and F. Nicolleau (2008), Dispersion of heavy particle sets in isotropic turbulence using Kinematic Simulation, *Phys. Rev. E*, **78**, 016310.

Advances in RDT and DNS for Coupled Effects of Shear, Rotation and Stratification

Alexandre Pieri[1], Claude Cambon[1], Fabien Godeferd[1], Aziz Salhi[2], Thierry Lehner[3]

[1] Laboratoire de Mécanique des Fluides et d'Acoustique, UMR 5509, Ecole Centrale de Lyon, France.

[2] Laboratoire de Physique, Tunis, Tunisia.

[3] Observatoire de Paris, Meudon, France.

1 Introduction

Important aspects of turbulence, subjected to mean shear, solid body rotation, density stratification and/or coupling with magnetohydrodynamics, can be understood in the context of Homogeneous Anisotropic Turbulence (HAT hereinafter), without explicit effect of solid boundaries.

Several studies, with the same starting point (see the foreword) range from linear theory, either applied to the prediction of statistics (so called Rapid Distortion Theory, RDT hereinafter), to stability of unimodal disturbances (Bayly 1986, Craik 1986, ref. in [19]), or to pseudo-spectral DNS in deformed cordinates (Rogallo 1981, Lesur 2007).

The other paper in the present issue, **Axisymmetric theory and DNS in rotating, stratified, and MHD turbulence**, deals with the cases without mean shear, in which axisymmetry is consistent with basic equations, and in which a spectral nonlinear theory can be applied in addition to DNS. These cases are essentially "without production", so that nonlinear dynamics and related modification of inter-scale energy cascade mediated by triple correlations is the main problem. Linear theory is useful for giving eigenmodes and dispersion laws, with a view to improve their nonlinear analysis. For instance, the basic linear Green's function, obtained analytically is a useful building block to incorporate in generalized EDQNM.

On the other hand, linear theory is crucial here, in the presence of mean shear or mean deformation, and the linear Green's function is often very complex. This yields a sophisticated "energy production" mechanism, which is more physical than an artificial forcing.

2 A generalized RDT approach

A historical survey of "Rapid Distortion Theory", *probably better coined as "Linear analysis in terms of mean-flow-advected Fourier modes"*, is drawn in the foreword. Very complete review of the essentials are given in [23] and in [19] , at the cross-road of three communities using different terminologies and often publishing in different journals: "RDT" historical community, Applied mathematics for hydrodynamic instabilities, Astrophysics. For instance, "shear wave" corresponds to "Kelvin mode" and is related to "Rogallo space". We have also recalled to which extent fully nonlinear computations using pseudo-spectral DNS in deformed boxes (Orszag / Patterson / Rogallo) are a natural extension of "RDT".

As a recap, our strategy for using generalized RDT, and to extend it towards nonlinear DNS, is generic with the following essentials:

1. Systematic use of a mean (or base) flow which is an exact solution of Euler equations: This "admissibility condition" allows us to balance the gyroscopic torque in a physical way, looking at the conservation of (mean) absolute vorticity derived from Euler equations.
2. Decomposition of the fluctuating flow in terms of advected Fourier modes with time-dependent wavevectors. These modes are called "Kelvin modes" (Applied Mathematics, probably following H. K. Moffatt in RDT) and "shear waves" (Astrophysics). The variable $\boldsymbol{X}$, with mean trajectory equation $x_i = F_{ij}(t,t_0)X_j$ corresponds to "Rogallo space" (engineering).
3. Fluctuating velocity modes are split using the Craya-Herring frame of reference, resulting in a minimal number (two) of solenoidal components, of toroidal and poloidal type.
4. The linear solution is generated by a complete deterministic Green's function, applied to the velocity-buoyancy-magnetic fluctuating field, for arbitrary initial data and possibly arbitrary forcing, prior to any calculation of statistics.
5. Classical conservation of potential vorticity is applied. In the RDT context, this yields to define an invariant of the motion, as the linearized absolute potential vorticity, *in which the vorticity of the mean shear* is involved.
6. Prediction of both synthetic realizations of the velocity field, as in KS (Kinematic simulation), and prediction of statistical quantities, as in conventional RDT, are given, in order to sweep the parameter range before applying much more costly DNS.

3 Rotating shear and beyond, shearing sheet approximation

The distorting mean shear flow sketched in Figure (1) (left, no rotation) is characterized by the following constant mean velocity gradient matrix and displacement (Cauchy) matrix:

$$A_{ij} = S\delta_{i1}\delta_{j2},\ F_{ij}(t,t_0) = \delta_{ij} + A_{ij}(t-t_0). \quad (1)$$

The indices 1, 2 and 3 refer to streamwise, cross-gradient, and spanwise directions. The general RDT solution by Moffatt [15] (1967, see the foreword) can be expressed in terms of two, toroidal and poloidal, velocity components. Several studies, such as [20], addressed the linear response of turbulence to the shear with spanwise rotation of rate Ω. This gives a model useful for predicting stabilisation or destabilisation by rotation in shear flows in term of the ratio $2\Omega/S$.

In this context of pure plane shear with spanwise rotation, the shearing sheet (or shearing box) approximation is a very important avatar of RDT and pseudo-spectral DNS in deformed box, with several applications to rotating accretion discs in astrophysics. The limit of a Taylor Couette flow with differential rotation in the radial (r) direction $\tilde{\Omega}(r) \sim r^{-q}$ is considered, so that the equivalent shear rate is

$$S = -r d\tilde{\Omega}/dr,$$

at a given r. Accordingly, streamwise, cross-gradient and spanwise directions in Cartesian coordinates correspond to peripheral, radial and axial directions, respectively, in cylindrical coordinates. For instance, the $k_1 = 0$ mode is called "axisymmetric mode" in the astrophysical context of rotating flows with radial variation of the angular velocity. The "Bradshaw (or rotational Richardson number) criterion" for the stability of rotating shear is related to the epicyclic frequency in astrophysics

$$\kappa^2 = 2\Omega(2\Omega + S),$$

and $\kappa^2 < 0$, or $-1 < \Omega/S < 0$ characterizes exponential instabillity in a simplified "pressure-less" analysis. For anticyclonic rotation of astrophysical discs, it is found that $\kappa^2 = 2(2-q)\tilde{\Omega}$, with the important result of the stability of the Keplerian disc, for which $q = 3/2$ and $\Omega/S = -4/3$, in this context.

Given the evidence that Keplerian accretion discs are turbulent, other effects were investigated. In our generalized RDT context, we have revisited stratorotational instability, in the presence of additional density stratification and buoyancy force, and magnetorotational instability (MRI) for magnetized discs. Other useful stability criteria are recovered and generalized, using linear theory, the Ertel theorem for conservation of absolute potential vorticity and its new established counterpart in MHD, replacing the vorticity by the magnetic vector potential [25].

For all cases subjected to the mean shear, even in the presence of additional body forces, Coriolis, buoyancy and Lorentz, analytical laws directly appear for disturbances with $k_1 = 0$, or equivalently with infinite wavelength in the streamwise direction. For instance, in magnetized accretion discs, magnetorotational instability (MRI) occurs at $k_1 = 0$ when the vertical magnetic tension is less than the centrifugal force intensity, in agreement with previous stability analyses (e.g. Balbus & Hawley, *A. P. J.*, 1991). A systematic use of the Levinson's theorem allows to treat the case $k_1 \neq 0$, except for some combinations of mean flow parameters with dominant rotation. Cases with and without MHD coupling, or for "active" and "dead" accretion discs, are investigated [25]. Generalized RDT offers very promising perspectives for transient growth and mode coupling in the context of rotating stratified shear flows, mainly discussed in the baroclinic context here. As in former meetings from the Henri Bénard PC, e.g. ASTROFLU in 2008, close collaboration between specialists of fluid mechanics and astrophysicists is encouraged.

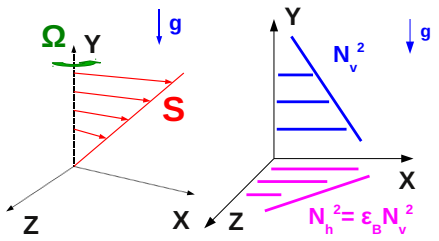

Figure 1: Sketch of the baroclinic mean flow.

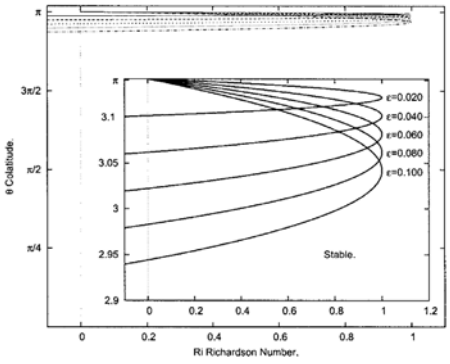

Figure 2: Neutral curves for the baroclinic flow obtained by RDT analysis for $k_1 = 0$ modes [21]. The figure shows the linear stability bound $Ri = 1$ in the (Ri, θ) plane.

4 Revisiting instability and turbulence in the baroclinic context

Combined effects of rotation, stratification and shear are a common feature of geophysical fluid dynamics. The baroclinic context, addressed by [17] as well, is characterized by a superposition of three coupled phenomena: (a) the Coriolis force, caused by earth rotation in geophysical flows; (b) stable stratification due to density gradients in the atmosphere, which lead to buoyancy forces in the vertical direction; (c) high vertical velocity gradients, as at the altitude of the tropopause in atmospheric flows, in the form of jet streams, which, in first approximation, are modelled by homogeneous shear. Following the introduction given above, the baroclinic context is addressed using "RDT" and DNS.

The first studies on baroclinic instability where done by Charney (1947) [4] using quasi-geostrophic equations in the β-plane approximation. He derived a necessary condition for instability to occur formulated simply by an inequality implying the Rossby radius of deformation. Further contribution by Eady (1949) [8] using the f-plane approximation was later added. Eady considered a

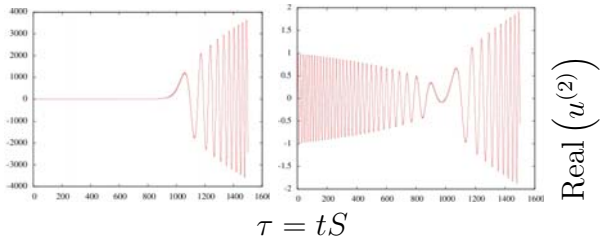

Figure 3: Transitional growth of the $u^{(2)}$ velocity component observed in RDT for $k_1 = 10^{-3}$. Left: with non-zero initial potential vorticity and strong coupling with the vortex mode. Right: zero initial potential vorticity (wave mode).

simpler model — a Couette-like configuration — of the atmosphere and obtained an instability condition resting on a critical wavenumber [16]. Unbounded shear is considered here and we also place the study within the f-plane approximation, or constant system vorticity.

Interest of "admissibility conditions" (Craya 1958, Craik 1989) is illustrated as for the precessing flow case in Section 5: The misalignment of (vertical) system rotation and (spanwise) mean-shear-vorticity induces a mean vorticity component in the streamwise direction, and this is exactly balanced by an additional buoyancy gradient in the horizontal direction. In other words, the fact that the mean flow ought to be an exact solution of Euler-Boussinesq equations implies a constraint on mean absolute vorticity, which amounts to the "geostrophic front adjustment" in geophysical flows. Accordingly, combination of both vertical and additional horizontal mean stratification results in tilting the isopycnal lines, triggering the baroclinic instability.

Investigations of homogeneous turbulent flows submitted to the separate effects of homogeneous shear, stable vertical stratification or rotation were done in the past decade [2, 9, 10, 13, 20]. Here, we focus on the following new approach: RDT and Direct Numerical Simulation (DNS) of homogeneous turbulence including the complete coupled three previous distorsions. Unlike the previously mentioned contexts, the baroclinic instability is a reservoir of energy which does not impose to add an artificial forcing to the simulations, or to have to deal with decaying flows. The aim of our study is first to provide a detailed characterization of the Eulerian properties of developped baroclinic turbulence. The parametric space is 4-dimensional (Pr, Re, Ri, ε_{B}), including the properties of turbulence itself, Reynolds number, cut-off wavenumbers, but also the choice of the intensities of rotation, stratification and shear. A reduction of the parametric space is obtained by considering the Richardson number defined as $Ri = N^2/S^2$ and the baroclinic parameter $\varepsilon_B = Sf/N^2$ which is also the mean slant angle of the isodensity surfaces. Here, $S = \partial_y U_x$ is the mean velocity gradient, $N = \left(-g\partial_y \overline{\rho}/\rho_0\right)^{1/2}$ is the Brunt-Väisälä frequency and $f = 2\Omega$ is the rotation rate. We shall investigate ranges of these parameters between $[0:2]$ for Ri and $[0:1]$ for ε_B.

4.1 Linear theory, towards mode coupling and transient growth

The basic problem, for stability analysis or RDT prediction, amounts to solve an initial-value system of ODE (Ordinary Differential Equations). This is a 2-rank system of ordinary equations with time-dependent coefficients using the general method (items (2) and (3) in Section 2): The fluctuating field in 5 components in physical space, 3 components for the velocity, one for the buoyancy and one for the pressure, reduces to a 3-component one in solenoidal Fourier space (Craya-Herring space), which generate toroidal kinetic, poloidal kinetic, and potential energy, respectively. The rank of the system is still reduced to a non-homogeneous system of two equations, thanks to item (5).

As discussed before, stability is analytically investigated at $k_1 = 0$, yielding the diagram in Figure (2) from [21]. It is shown that the domain of exponential instability can be shifted towards $R_i = 1$. This domain is restricted to $R_i < 0$ (unstable stratification) for stratified shear flows —without rotation— in RDT, and only extended to small positive values $R_i \sim 0.1$ using DNS, as investigated by [10].

In addition to investigation of exponential instability, RDT is capable of predicting dramatic — even if algebraic— transient growth, as a non-standard non-modal stability analysis. This is due to the fact that spatial structure of modes, advected Fourier modes in RDT, is prescribed, but not at all their temporal dependence when solving the initial-value, linear system of ODE. Mode coupling underlying this dramatic transient growth can be related to a generalized wave-vortex decomposition [3], in which the "vortex" mode is the linearized potential vorticity mode. In Figure (3), it is shown that the transient growth is important only for nonzero value of the vortex mode, in a domain $R_i > 1$ shown as "exponentially" stable.

The linear stability analysis of Salhi & Cambon [21] and in [3] is continued here using a stochastic RDT-based Kinematic Simulation model, whose results are compared to DNS ones.

4.2 DNS results, and perspectives

The Navier-stokes equations in the Boussinesq approximation are solved using pseudo-spectral Direct Numerical Simulation. Periodicity is assumed in the three directions. Under the action of shear, the mesh is deformed and a periodic remeshing is needed using the algorithm by Rogallo [18] (the anisotropic adaptation of the Orszag-Patterson algorithm) in spectral space. Dealisasing is done following Delorme [6] method. The code used in this study is a MPI-based parallel code : the turbulence box is cut into slabs following the algorithm by Coleman [5]. Time-advancing is done according to the third order Runge-Kutta (RK3) method. Lastly, the rotational form of the non-linear term has been implemented.

We start by considering two-point spectra of Eulerian velocity and buoyancy fields, as well as the evolution of additional scalars which are introduced in the flow, with different Schmidt numbers. The time evolution of quantities such as the deviatoric part of the Reynolds stress tensor, the componentality and dimensionality tensors [1, 11], potential and kinetic energy directional spectra are analized to bring out and understand the complex anisotropic structure of the flow. A link with extended structure functions is also proposed, in order to assess the possible application, or disagreement, of scalings available for isotropic turbulence in the context of Kolmogorov theory. We will also study two-point correlations for characterizing the turbulent structures, and their properties. Large scale structures will be quantified with directional correlation length obtained from the velocity correlation tensor, whereas two-point vorticity correlations put to the fore smaller turbulent structures. The Lagrangian properties are also studied, and related to Eulerian data, especially considering the dual characterization of anisotropy. To refine our study, we thus obtain results concerning mixing properties of the flow by looking at both the stratifying agent concentration (see for instance the distribution of buoyancy on Figure (4)) and passive scalars advection (on Figure (5)). We also put the emphasis on the analysis of possibly unstable dynamics of turbulence within the baroclinic context, in a second part. Inertial transfers will be investigated, considering energy exchanges between the kinematic and the potential modes, but also the interscale and directional energy drain. This structuring of the flow, of nonlin-

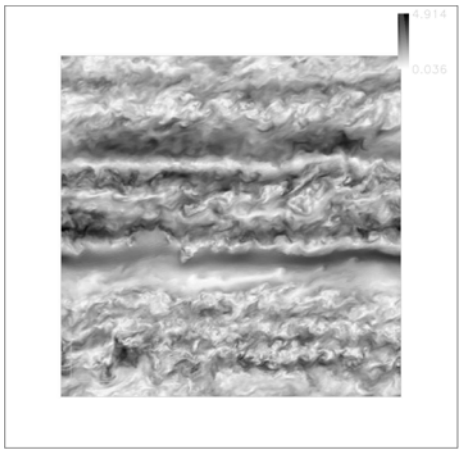

Figure 4: Buoyancy in the vertical-longitudinal plane for $Ri = 0.99$ and $\varepsilon_B = 0.2$ at time $\tau = tS = 13.2$. $Re_\lambda(0) = 66$. DNS $256 \times 384 \times 256$. G. Simon, PhD thesis (2007).

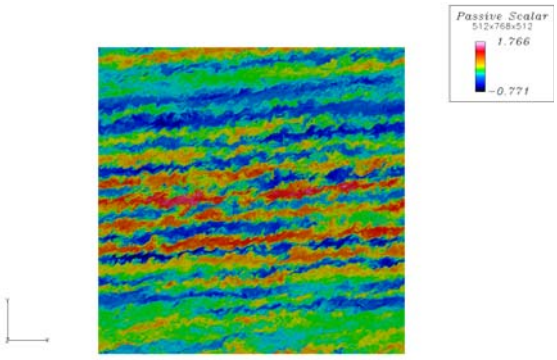

Figure 5: Passive scalar distribution in the vertical-longitudinal plane. DNS with 512x768x512 degrees of freedom with Richardson number $Ri = 0.5$ and baroclinicity parameter $\varepsilon_B = 0.2$. $Re_\lambda(0) = 122$ and $\frac{Sk}{\epsilon_\nu} = 4.55$. With ϵ_ν the kinetic energy dissipation. $\tau = tS = 7$.

ear, irreversible nature since it is due to quadratic terms in the equations, is also compared to the predictions of linear theory (often called Rapid Distorsion Theory, RDT). It provides lots of valuable information on the spectral energy distribution reorganization by the mere body forces (Coriolis and buoyancy) and shear. Since RDT is also computationally much lighter than DNS, it also permits a preliminary opening of the parametric space, allowing to choose the most relevant parameters for the high resolution simulations. At zero baroclinicity, the numerical results are checked with the ones by Jacobitz, Sarkar and van Atta (1997). New results show the kinetic energy growth rate and the development of Reynolds stress tensor anisotropy. Finally, some passive scalar diffusion visualizations are presented (see Figure (5)) showing that mixing is typically structured in the stable case with very different horizontal layers.

5 Precessing flows

Very recently, the interest for such flows and related above-mentioned techniques was renewed with precessing rotating flows. It can be shown that the gyroscopic torque induced by the misalignment of main solid body rotation and weak additional precessing rotation (see

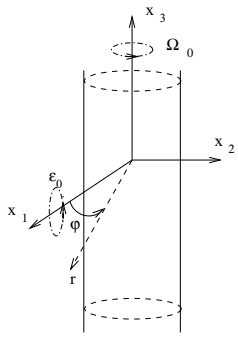

Figure 6: Sketch of the precessing mean flow. Figure taken from [22].

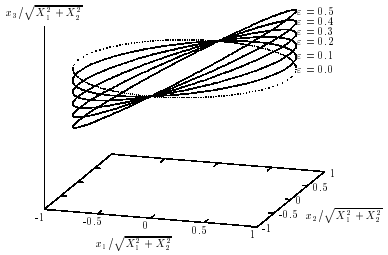

Figure 7: Elliptical streamlines of the precessing flow. Figure taken from [22].

Figure (6)) can be exactly balanced by an additional shear [22]. The resulting background mean flow is characterized by elliptical streamlines (see Figure (7)), so that it can trigger instabilities for the fluctuating part very close to the generic *elliptical flow instability*. Application of the Rogallo technique to the case of mean elliptical streamlines was addressed by a single, almost unpublished, study (Blaisdell and Shariff, CTR Annual Briefs, 1996), and this merits to be revisited and extended with new flow cases. In addition to technical advantages — no need for periodic remeshing with interpolation as for unclosed streamlines— , the precessing flow case present interest for geophysical and astrophysical applications, including MHD [24], such as the geodynamo in the earth's core, and allows us to explore a new route to turbulence and mixing via generic instabilities. In the unbounded case at least, ellipticity is not given a priori as in the conventional "elliptical flow instability" (e.g. Bayly 1986) but results from the sole gyroscopic torque balanced by the shear, and is completely controlled by the Poincaré parameter, ratio of precessing to main angular velocity. Recent theoretical, experimental, and numerical studies are carried out in different teams, such as the one by Shigeo Kida (Tokyo), IRPHE (Marseille), Observatoire de Meudon (near Paris), and in Dresden, but this list is far to be exhaustive.

6 Perspectives

Generalized RDT can be used as a non-standard tool of linear stability analysis, predicting both exponential instability and algebraic dramatic transient growth by wave-vortex mode coupling. In addition, it remains a predictive model for classical Eulerian statistics, and, incorporated in KS, gives also access to random realizations and Lagrangian statistics. Nonlinear effects are investigated in pseudo-spectral DNS in a comoving frame, which follow the characteric curves given by RDT and reproduce their linear operators with good precision. Strong efforts are done to increase the resolution and

therefore the Reynolds numbers in these DNS. Search for marginal nonlinear stability, with an almost balance between production and dissipation, is a very promising way, extending to baroclinic and precessing effects the study of, e.g, stratified shear flow [10]. Cumulative errors for long-time evolution, especially in the case of transient growth, are probably important in DNS due to the periodic remeshing in time for mean flows with rectilinear streamlines. This drawback is avoided for mean flows with close streamlines, such as the elliptic ones recovered in precessing flows. New DNS have to be done in this case.

For long-term perspectives, effects of confinment could be incorporated in DNS via immersed boundary conditions and penalisation technique. Modelling of simple boundary effects are investigated in close connection with our linear and nonlinear statistical equations in Fourier space (Lin type), as suggested by some recent analyses of the plane Couette flow [12].

References

[1] C. Cambon, L. Jacquin & J. L. Lubrano (1992), Toward a new Reynolds stress model for rotating turbulent flows, *Phys. Fluids A*, **4**, pp. 812-824.

[2] C. Cambon, F. S. Godeferd, F. Nicolleau & J. C. Vassilicos (2004), Turbulent diffusion in rapidly rotating flows with and without stable stratification, *J. Fluid Mech.*, **499**, pp. 231-255.

[3] D. Chagelishvili, A. G. Tevzadze, G. Bodo & S. S. Moiseev (1997), Linear mechanism of wave emergence from vortices in smooth shear flows, *Phys. Rev. Lett.* **79**, 3178.

[4] J. G. Charney & M. E. Stern (1962), On the Stability of internal Baroclinic Jets in a rotating atmosphere, *J. Atm. Sc.*, **19**, pp. 159-172.

[5] G. N. Coleman, J. Kim, & P. R. Spalart (2000), A numerical study of strained three-dimensional wall-bounded turbulence, *J. Fluid Mech.* **416**, 107.

[6] P. Delorme (1985), Simulation numérique de turbulence homogène compressible avec ou sans cisaillement imposé, *PhD Thesis*, ONERA.

[7] P. G. Drazin & W. H. Reid (1981), Hydrodynamic stability, *Cambridge University Press.*

[8] E. T. Eady (1949), Long waves and cyclonic waves, *Tellus*, **1**, pp. 33-52.

[9] F. S. Godeferd & C. Cambon (1994), Detailed investigation of energy tra sfers in homogeneous stratified turbulence, *Phys. Fluids*, **6**, pp. 2084-2100.

[10] F. G. Jacobitz, S. Sarkar & C. W. Van Atta (1997), Direct numerical simulations of the turbulence evolution in a uniformly sheared and stably stratified flow, *J. Fluid Mech.*, **342**, pp. 231-261.

[11] S. C. Kassinos, W. C. Reynolds & M. M. Rogers (2001), One-point turbulence structure tensors, *J. Fluid Mech.*, **428**, pp. 213-248.

[12] G. Khujadze, M. Oberlack & G. Chagelishvili (2006), Direct numerical simulation of stochastically forced laminar plane peculiariaties of hydrodynamic fluctuations, *Phys. Rev. Letters*, **97**.

[13] L. Liechtenstein, F. S. Godeferd & C. Cambon (2005), Nonlinear formation of structures in rotating stratified turbulence, *J. Turbulence*, **6**, pp. 1-18.

[14] G. R. Mamatsashvili *et al.* (2010), Transient Dynamics of Nonsymmetric Perturbations versus Symmetric Instability in Baroclinic Zonal Shear Flows, *J. Atmos. Sc.*, **67**, pp. 2972-2989.

[15] H. K. Moffatt (1967), The interaction of turbulence with strong shear, *Proceedings of the URSI-IUGG International Colloquium*, pp. 139-154.

[16] J. Pedlowsky (1987), Geophysical Fluid Dynamics, *Springer-Verlag.*

[17] A. Pieri, C. Cambon & F. S. Godeferd (2011), A study of homogeneous turbulence within a baroclinic context, *Journal of Physics-Conference series, ETC13 Conference in Warsaw.*

[18] R. S. Rogallo (1981), Numerical experiments in homogeneous turbulence, *Nasa Technical Memorandum*, **81315**.

[19] P. Sagaut & C. Cambon (2008), Homogeneous Turbulence Dynamics, *Camb. U. Press* , pp. 463.

[20] A. Salhi & C. Cambon (1997), An analysis of rotating shear flow using linear theory and DNS and LES results, *J. Fluid Mech.*, **347**, pp. 171-195.

[21] A. Salhi & C. Cambon (2006), Advances in RDT, from rotating shear flows to the baroclinic instability, *J. Appl. Mech.*, **73**, pp. 449-460.

[22] A. Salhi & C. Cambon (2009), Precessing rotating flows with additional shear: Stability analysis *Phys. Rev. E*, **79**, 036303.

[23] A. Salhi & C. Cambon (2010), Stability of rotating stratified shear flow: An analytical study, *Phys. Rev. E*, **81**, 026302.

[24] A. Salhi, T. Lehner & C. Cambon (2010), Magnetohydrodynamic instabilities in rotating and precessing sheared flows: An asymptotic analysis, *Phys. Rev. E*, **82**, 016315.

[25] A. Salhi, T. Lehner, F. S. Godeferd & C. Cambon (2011), Magnetized stratified rotating shear waves, *Phys. Rev. E*, to appear.

Statistical Theories of Turbulence: Non-Gaussianity and Coherence

Wouter J.T. Bos[1], Robert Rubinstein[2]

[1] LMFA, CNRS, Ecole Centrale de Lyon, Université de Lyon 69134 Ecully Cedex, France.

[2] Newport News, VA, USA.

Abstract

Turbulence is a fascinating mixture of randomness and coherence. On the one hand, the randomness of the phenomenon naturally motivates the use of a statistical characterisation of the turbulent flow properties and the search for theories that can describe and predict these statistics. The coherence, on the other hand, makes it tempting to look at the intriguing beauty of instantaneous vorticity fields and to identify generic mechanisms that describe the dynamics of coherent flow structures. Both approaches are complementary, but in general it is hard to transpose concepts of one approach to the other. For this to be successful statistical theories should be able to describe the statistical imprint of coherence and generic mechanisms of the dynamics of coherent structures should be characterized statistically. In this article we will focus on the first part and we will illustrate that the origin of coherence, the suppression of nonlinearity, can be captured by statistical theory. We will not address questions on the importance of coherent structures, since to answer this, one needs to be able to define a coherent structure and this remains a highly debated issue. A brief historical survey of analytical closure theories, which are the most successful statistical theories available, is given first.

1 Introduction: two-point closures, a short historical review

The statistics of a turbulent flow can be studied in different ways. In this work we will discuss the statistics of turbulence as obtained as a result from analytical closure theory, the founding activity of the Special Interest Group 35 of Ercoftac. We do not try to give an exhaustive presentation of the enormous amount of results in literature, but rather cite some seminal references, in particular to the contributions of Robert Kraichnan. Recent results and illustrations are taken from different works of the authors, so that the presentation will be necessarily biased in this respect.

Statistical theories of turbulence have to deal, one way or another, with the closure problem since the averaged Navier-Stokes equations contain more unknowns then equations. This is due to the nonlinear term, which, when averaged, introduces additional unknowns. Analytical closure approaches are an attempt to overcome this problem by relating the unknowns by physical assumptions and hereby reducing the number of unknowns or increasing the number of equations. Early approaches, such as the quasi-normal approach [1, 2], in which the unclosed hierarchy of moments was closed by assuming joint-Gaussian statistics of the fourth order moments of Fourier-modes of the velocity field, did not yield physical results. Negative kinetic energy distributions were observed as a consequence of that closure assumption.

A great step forward was the introduction of the Direct Interaction Approximation (DIA) [3], in which the importance of the time-history in the dynamics was recognized by introducing an evolution equation for the response function of a Fourier mode. This quantity characterizes in some sense the time correlation of turbulent fluctuations. DIA thereby not only models the multiscale structure of turbulence but also the non-Markovian (or multi-time) character. An important property of DIA is its realizability. This means that the energy spectrum is non-negative, which was not the case for the Quasi-Normal approximation. This property can be proven because the DIA equations correspond to the dynamics of a generalized Langevin equation for the velocity (*e.g.* reference [4]), which implies that the energy and all other even moments of the velocity field are positive.

The resulting energy distribution predicted by DIA is proportional to $k^{-3/2}$ with k the wavenumber. This is in disagreement with Kolmogorov's phenomenological theory proposed in 1941 [5]. We recall here that in Kolmogorov's theory scale-locality is assumed, which means that at very high Reynolds numbers, in which the forcing scale is much larger then the dissipative scale, the intermediate scales are only determined by the local energy flux and the wavenumber. Later, it was argued that this disagreement could be caused by an incorrect representation of the time-history of the Fourier modes in the DIA [6]. Since DIA is a two-time theory, it takes into account the time-history of the correlations of Fourier modes. In the original formulation of DIA, this time-history is computed at a fixed point in the laboratory frame. The decorrelation of a Fourier mode can then be caused by either nonlinear distortion (such as vortex stretching, straining or other multi-scale processes), or by the advection of an arbitrary large scale or flow component or a uniform advecting velocity. This latter dependence is spurious in the sense that the dynamics of a velocity fluctuation governed by the Navier-Stokes equations should be invariant if we add an arbitrary large scale uniform mean flow, a concept better known as Galilean Invariance. This problem of DIA can be solved by recasting the approximation into a Lagrangian reference frame [7]. By doing so the dynamics of a Fourier mode at a certain scale become insensitive to the sweeping of an arbitrary large flow scale. This shows that the scale-locality assumption of Kolmogorov can be directly linked to the Lagrangian character of the time-correlation of the Fourier modes.

The biggest problem of the Lagrangian DIA is perhaps

its analytical complexity, in particular due to the dependence of the time-history of Fourier modes over Lagrangian trajectories. In order to deal with this, approximations have been proposed which model this time history. The assumption that the time-correlation is of exponential form leads to a simplified set of equations in which the time-scale appearing in the exponential is to be modeled. This time-scale should take into account the Galilean invariant character of the time-history. The decorrelation should then only be caused by the decorrelation through the effects of pressure and viscous stresses and not through the effect of advection, since it is this advection which is responsible for the violation of Galilean Invariance. The decorrelation by viscous stresses is easily modeled since it is a local, linear process (in scale space), but the decorrelation by the pressure, involving scale-interactions is more delicate. Kraichnan proposed an elegant way of modeling the pressure decorrelation by pointing out that the effect of pressure is to remove the energy which is contained in Fourier-modes parallel to the wavevector. By solving an equation for a vector-field, the test-field, which is governed by pressureless dynamics, the time-scale at which energy is transferred towards the parallel modes is taken as the decorrelation time of the Fourier modes [8]. Another way to measure the decorrelation is to write an equation for the displacement vector of a fluid particle. Since the displacement vector is the time integral of the Lagrangian velocity, it measures the correlation-time of a fluid particle. The resulting model is described in [9] and in Figure (1) we illustrate the comparison of results obtained by this model with Kolmogorov's 1941 inertial range prediction.

A further simplification of this approach leads to the Eddy-Damped Quasi-Normal Markovian approximation [10], in which no equation is solved for the time-scale but in which it is modeled directly. Since this last approach gives reasonable results in most cases, it is, by far, the most generally used two-point closure in turbulence research and most of the results presented in the following are obtained using this closure.

We will not discuss the further attempts by Kraichnan to model turbulence, which in particular aimed at correctly predicting dissipation-rate fluctuations, but we will discuss some results which can be obtained by DIA and EDQNM type closures. In this review the focus will be on isotropic turbulence. An extensive review of two-point closures applied to study anisotropic turbulence can be found in reference [11]. A large body of work has already been devoted to two-point closures for isotropic turbulence. The present contribution can not treat in detail every aspect and we refer to some existing monographs for the interested reader. References [12–14] give a fair overview of closure-theory approaches developed until the nineties. The first of these books is mainly devoted to DIA, the second book uses extensively the EDQNM closure to study turbulence dynamics. In the last book, among others, the Local Energy Transfer (LET) theory is discussed, a theory which reconciles Kolmogorov's 1941 concepts and Eulerian turbulence theories.

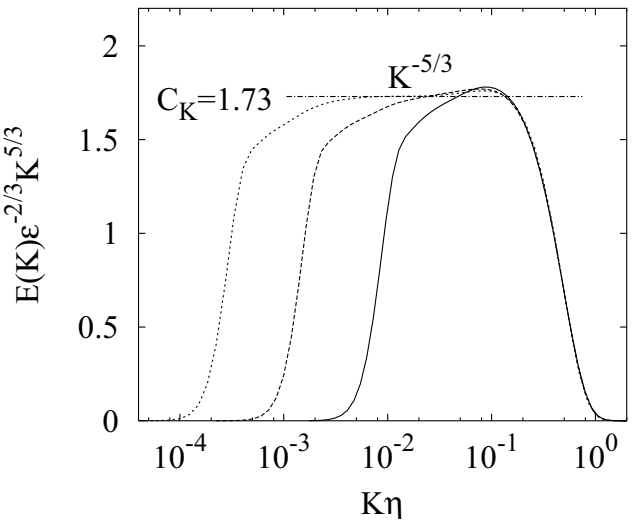

Figure 1: Single-time two-point closures derived from the Direct Interaction Approximation by using an assumption on the time-dependence of the response function (a procedure also called Markovianization) yield generally agreement with Kolmogorov's scaling arguments if the Lagrangian character of the time-history is properly taken into account. Shown in the figure are the compensated energy spectra obtained using the Lagrangian Markovianized Field Approximation [9].

2 Gaussianity, statistical mechanics and relaxation to thermal equilibium

A Gaussian field does not contain structures. It represents a state of maximum disorder. If one therefore wants to measure the coherence of a field, which is the aim of the present review, a logical thing is to compare with a Gaussian field. We will first digress a little from the actual problem of turbulence and discuss some features of a Gaussian field and then we will discuss how turbulence develops from a Gaussian initial state.

We consider the Fourier transform of a three-dimensional field, which in the following will represent the velocity field or the scalar fluctuation field. Instead of the coordinate $\bar{b}x$, we now have the wavevector $\bar{b}k$ that indicates the position of a vector or scalar. The Fourier-transformed quantities are complex. Each component of the vector is therefore determined by its norm and its phase. The important property of a Gaussian field is that this phase is a random variable. This translates the fact that there are no structures. The norm is however a free variable and one can have random Gaussian fields with different variance distributions with respect to the lengthscale. In the case of white noise the variance averaged over a spherical shell is constant. This means that on average the mean-quare variance of a Fourier mode is independent of its wavenumber. Modes in thermal equilibrium will have such an energy distribution. One can ask what the relevance is of this type of distribution for turbulence, in which the energy is generally dominant in the large scales so that the distribution is far from thermal equilibrium. It can however be shown that the Euler equations will relax to a state displaying such a behavior if a Galerkin trunctation is applied to the system. A Galerkin truncation means that we consider a fixed range of wavemodes, limited by a cut-off wavenumber k_f and

modes with $k \leq k_f$ do not interact with modes $k > k_f$.

In order to study the non-Gaussianity induced by the nonlinear term in the Navier-Stokes or Euler equations, one can perform the following (numerical) experiment: we start with an initial Gaussian energy distribution confined to the large scales, *i.e.*, the small wavenumbers and let the system evolve according to the Euler equations in a Galerkin truncated domain. The system is not in thermal equilibrium since the energy is not equally distributed over the different wavelengths. However, a Gaussian vectorfield will, on average, not transfer energy to modes of another wavenumber shell. This can easily be seen by the fact that the mean transfer between modes is directly related to the skewness of the distribution, or rather the skewness of its gradients, and this skewness is zero in a Gaussian field. Some non-Gaussianity needs to be developed from the initial Gaussian state to relax to equilibrium, since the initial conditions are not in statistical equilibrium. This non-Gaussianity needs to be due to the quadratic term in the Euler-equations, since the pressure term only ensures incompressibility and will be zero if the nonlinear term is zero. The way in which this system will relax to this equilibrium-state is perhaps one of the cleanest situations to study non-Gaussianity, since no non-Gaussian forcing or initial condition is imposed so that all non-Gaussian features stem directly from the nonlinear dynamics of the Euler equations. The end-state, which is the thermal equilibrium state, is Gaussian again. The ensemble of Fourier-modes will thus only transiently be non-Gaussian. This non-Gaussian transient, in which energy is transferred from an initial Gaussian state with non-equipartitioned energy to a thermal equilibrium follows a two-stage procedure, which will now be described.

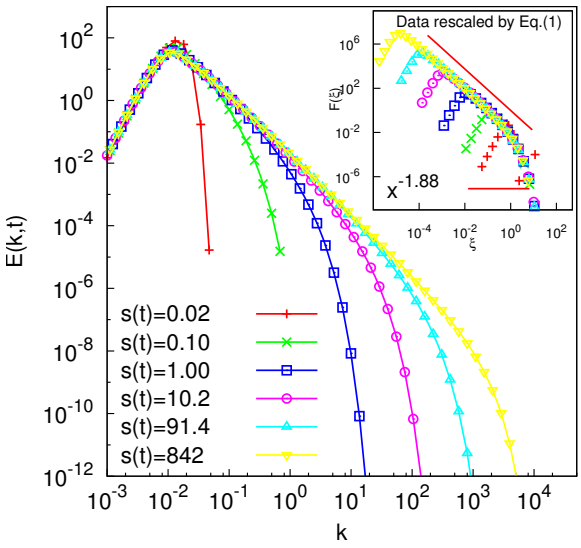

Figure 2: The development of the nonlinear cascade of energy governed by the Euler or Navier-Stokes equations displays a scaling which is not the same as proposed by Kolmogorov for constant flux cascades. The steeper slope, with a power-law exponent of order 1.89, has not yet been described by a simple dimensional analysis [15].

In the initial stage the scales will pass their energy to smaller and smaller scales in a completely inertial way, meaning that no damping is experienced by the modes. This stage should be identical for both Navier-Stokes dynamics at very high Reynolds number and Euler-dynamics, since the viscous term is neglibible if the initially excited modes are initially confined to a sufficiently small wavenumber range. It was recently shown that in this stage the energy distribution displays a power-law behaviour with an exponent between $-5/3$ and -2. In Figure (2) (from [15]) we illustrate this behavior. We note here that in this particular simulation not the Euler equations are solved but the Navier-Stokes equations at very high Reynolds number. As stated before, it is expected that during the initial stage this difference will not be important for the dynamics. Currently, no dimensional analysis is known to predict or explain the value of the power-law exponent, like the one proposed by Kolmogorov for the inertial range energy spectrum of a high-Reynolds number turbulent flow. Its value is numerically close to the fraction $-17/9 \approx -1.89$, but it is for the moment not even clear if a dimensional analysis predicting this exponent and corresponding to the physical mechanism should exist.

In the second stage of the evolution, the smallest scales of the system have received energy and the energy piles up at these modes, filling up a *reservoir* of thermalized modes, displaying a k^2 spectrum. At this point the modes transferring energy will experience a damping. Indeed, the thermalized modes will act, through nonlocal interaction, as an effective viscosity on the active modes and the latter will behave as in a constant flux energy cascade, obeying approximately the Kolmogorov 1941 inertial range phenomenology. This transient behavior is illustrated in Figure (3) (from [16]). We note that this behavior was predicted by Kraichnan in 1975 [17].

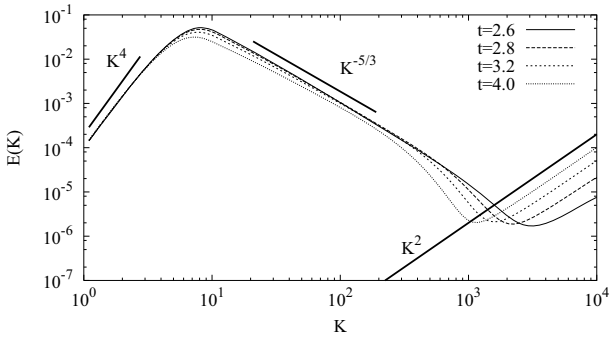

Figure 3: When the truncated Euler equations are solved starting from an initial condition in which the energy is confined to the large scales, the dynamics will tend to relax the system to a state in thermal equilibrium. In this final state the energy spectrum is proportional to k^2. During the transient a Kolmogorov inertial range can coexist with modes in thermal equilibrium at the smallest wave-lengths. These thermalized modes act as an effective viscosity on the modes out of equilibrium [16].

The final state will be statistically static, displaying an energy spectrum proportional to k^2. The transient nonlinear and non-Gaussian phase shares the essential feature of nonlinear mode-coupling with real Navier-Stokes turbulence. We still did not answer the question how non-Gaussian the transient is. To characterize non-Gaussianity, one can compare statistics to those obtained from a Gaussian field. We will consider two quantities, the skewness, which is related to triple velocity correlations and the mean-square nonlinearity, a quantity which contains quadruple velocity correlations.

3 Third-order moments and inertial range energy flux

In a Gaussian field all odd moments of the field-variable are zero. Hereby it can be shown that no net energy transfer can take place, since this is related to the third-order moment of the velocity field. Therefore the energy transfer in a turbulent flow is a direct measure of the non-Gaussianity. In the present section we will discuss the energy transfer in more detail, in particular focusing on its scale dependence in physical space and on the difference between the energy flux and the viscous dissipation rate.

The nonlinear transfer can be related to the third-order structure function in physical space. The longitudinal structure function of order n, is defined by $\delta u_n = \overline{\left[\left(\overline{b}u(\overline{b}x) - \overline{b}u(\overline{b}x + \overline{b}r)\right) \cdot (\overline{b}r/r)\right]^n}$. Both wavenumber spectra and structure functions measure scale distributions of moments of the velocity field. An exact correspondence between the two types of quantities exists. Well known examples of the relations between second- and third-order structure functions on the one hand and energy and transfer spectra on the other can be found in reference [18]. Even though the relations exist, the transformations are not always bijective. For example, if an energy distribution in wavenumber-space is steeper then k^{-3}, the corresponding second order structure function will become insensitive to the exponent and will show a scale-distribution following a power-law proportional to r^2, corresponding to a perfectly smooth velocity distribution. With respect to this aspect, wavenumber spectra are more sensitive tools, since they can probe the wavenumber distribution of these steep energy distributions.

When it comes to higher order statistics, δu_n for $n > 2$, most investigations have focused on structure functions rather then wavenumber spectra, in particular to measure the deviations from Kolmogorov's 1941 proposition for inertial range scaling. This issue, adressing so-called anomalous scaling, has received a disproportionate amount of attention. The original work suggesting a possible correction to Kolmogorov's prediction for the energy spectrum (or structure function), was due to Kolmogorov himself [19] and presented at a famous conference in Marseille 50 years ago. The autocriticism of Kolmogorov was motivated by the observation that scale-dependent fluctuations of the energy dissipation rate introduce an additional possible parameter in the dynamics of the inertial range, so that the scale dependence of the energy spectrum cannot be determined by dimensional analysis only, as was the case for the 1941 theory. These scale dependent fluctuations of the dissipation rate were indeed observed. As correctly pointed out by Kraichnan [20], however, the relevant quantity determining the inertial range is not the energy dissipation, but the energy flux through scales. Even though these quantities have the same mean value in a statistically stationary state, they are not neccesarily the same, since they reflect different physical mechanisms. The energy flux represents the nonlinear interaction between modes, whereas the energy dissipation corresponds to the diffusion of momentum fluctuations through the action of viscous stresses. Note that for the same reason the normalized dissipation rate $\epsilon\mathcal{L}/\mathcal{U}^3$, a quantity which in numerous engineering turbulence models is taken to be constant, is a function of the type of flow considered (see the discussion in the caption of Figure (4)).

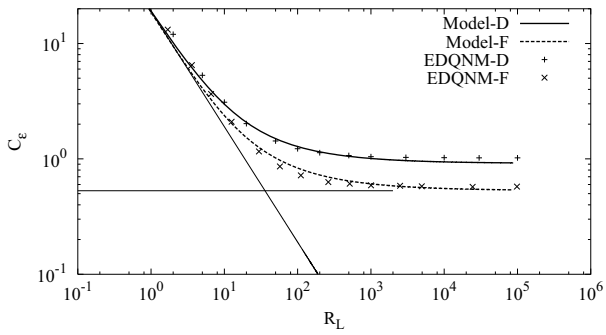

Figure 4: The normalized dissipation rate is defined as $C_\epsilon = \epsilon\mathcal{L}/\mathcal{U}^3$ in which ϵ is the viscous dissipation rate and $\mathcal{L}$ and $\mathcal{U}$ correspond to the integral length and velocity scales, respectively. $\mathcal{U}^3/\mathcal{L}$ corresponds roughly to the rate at which the large scales lose their energy through nonlinear interaction. This energy will cascade to the small scales and will there be dissipated. In a steady state the energy flux and dissipation are statistically identical at high enough Reynolds number (at low Reynolds numbers the energy-flux is smaller since the large scales are directly dissipated by viscous dissipation). In unsteady turbulence, the cascade-time, or time it takes for the energy to reach the smallest scales, introduces an imbalance which is characterized by a variation of C_ϵ. In the figure this is illustrated by comparing stationary, forced turbulence (indicated by **F**) with a canonical case of unsteady turbulence: freely decaying turbulence (indicated by **D**). The curves correspond to a simplified model prediction of the Reynolds number behaviour based on this idea of a cascade time. From [21].

From first principles, *i.e.*, starting from the Navier-Stokes equations, it has not been possible yet to prove or disprove the existence of anomalous scaling. In favour of the partisans of anomalous scaling we can mention that it is possible to show deviations from normal, dimensional scaling, for structure functions of a passive scalar advected by a model velocity field [22]. Similarly, anomalous scaling can be shown to exist for the Burgers' equation. Both examples differ from the Navier-Stokes equation by the absence of a pressure term. Experiments seem to indicate anomalous scaling. However, it is not evident to disentangle anomalous effects from effects which reduce the extent of the inertial range, such as the finiteness of the Reynolds number and the energy input in the large scales by some forcing mechanism. This issue is adressed in [18], in which it is shown that that for Reynolds numbers currently available in simulations and experiments the deviations from Kolmogorov scaling as described by formalisms describing anomalous scaling are of the same order of magnitude as finite Reynolds number effects for second order structure functions (see Figure (5)).

4 Fourth-order correlations and depletion of nonlinearity

In one of the original papers introducing DIA [3], it was already mentioned that the theory was applicable to describe statistical moments of arbitrary order. It was however not until thirty years later that it was shown by Kraichnan and coworkers [23] how this could be done in practice. In that investigation it was outlined how arbitrary order cumulants (the non-Gaussian contributions) can be computed by DIA. It was shown that DIA

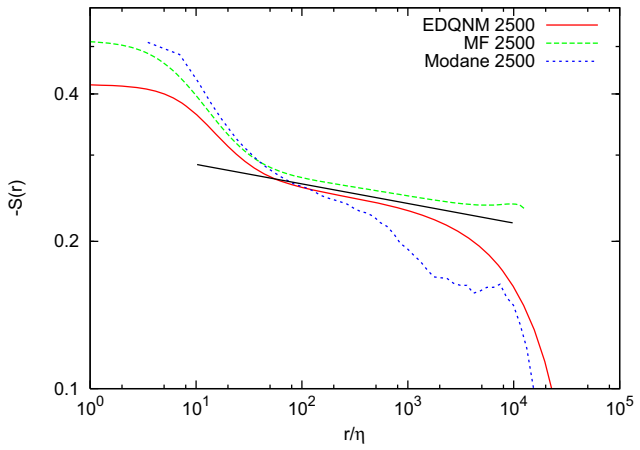

Figure 5: In the framework of Kolmogorov's 1941 theory, the skewness of the velocity increments should display a scale-independent plateau at very high Reynolds numbers. In his 1962 theory this was not any longer the case and a power-law was predicted with a small power-law coefficient. Formalisms such as multifractality were applied to hydrodynamic turbulence to describe these effects, which are absent in two-point closure theories. However, at least at the level of the velocity increment skewness, this power-law coefficient is of the same order of magnitude as finite Reynolds number corrections for Reynolds numbers upto roughly 10^4. This is a very high value which has not yet been obtained in controlled experiments. In the figure results of an EDQNM simulation, the multifractal formalism and a wind-tunnel experiment for the velocity increment skewness are compared at a Taylor-scale Reynolds number of 2500. From [18].

did not yield only successful results. In particular, non-Gaussian fluctuations of the dissipation rate were not captured by DIA. An important quantity that is correctly predicted is the spectrum of the nonlinear term. Closure can therefore be used to study the important phenomenon "depletion of nonlinearity", introduced by Kraichnan and Panda in 1988 [24]. In particular it was argued that a system containing a quadratic nonlinearity tends to a state in which the strength of the nonlinearity is reduced. One particular manifestation of this tendency is the appearance of vortex filaments in the small scales of three-dimensional turbulence.

An impressive manifestation of depletion of nonlinearity is observed in two-dimensional turbulence. If we consider the rather academic case of freely evolving two-dimensional turbulence in a periodic domain, the end state, long before all energy is dissipated, consists in a longliving counter-rotating vortex pair. This *final state*, in which nonlinear interaction is absent can be predicted by statistical mechanics, as was first suggested by Onsager [25]. In axisymmetric three-dimensional turbulence progress has recently be made to apply statistical mechanics in a predictive way [26]. For non-axisymmetric three-dimensional turbulence no fully successful attempts can be reported. However, the fact that an important depletion of nonlinearity is observed in both two- and three-dimensional turbulence, gives some hope that some features can be predicted in three dimensions by similar approaches. This constitutes an exciting challenge for turbulence theory.

In a recent investigation [27] we tested the concept of depletion of nonlinearity for the case of a passive scalar advected by turbulence. The scalar equation is linear, but the advection term plays for the scalar a similar role as the nonlinearity of the Navier-Stokes equations with respect of the coupling of different modes. Indeed all products of fields correspond to convolution products in Fourier space, which couple all different length scales. It was found that also the dynamics of the scalar tend to a state depleted of advection. In particular in the small scales of the scalar it was observed that the strength of the advection term was reduced substantially compared to its Gaussian estimate (see Figure Figure (6)). The consequence in the case of the scalar might be the appearance of fronts, since fronts are stabilized when the scalar gradient is perpendicular to the velocity field, as is the case when the advection term is reduced.

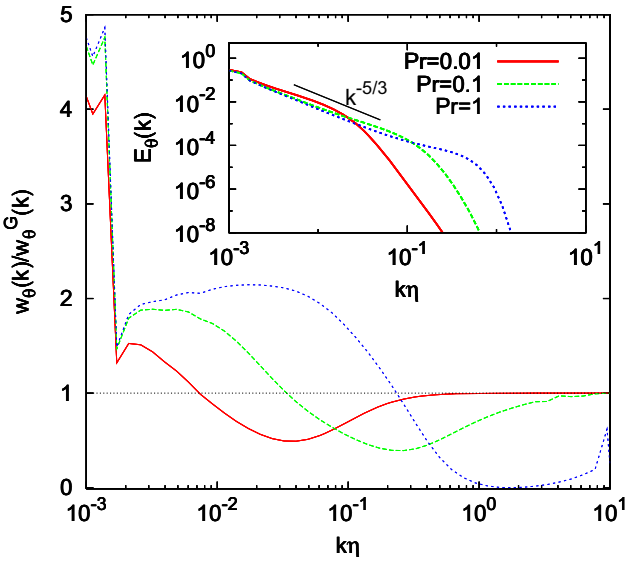

Figure 6: Comparison of the spectrum of the mean square advection term of the scalar equation in isotropic turbulence to its Gaussian value at a Taylor-scale Reynolds number of 1000 and $\mathcal{S}c = 0.01, 0.1, 1$. These results show clearly that the depletion of advection is a persistent phenomenon in the small scales of the scalar field. Inset: scalar variance spectra. From reference [27].

In both the case of the turbulent velocity field and the mixing of a passive scalar, the statistical imprint of coherence can thus be probed by computing the depletion of nonlinearity. The manifestation of this phenomenon in instantaneous velocity or scalar fields corresponds to coherent structures or fronts.

5 Two-point closures and structures

It might seem surprising that, if the depression of advection is linked to the marked fronts observed in the fine scales, it could be captured by statistical closures. A similar thing can be said about the depletion of nonlinearity and its relation to coherent structures. Indeed it is often mistakenly assumed that these statistical approaches can not predict anything on structure related issues since all phase-information is averaged out. However, structures are a dynamical consequence of the underlying equations and the statistical theories are derived from these equations. It is therefore not completely surprising that, if the assumptions used in deriving the closures are physically sound, the statistics observed from closures can be related to the structures observed in experiments and simulations.

References

[1] M. Millionschikov. On theory of homogeneous isotropic turbulence. *Dokl. Akad. Nauk SSSR*, 32:615, 1941.

[2] I. Proudman and W.H. Reid. On the decay of a normally distributed and homogeneous turbulent velocity field. *Phil. Trans. R. Soc. Lond. A*, 247:163–189, 1954.

[3] R.H. Kraichnan. The structure of isotropic turbulence at very high Reynolds numbers. *J. Fluid Mech.*, 5:497–543, 1959.

[4] R.H. Kraichnan. Convergents to turbulence functions. *J. Fluid Mech.*, 41:189, 1970.

[5] A.N. Kolmogorov. The local structure of turbulence in incompressible viscous fluid for very large Reynolds numbers. *Dokl. Akad. Nauk. SSSR*, 30:301, 1941.

[6] R.H. Kraichnan. Kolmogorov's hypotheses and eulerian turbulence theory. *Phys. Fluids*, 7:1723, 1964.

[7] R.H. Kraichnan. Lagrangian-history closure approximation for turbulence. *Phys. Fluids*, 8:575, 1965.

[8] R.H. Kraichnan. An almost-Markovian Galilean-invariant turbulence model. *J. Fluid Mech.*, 47:513, 1971.

[9] W.J.T. Bos and J.-P. Bertoglio. A single-time two-point closure based on fluid particle displacements. *Phys. Fluids*, 18:031706, 2006.

[10] S.A. Orszag. Analytical theories of turbulence. *J. Fluid Mech.*, 41:363, 1970.

[11] P. Sagaut and C. Cambon. *Homogeneous Turbulence Dynamics*. Cambridge University Press, 2008.

[12] D.C. Leslie. *Developments in the theory of turbulence*. Oxford University Press, 1973.

[13] M. Lesieur. *Turbulence in fluids*. Kluwer Dordrecht, 1990.

[14] W.D. McComb. *The physics of fluid turbulence*. Oxford University Press, 1992.

[15] W.J.T. Bos, C. Connaughton, and F.S. Godeferd. Developing homogeneous turbulence. *Phys. D, In press*, 2011.

[16] W. J. T. Bos and J.-P. Bertoglio. Dynamics of spectrally truncated inviscid turbulence. *Phys. Fluids*, 18:071701, 2006.

[17] R.H. Kraichnan. Remarks on turbulence theory. *Adv. Math.*, 16:305, 1975.

[18] W.J.T. Bos, L. Chevillard, J.F. Scott, and R. Rubinstein. Reynolds number effect on the velocity increment skewness in isotropic turbulence. *arXiv:1101.4726*, 2011.

[19] A.N. Kolmogorov. A refinement of previous hypotheses concerning the local structure of turbulence in a viscous incompressible fluid at high Reynolds number. *J. Fluid Mech.*, 13:82, 1962.

[20] R.H. Kraichnan. On kolmogorov's inertial-range theories. *J. Fluid Mech.*, 62:305, 1974.

[21] W.J.T. Bos, L. Shao, and J.-P. Bertoglio. Spectral imbalance and the normalized dissipation rate of turbulence. *Phys. Fluids*, 19:045101, 2007.

[22] R.H. Kraichnan. Anomalous scaling of a randomly advected passive scalar. *Phys. Rev. Lett.*, 72:1016, 1994.

[23] H. Chen, J.R. Herring, R.M. Kerr, and R.H. Kraichnan. Non-gaussian statistics in isotropic turbulence. *Phys. Fluids A*, 1:1844, 1989.

[24] R.H. Kraichnan and R. Panda. Depression of nonlinearity in decaying isotropic turbulence. *Phys. Fluids*, 31:2395, 1988.

[25] L. Onsager. Statistical hydrodynamics. *Il Nuovo Cimento*, 6:279, 1949.

[26] A. Naso, S. Thalabard, G. Collette, P.-H. Chavanis, and B. Dubrulle. Statistical mechanics of beltrami flows in axisymmetric geometry: equilibria and bifurcations. *J. Stat. Mech.*, 2010:P06019, 2010.

[27] W.J.T. Bos, R. Rubinstein, and L. Fang. Scalar beltramization in turbulent flow. *arXiv:1107.0791*, 2011.

Turbulent Rotating Convection: Desktop Geophysics

Rudie P.J. Kunnen[1,3], Herman J.H. Clercx[1,2], and Bernard J. Geurts[1,2]

[1]Department of Physics and J.M. Burgers Centre for Fluid Dynamics,
Eindhoven University of Technology, P.O. Box 513, 5600 MB Eindhoven, The Netherlands
[2]Department of Applied Mathematics and J.M. Burgers Centre for Fluid Dynamics,
University of Twente, P.O. Box 217, 7500 AE Enschede, The Netherlands
[3]E-mail: r.p.j.kunnen@tue.nl

1 Introduction

The paradigm of buoyancy-driven flows is the Rayleigh–Bénard problem: a layer of fluid bounded from above and below by solid plates is heated from below and cooled from above. It is a particularly appealing system to investigate experimentally as well as numerically: its implementation is rather straightforward yet it provides rich flow dynamics [1, 2]. Here we consider a relevant extension to the classical Rayleigh–Bénard setting: a rotation is added with its axis directed vertically, perpendicular to the plates and antiparallel to gravity. The effects of rotation in convective turbulence are recognised in large-scale geophysical and astrophysical flows such as oceanic deep convection [3] and convection in the outer layers of the Sun [4]. They may also arise in specific technological applications, for example in turbomachinery [5] or in crystal growth processes using a rotating heated deposition target [6].

The flow in such a convective system is governed by three dimensionless parameters, viz. the Rayleigh number Ra, the Prandtl number σ and the Rossby number Ro:

$$Ra = \frac{g\alpha\Delta T H^3}{\nu\kappa}\,, \tag{1}$$

$$\sigma = \frac{\nu}{\kappa}\,, \tag{2}$$

$$Ro = \frac{1}{2\Omega}\sqrt{\frac{g\alpha\Delta T}{H}}\,, \tag{3}$$

where g denotes the gravitational acceleration, α, ν and κ are the thermal expansion coefficient, kinematic viscosity and thermal diffusivity of the fluid, respectively, ΔT is the applied temperature difference between bottom and top plate, H is the plate separation, and Ω is the angular velocity of rotation. The Rayleigh number Ra is a dimensionless form of the forcing strength. The Prandtl number σ designates the diffusive properties of the fluid. The Rossby number Ro compares the buoyant time scale $\tau_b = \sqrt{g\alpha\Delta T/H}$ to the time scale of rotation $\tau_\Omega = 1/(2\Omega)$; it essentially gives the relative importance of buoyancy and rotation, i.e. strong rotation implies $Ro \ll 1$. In practical applications another parameter occurs that describes the geometry. An upright cylinder is the preferred geometry, which provides as extra parameter the diameter-to-height aspect ratio $\Gamma = D/H$. Here we shall mostly consider cylindrical geometries with $\Gamma = 1$.

The primary questions in this research are the effects of rotation on the flow phenomenology, the turbulence statistics and the convective heat transfer. The last quantity is indicated by the Nusselt number Nu, which compares the convective heat flux to the flux due to conduction that would be found in absence of fluid motion. We have used experiments and numerical simulations to investigate this flow problem.

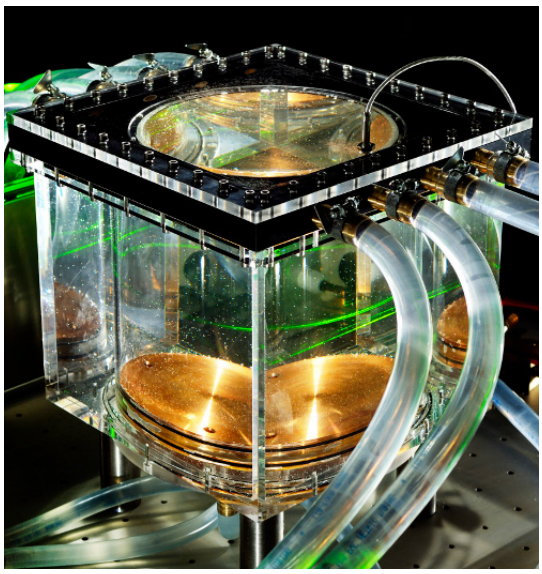

Figure 1: The convection experiment.

This paper is organised as follows. In section 2 the experimental and numerical methods employed in this work are presented. The flow phenomenology that is found at various rotation rates is treated in section 3. Section 4 is on the convective heat transfer under influence of rotation. In section 5 we consider the rotational dependence of turbulence intensities (root-mean-square velocity and vorticity). A description of anisotropy is presented in section 6. Conclusions are drawn in section 7.

2 Experimental and numerical methods

The experimental setup is shown in Figure (1) [7]. The working fluid (water) seeded with PIV tracer particles is placed inside a Plexiglas cylinder of equal height and diameter $H = D = 23$ cm, which is closed from below by a copper plate with an electric heater underneath, keeping the bottom plate at a constant temperature. A transparent cooling chamber is mounted on top; a cooling bath circulates water through the cooling chamber to

maintain a constant temperature there. The cell is transparent from above. A square container is placed around the cylinder with the volume in between also filled with water; thereby allowing for optical access from the sides. A laser light sheet traverses the flow domain horizontally. Two cameras mounted above the cell (not visible in the photograph), placed at different viewpoints, are used to record the seeding particle images, which can be processed with a stereoscopic PIV algorithm [8] to simultaneously extract the three components of velocity in many positions in the laser light sheet plane. All of the aforementioned equipment is mounted on a rotating table.

It must be noted that experimental investigations on convection cannot reliably combine precise heat transfer measurements with investigation of the flow inside the convection cell. Flow measurements require a cell that is optically accessible, while for the determination of the heat transfer it is important to thermally insulate the entire cell to avoid stray heat currents, see e.g. Ref. [9].

Next to the experiment we have carried out direct numerical simulations (DNS) of turbulent rotating convection in a cylindrical domain. The nondimensionalised equations of motion to be solved are

$$\frac{\partial \mathbf{u}}{\partial t} + (\mathbf{u}\cdot\boldsymbol{\nabla})\,\mathbf{u} + \frac{1}{Ro}\hat{\mathbf{z}}\times\mathbf{u} = -\boldsymbol{\nabla} p + T\hat{\mathbf{z}} + \sqrt{\frac{\sigma}{Ra}}\nabla^2\mathbf{u}\,, \tag{4}$$

$$\frac{\partial T}{\partial t} + (\mathbf{u}\cdot\boldsymbol{\nabla})\,T = \frac{1}{\sqrt{\sigma Ra}}\nabla^2 T\,, \tag{5}$$

$$\boldsymbol{\nabla}\cdot\mathbf{u} = 0\,, \tag{6}$$

which describe the evolution in time t of the velocity $\mathbf{u}$ and temperature T; $\hat{\mathbf{z}}$ is the vertical unit vector pointing upwards. The reduced pressure $p = P - \frac{1}{2}\Omega^2 r^2$ incorporates the centrifugal acceleration $\Omega^2 r$ in potential form. To shed the equations in this dimensionless form, distances are scaled with the domain height H, time with the buoyant time scale τ_b; temperatures are scaled according to $T = (T^* - T_0)/\Delta T$, with T^* the actual temperature and T_0 the temperature of the top plate. In the equations of motion the Boussinesq approximation is applied: variations of density with temperature are only considered in the gravitational term and linearised with constant of proportionality α. Furthermore, the fluid properties α, ν and κ are assumed constant (independent of temperature). The horizontal plates are kept at constant temperatures, while the sidewall is adiabatic.

The discretisation used second-order finite-difference formulations in space and a third-order Runge–Kutta time integration scheme is applied. The formulation in cylindrical coordinates requires some special attention to avoid the singularity on the axis $r = 0$ due to terms $1/r$ occurring in the Navier–Stokes [10, 11].

3 Flow phenomenology

Rotation has a profound effect on the formation of coherent structures in the convective turbulent flow. We know from turbulent convection without rotation that the individual plumes cluster together to form a domain-filling large-scale circulation (LSC) [1], i.e. warm fluid rises on one side of the cylinder while cold fluid sinks on the opposite side. This can be nicely visualised in DNS (upper left plot of Figure (2)): three-dimensional

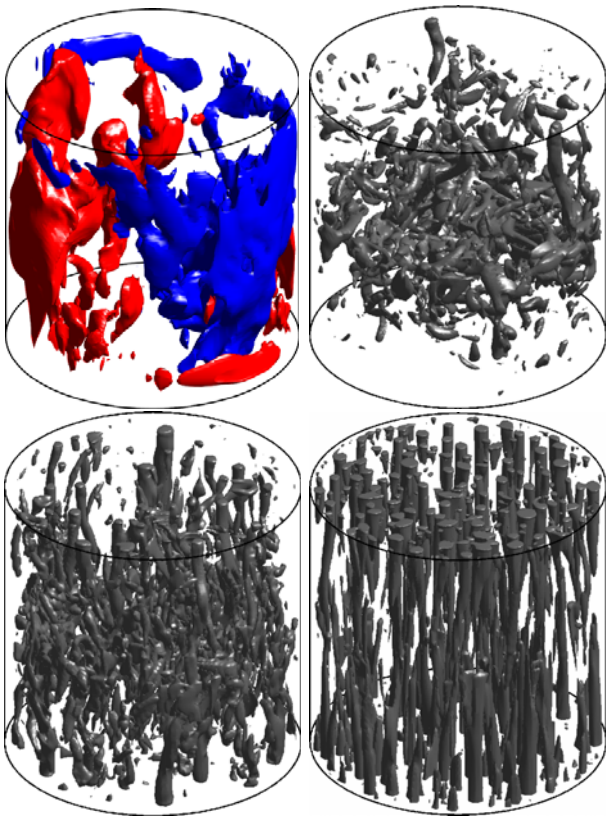

Figure 2: Flow structures in DNS at $Ra = 1 \times 10^9$ and $\sigma = 6.4$ (water). Top left: positive (red) and negative (blue) vertical-velocity isosurfaces in the non-rotating case. The other plots show isosurfaces of the Q criterion marking rotation-dominated regions (vortices), top right $Ro = 0.72$, bottom left $Ro = 0.18$, bottom right $Ro = 0.045$.

isosurfaces of positive (red) and negative (blue) vertical velocity visualise the LSC. Weak rotation does not affect the LSC that much, although it shows a retrograde precession caused by the Coriolis force acting on its horizontal branches [12]. However, at a critical Rossby number $Ro_c = 2.5$ (dependent on the cylinder aspect ratio Γ) a transition occurs [12–14]: the LSC disappears and instead smaller vertically aligned vortical plumes are formed. These vortices can be visualised with contours of the so-called Q criterion [15] that distinguishes strain-dominated regions from rotation-dominated structures, i.e. vortices. The tendency to form coherent vortices as the Rossby number decreases (rotation increases) can be clearly recognised from the three other plates in Figure (2). Additionally, the columnar flow structuring typical for rapidly rotating flows is also observed: a manifestation of the Taylor–Proudman theorem [16] which describes the suppression of vertical velocity gradients by rotation.

These columnar vortices have a peculiar internal structure. There exist 'warm' and 'cold' vortices, depending on from which plate they originate (bottom or top). Close to its plate of origin such a vortex gains strong positive vorticity due to spin-up (conservation of angular momentum) of the converging flow in the boundary layer feeding it. While traversing the domain vertically, it gradually loses its vorticity. As it approaches the vertically opposite plate it spins down, gains negative vorticity and the feeding flow is deviated radially outward. They obey to first approximation an up-down symme-

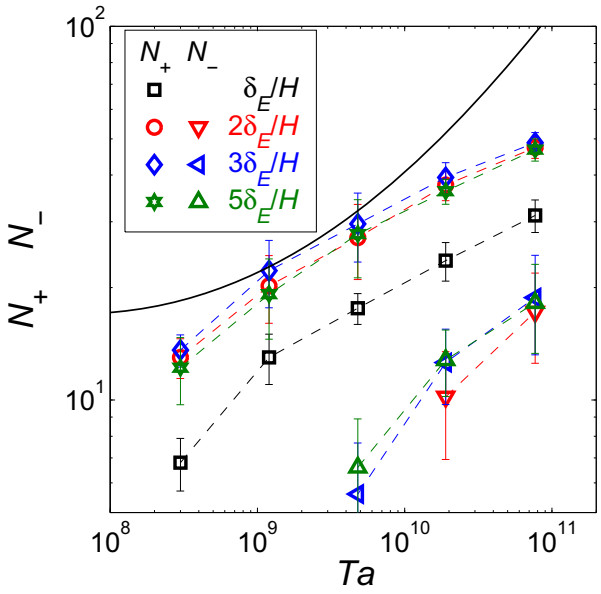

Figure 3: Mean number of cyclonic (N_+) and anticyclonic (N_-) vortices found in a horizontal cross-section of the domain as a function of rotation (Taylor number Ta), at $Ra = 6 \times 10^8$ and $\sigma = 6.4$. From left to right, the points correspond to Rossby numbers $Ro = 0.56$, 0.28, 0.14, 0.07 and 0.035. Various vertical measurement positions are included. The solid line is the prediction of a theoretical model by Sakai [19].

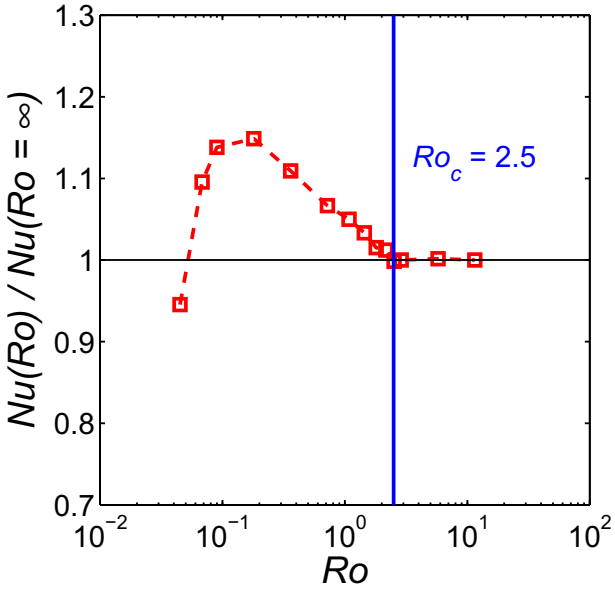

Figure 4: The Nusselt number Nu as a function of Rossby number Ro. To emphasize effects of rotation the results are normalised with the Nu value found in absence of rotation ($Ro = \infty$). The blue vertical line indicates the critical Rossby number $Ro_c = 2.5$.

try that, when enforced in the Navier–Stokes equations, provide a fitting theoretical model for these vortices [17]. This also means that in a given horizontal cross-section of the domain, one can find both cyclonic (rotating in the same direction as the convection cell) and anticyclonic (of opposite rotation) vortices.

Another observation from the visualisations of Figure (2) is that the number of vortices depends on the rotation rate. We have used the vortex detection criterion Q to count the number of vortices as a function of rotation rate [18]. To compensate for the height of the boundary layer that changes with rotation, we investigated horizontal cross-sections at vertical positions that are multiples of the Ekman boundary layer height $\delta_E = \sqrt{\nu/\Omega}$ [16]. The theoretical Ekman layer thickness is found to be a good approximation for the boundary layer thickness in the rotating turbulent convective flow [7]. In Figure (3) the mean number of vortices found in a horizontal cross-section of the cylinder are depicted at several measurement heights $z = \delta_E$ (black), $2\delta_E$ (red), $3\delta_E$ (blue) and $5\delta_E$ (green). Cyclonic (N_+) and anticyclonic (N_-) vortices are counted separately. They are depicted as a function of the Taylor number $Ta = Ra/(\sigma Ro^2) \sim \Omega^2$, another dimensionless representation of the rotation rate. It is seen that cyclonic vortices are formed in a boundary layer of approximate thickness $2\delta_E$. In this layer no anticyclonic vortices are detected. The strong cyclonic vortices remain stable when going to other vertical positions (their number remains constant). For $z \geq 2\delta_E$ some anticyclonic vortices are detected, however there are considerably less anticyclonic vortices than their cyclonic counterparts ($N_+ > N_-$). The total number of vortices increases as Ta grows, so there are indeed more vortices at higher rotation rates.

4 Heat transfer

The convective heat transfer through a convection cell depends on the rotation rate in an unexpected way. In Figure (4) we show the results of a series of DNS at several Rossby numbers and $Ra = 1 \times 10^9$, $\sigma = 6.4$ [12]. The Nusselt number $Nu(Ro)$ is normalised by the value found in absence of rotation $Nu(Ro = \infty)$. At small rotation rates (high Ro) rotation has no effect on the heat transfer. However, at the critical Rossby number $Ro_c = 2.5$ introduced before, there is a 'kink' in the graph. As the Rossby number decreases past Ro_c the heat transfer *increases*, with a maximal increase of 15% around $Ro \approx 0.1$. For $Ro < 0.1$ the heat transfer is reduced by rotation. The increased heat transfer was first noticed in a pioneering experiment by Rossby [20] in which he also explained its origin: the vortices that are formed in the flow act as pumps that entrain fluid from close to the plates (which is either very hot or very cold) and transport it efficiently to the vertically opposite side. This pumping action is known as Ekman pumping [16]. Zhong et al. [21] and Stevens et al. [22] have recently shown that the heat transfer enhancement is strongly dependent on the Prandtl number and that it is most effective at moderate Rayleigh numbers of $O(10^7 - 10^9)$. In fact, in rotating-convection experiments in liquid helium at very high Rayleigh numbers $Ra = 10^{11} - 4 \times 10^{15}$ only a reduction of heat transfer by rotation is observed [23]. The reduction of heat transfer by strong rotation (low Rossby numbers) is a manifestation of the stabilising effect of rotation: vertical velocity fluctuations are damped, reducing the convective heat transport. Indeed, linear stability analysis [24] reveals that at sufficiently large rotation all convective motions will be suppressed and an exclusively conductive state remains with $Nu = 1$. This damping of fluctuations will be further quantified in the next section.

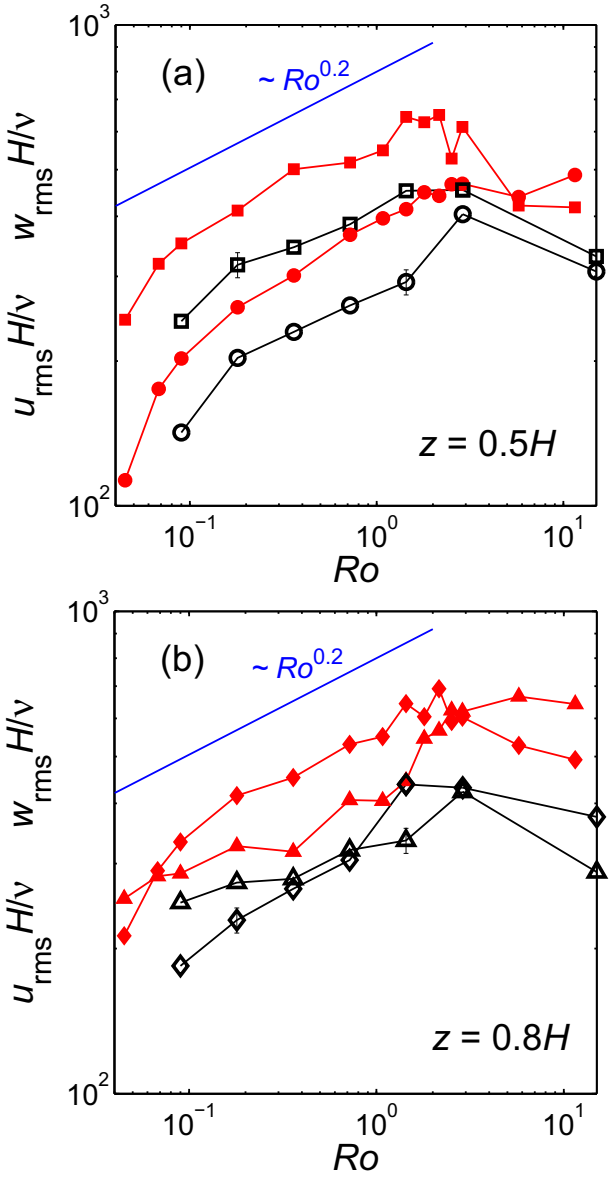

Figure 5: Horizontal and vertical rms velocities measured at two heights: (a) $z = 0.5H$ (mid-height), with horizontal (circles) and vertical (squares) components; (b) $z = 0.8H$ (closer to the top plate), with horizontal (triangles) and vertical (diamonds) components. In both panels the experimental results are plotted in black and the DNS results in red. The black symbols on the right-hand side boundary represent the non-rotating case $Ro = \infty$. The blue line indicates an approximate Rossby number scaling.

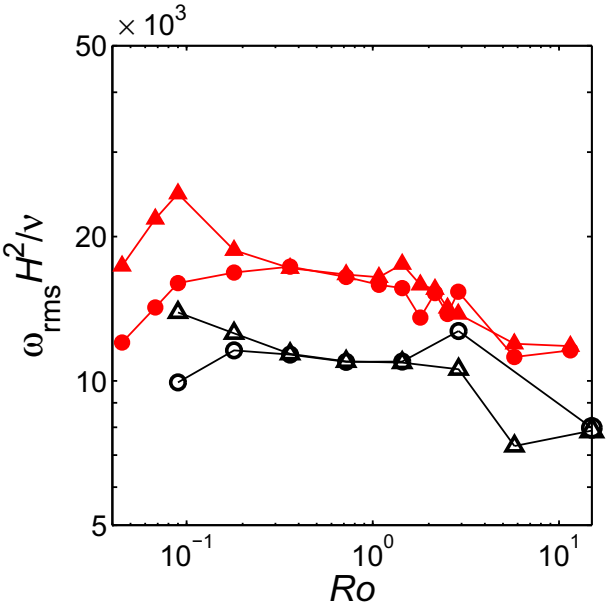

Figure 6: Root-mean-square vertical vorticity from experiment (black) and DNS (red). Circles denote $z = 0.5H$; triangles are for $z = 0.8H$. The black symbols on the right-hand side boundary are from an experiment without rotation ($Ro = \infty$).

5 Turbulence statistics

The fact that the critical Rayleigh number for onset of convective motion goes up as rotation is added [24] is generally interpreted as a sign that rotation stabilizes the turbulence; i.e. rotation weakens the turbulent fluctuations. This is found to be only partially true, when considering the Rossby number dependence of the root-mean-square (rms) velocity fluctuations [7], see Figure (5). The values are rendered dimensionless with the viscous velocity scale ν/H. Results from experiment and DNS are compared; a good qualitative agreement is observed. The quantitative difference is due to different Rayleigh numbers, $Ra = 6 \times 10^8$ in the experiment and $Ra = 1 \times 10^9$ in the DNS [7]. For Rossby numbers smaller than Ro_c it is indeed observed that a reduction of Ro (increased rotation) leads to reduced fluctuations. However, around Ro_c the rms velocities are higher than without rotation. The reason for this is not clear, although we expect that it is linked to the azimuthal drift of the LSC [12]. At the cell mid-height $z = 0.5H$ the vertical rms velocities are always higher than their horizontal counterparts, with a remarkably constant spacing between them. Closer to the top plate at $z = 0.8H$ the horizontal rms velocities can actually become larger than the vertical fluctuations. This is related with spin-up and spin-down of the vortical tubes, occurring close to the plates, that generate horizontal velocity. A final remark can be made concerning the lowest Rossby numbers considered in this plot: the steeper curves indicate a state with a more pronounced rotation dependence.

We also considered the rms values of the vertical vorticity component, as this component is linked to the vertically aligned vortical tubes. These vortices should be represented in the vorticity statistics. These values are presented in Figure (6), nondimensionalised with the viscous time scale H^2/ν. The quantitative difference between experiment and DNS due to different Ra remains, but again a nice qualitative agreement is found. The rms vorticity under rotation is consistently larger than in the non-rotating case. The spin-up process that produces strong vorticity is found to start somewhere between $Ro = 3$ and 6. For the most part the rms vorticity is of equal magnitude on both considered measurement heights. However, around $Ro = 0.1$ the vorticity closer to the plate shows a distinct peak while at mid-height it is reduced in strength. For $Ro < 0.1$ the increased sensitivity can also be noted in this graph.

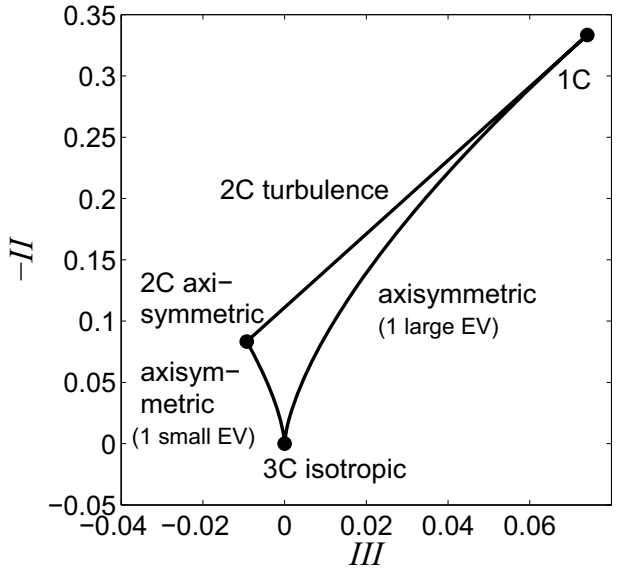

Figure 7: Map of realizable turbulent states (Lumley triangle) in terms of the invariants II and III (after figure 1 of [27]).

6 Anisotropy

The anisotropy identified in the rms velocity plots can be quantified in the so-called Lumley triangle [25,26]. It builds on the tensor invariants of the deviatoric part b_{ij} of the Reynolds stress tensor R_{ij}:

$$b_{ij} = \frac{R_{ij}}{R_{kk}} - \frac{1}{3}\delta_{ij}\,, \qquad (7)$$

where $R_{ij} = u_i\bar{u}_j$ and δ_{ij} is the second order Kronecker tensor; summation is implied over repeated indices. b_{ij} is a symmetric tensor with zero trace by definition. Hence the first tensor invariant, which is the trace, is always zero. The second and third invariants are defined as $II = -b_{ij}b_{ji}/2$ and $III = b_{ij}b_{jk}b_{ki}/3 = \det(b_{ij})$.

A plot of all physically realizable turbulence states in terms of the invariants II and III reveals a triangular region, the Lumley triangle, see Figure (7), which is based on figure 1 of Ref. [27]. The limit of three-component (3C) isotropic turbulence is the bottom point of the diagram. From this point, the leftward boundary represents axisymmetric turbulence in which the anisotropy tensor has one small eigenvalue (EV) and two larger EVs of equal magnitude. This corresponds to a turbulent state in which one direction has a reduced turbulence intensity; it is also referred to as pancake-shaped or disk-like turbulence. From the bottom point to the right the anisotropy tensor has one large EV and two equal smaller EVs. One direction has stronger than the other two; this turbulence is described as cigar-shaped or rod-like. These descriptions, while often strikingly good in practice, must be used with caution as it actually states the shape of the anisotropy tensor, not of the resulting flow structures [26,27]. The leftmost point in the triangle represents the state of two-component (2C) axisymmetric turbulence (the two nonzero components are of equal magnitude). The rightmost point is the theoretical limit of turbulence with one nonzero component (1C). On the connecting line between the 1C and 2C axisymmetric points the 2C states with a preferred direction (and one component zero) are found.

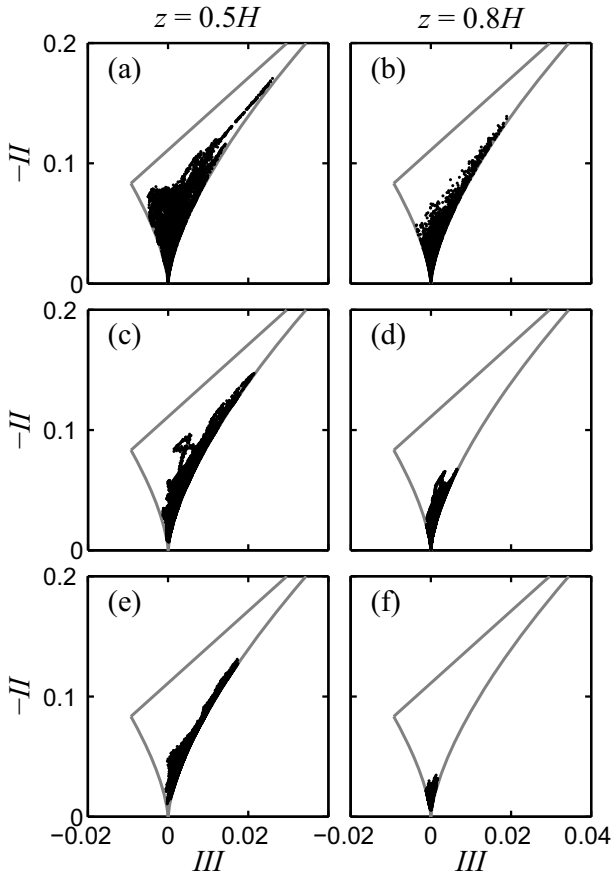

Figure 8: Time traces of the invariants calculated from the experiments, plotted in the Lumley triangle at different Ro: (a,b) $Ro = \infty$; (c,d) $Ro = 1.44$; (e,f) $Ro = 0.09$. Plates (a,c,e) are measured at vertical position $z = 0.5H$, plates (b,d,f) at $z = 0.8H$. The grey lines indicate the bounding curves of the Lumley triangle.

We considered the anisotropy of turbulent rotating convection according to this procedure [7,28]. The invariants have been calculated from velocity snapshots of the flow. Time traces of the invariants are plotted in Figure (8) at three different Rossby numbers, viz. $Ro = \infty$, $Ro = 1.44$ and $Ro = 0.09$. It can be seen that the effect of rotation on the anisotropy is different at the two vertical positions under consideration. At mid-height $z = 0.5H$ the trajectory in the Lumley triangle is found in a thin region near the right-hand-side bounding curve: turbulence with one preferred direction. Indeed, in the velocity rms plot (Figure (5)a) it can be seen that vertical fluctuations are stronger than the horizontal ones. At $z = 0.5H$ the vertical velocity inside the vortical columns is stronger than the horizontal components. However, at $z = 0.8H$ it is found that under rotation the trajectory is confined to a reduced area close to the 3C isotropic point. Thus we can conclude that rotation leads to a more isotropic state at this measurement height: the spin-up and spin-down of vortex tubes apparently induces horizontal velocities that are comparable in magnitude to the vertical velocities. A similar analysis of the DNS results revealed the same picture [7].

This result marks a sharp contrast with isothermal rotating turbulence [29], where fluctuations of the two velocity components perpendicular to the rotation axis are dominant over the smaller component parallel to the rotation vector.

7 Conclusion

Turbulent rotating convection in a cylindrical domain has been investigated using experiments employing stereoscopic PIV and DNS. We have presented an overview of the effects of rotation on the formation of coherent structures, the convective heat transfer and several statistical properties of the turbulence. Based on these analyses it is appropriate to suggest a division into three regimes based on the Rossby number Ro:

$Ro > Ro_c$**:** These modest rotation rates have practically no effect on the convective motion. The large-scale circulation is the dominant flow structure. All of the statistics remain at the values found in the non-rotating case.

$0.1 \lesssim Ro < Ro_c$**:** The formation of coherent column-like vortices increases the velocity and vorticity fluctuations. Ekman pumping inside these vortices enhances the convective heat transfer. This effect is stronger than the damping of velocity fluctuations by rotation: even though the rms velocities decrease as rotation is enhanced (Ro is lowered), the heat transfer (Nusselt number) actually increases at the same time.

$Ro \lesssim 0.1$**:** The damping action of rotation is dominant in this regime. Velocity fluctuations are strongly reduced, as is the convective heat transfer. A strong enough rotation can suppress all convective motion [24].

This work is part of a group of investigations on the effects of rotation on turbulence carried out in our laboratory. Other works (partially) carried out by people from our group include experimental [29,30] and numerical [31] studies on isothermal rotating turbulence.

R.P.J.K. wishes to thank the Foundation for Fundamental Research on Matter (Stichting voor Fundamenteel Onderzoek der Materie, FOM) for financial support. This work was sponsored by the National Computing Facilities Foundation (NCF) for the use of supercomputer facilities, with financial support from the Netherlands Organisation for Scientific Research (NWO).

References

[1] G. Ahlers, S. Grossmann, and D. Lohse. Heat transfer and large-scale dynamics in turbulent Rayleigh–Bénard convection. *Rev. Mod. Phys.*, 81:503–537, 2009.

[2] D. Lohse and K.-Q. Xia. Small-scale properties of turbulent Rayleigh–Bénard convection. *Annu. Rev. Fluid Mech.*, 42:335–364, 2010.

[3] J. Marshall and F. Schott. Open-ocean convection: observations, theory, and models. *Rev. Geophys.*, 37:1–64, 1999.

[4] M. S. Miesch. The coupling of solar convection and rotation. *Solar Phys.*, 192:59–89, 2000.

[5] J. P. Johnston. Effects of system rotation on turbulence structures: a review relevant to turbomachinery flows. *Int. J. Rot. Mach.*, 4:97–112, 1998.

[6] H. van Santen, C. R. Kleijn, and H. E. A. van den Akker. On turbulent flows in cold-wall CVD reactors. *J. Cryst. Growth*, 212:299–310, 2000.

[7] R. P. J. Kunnen, B. J. Geurts, and H. J. H. Clercx. Experimental and numerical investigation of turbulent convection in a rotating cylinder. *J. Fluid Mech.*, 642:445–476, 2010.

[8] M. Raffel, C. Willert, and J. Kompenhans. *Particle Image Velocimetry*. Springer, Berlin, 1998.

[9] J.-Q. Zhong and G. Ahlers. Heat transport and the large-scale circulation in rotating turbulent Rayleigh–Bénard convection. *J. Fluid Mech.*, 665:300–333, 2010.

[10] R. Verzicco and P. Orlandi. A finite-difference scheme for three-dimensional incompressible flow in cylindrical coordinates. *J. Comput. Phys.*, 123:402–413, 1996.

[11] R. Verzicco and R. Camussi. Numerical experiments on strongly turbulent thermal convection in a slender cylindrical cell. *J. Fluid Mech.*, 477:19–49, 2003.

[12] R. P. J. Kunnen, H. J. H. Clercx, and B. J. Geurts. Breakdown of large-scale circulation in turbulent rotating convection. *Europhys. Lett.*, 84:24001, 2008.

[13] R. J. A. M. Stevens, J.-Q. Zhong, H. J. H. Clercx, D. Lohse, and G. Ahlers. Transitions between turbulent states in rotating Rayleigh–Bénard convection. *Phys. Rev. Lett.*, 103:024503, 2009.

[14] S. Weiss, R. J. A. M. Stevens, J.-Q. Zhong, H. J. H. Clercx, D. Lohse, and G. Ahlers. Finite-size effects lead to supercritical bifurcations in turbulent rotating Rayleigh–Bénard convection. *Phys. Rev. Lett.*, 105:224501, 2010.

[15] J. C. R. Hunt, A. Wray, and P. Moin. Eddies, stream, and convergence zones in turbulent flows. Report CTR-S88, Center for Turbulence Research, 1988.

[16] H. P. Greenspan. *The Theory of Rotating Fluids*. Cambridge University Press, Cambridge, 1968.

[17] J. W. Portegies, R. P. J. Kunnen, G. J. F. van Heijst, and J. Molenaar. A model for vortical plumes in rotating convection. *Phys. Fluids*, 20:066602, 2008.

[18] R. P. J. Kunnen, H. J. H. Clercx, and B. J. Geurts. Vortex statistics in turbulent rotating convection. *Phys. Rev. E*, 82:036306, 2010.

[19] S. Sakai. The horizontal scale of rotating convection in the geostrophic regime. *J. Fluid Mech.*, 333:85–95, 1997.

[20] H. T. Rossby. A study of Bénard convection with and without rotation. *J. Fluid Mech.*, 36:309–335, 1969.

[21] J.-Q. Zhong, R. J. A. M. Stevens, H. J. H. Clercx, R. Verzicco, D. Lohse, and G. Ahlers. Prandtl-, Rayleigh-, and Rossby number dependence of heat transport in turbulent rotating Rayleigh–Bénard convection. *Phys. Rev. Lett.*, 102:044502, 2009.

[22] R. J. A. M. Stevens, H. J. H. Clercx, and D. Lohse. Optimal Prandtl number for heat transfer in rotating Rayleigh–Bénard convection. *New J. Phys.*, 12:075005, 2010.

[23] J. J. Niemela, S. Babuin, and K. R. Sreenivasan. Turbulent rotating convection at high Rayleigh and Taylor numbers. *J. Fluid Mech.*, 649:509–522, 2010.

[24] S. Chandrasekhar. *Hydrodynamic and Hydromagnetic Stability*. Oxford University Press, Oxford, 1961.

[25] J. L. Lumley and G. R. Newman. The return to isotropy of homogeneous turbulence. *J. Fluid Mech.*, 82:161–178, 1977.

[26] K.-S. Choi and J. L. Lumley. The return to isotropy of homogeneous turbulence. *J. Fluid Mech.*, 436:59–84, 2001.

[27] A. J. Simonsen and P.-Å. Krogstad. Turbulent stress invariant analysis: clarification of existing terminology. *Phys. Fluids*, 17:088103, 2005.

[28] R. P. J. Kunnen, H. J. H. Clercx, and B. J. Geurts. Enhanced vertical inhomogeneity in turbulent rotating convection. *Phys. Rev. Lett.*, 101:174501, 2008.

[29] L. J. A. van Bokhoven, H. J. H. Clercx, G. J. F. van Heijst, and R. R. Trieling. Experiments on rapidly rotating turbulent flows. *Phys. Fluids*, 21:096601, 2009.

[30] L. Del Castello and H. J. H. Clercx. Lagrangian velocity autocorrelations in statistically steady rotating turbulence. *Phys. Rev. E*, 83:056316, 2011.

[31] L. J. A. van Bokhoven, C. Cambon, L. Liechtenstein, F. S. Godeferd, and H. J. H. Clercx. Refined vorticity statistics of decaying rotating three-dimensional turbulence. *J. Turbul.*, 9:N6, 2008.

Axisymmetric Theory and DNS in Rotating, stratified, and MHD Turbulence

Fabien Godeferd[1], Claude Cambon[1], Benjamin Favier[2], Alexandre Delache[3]

[1] Laboratoire de Mécanique des Fluides et d'Acoustique, UMR 5509,

Ecole Centrale de Lyon, 69134 Ecully Cedex, France.

[2] University of Newcastle, UK.

[3] LMFA Université Saint-Etienne, France.

1 Introduction

Homogeneous Anisotropic Turbulence (HAT) is often considered as a marginal theme among 'canonical' turbulence studies. Isotropy is often automatically associated with homogeneity, and the search for more or less universal behaviour of inertial scales, considered as homogeneous, isotropic, and intermittent, remains an important activity, even when analysing flows that are nonetheless anisotropic and even inhomogeneous at largest scales. On the other hand, HAT is of interest in the geophysical context, especially for turbulent flows dominated by rotation and/or stable stratification. Another domain is magnetohydrodynamics (MHD) flows, for electrically conducting fluids, and all aspects particularly relevant in astrophysics or geodynamo.

It can be shown that these flows are very important for a better understanding of anisotropic cascade phenomena, with a general implication in the modelling of turbulence. For instance, very high resolution direct numerical simulations (DNS) are developed to investigate 'purely' rotating flows with helical and non-helical forcing at the largest scales (Mininni *et al.*, with A. Pouquet, lots of recent papers); such studies are relevant for turbulence theory, although much less directly applicable to actual flows in a dedicated geophysical context or in turbomachinery.

Our studies presented here are set in this context, but, in contrast with other recent analyses, we consider that anisotropy is the main characteristic and deserves a complete investigation.

In addition to DNS, additional insight can be obtained thanks to the renewed interest for the development of closure methods and theories ranging from dynamical equations of Navier-Stokes type to the related dynamical equations for multipoint statistical correlations. As presented in the foreword, on the one hand, rather recent analyses starting from Kármán-Howarth-like equations for two-point second-order velocity correlations, are really *two-point approaches*. On the other hand, techniques formerly referred to as *two-point closures* or *two-point theories*, developped in Fourier space from Kraichnan's and Orszag's legacy, tackle the problem of cascade at the level of three-point third-order dynamics: it is suggested to call these approaches *triadic* that rather *two-point* . The interest of this spectral, triadic, approach, is discussed for strongly anisotropic turbulence, and involves the rigorous removal of pressure fluctuations and detailed conservation laws, following [24].

Generalized rapid distorsion theory (RDT) is only used to give a 'linear ground 0', say, in order to display, by comparison with DNS and EDQNM, which is the exact contribution of nonlinearity. In addition, it is used to identify the eigenmodes and the basic dispersion laws, when waves are present, which serve as a base for improving the nonlinear analysis. Similarly, the linear Green's function—*e.g.* expressed by diagonalization in the basis of eigenmodes—is incorporated in generalized EDQNM models, thus including the rapid distortion of cubic correlations. The flow cases considered here are essentially 'without production' so that the body force has a direct impact on cubic correlations, and therefore on the cascade process. Anisotropy deeply penetrates towards rather small structures in the inertial range, and can affect more these structures than the largest ones, in the absence of artificial forcing. A similar set of three cases, rotating, stratified, MHD, has been investigated by other teams, but only looking at weak anisotropy (e.g. Y. Kaneda and coworkers), or based of a priori semi-empirical scalings for Reynolds stress components and integral lengthscales. In particular, the approach by Davidson (2011) [7] overestimates the purely linear effects for the formation of structures in rotating turbulence, and implicitely supports a *critical balance* between linear and nonlinear effects for stratified turbulence, as also advocated by Lindborg and coworkers, as rediscussed in Section 3. A questionnable amalgam between the three cases is proposed by S. V. Nazarenko and A. A. Schekochihin, conjecturing the critical balance as well. Based on these three cases, rotating turbulence in section 2, stratified turbulence in Section 3 and MHD turbulence in Section 4, we illustrate here a full theory for axisymmetric turbulence, which does not use a priori scaling analysis.

2 Rotating turbulence

In the linear limit, rotating homogeneous turbulence is thus the superposition of inertial waves, structured in wave packets according to the initial conditions. Apart from a preferential short time concentration of energy propagation due to the inertial waves dispersion law, from *e.g.* initial inhomogeneous blobs of turbulence, the long term structure of rotating turbulence predicted by RDT cannot become strongly anisotropic in a permanent way. By contrast, DNS of homogeneous rotating turbulence has shown that the initial isotropic turbulence eventually evolves toward a flow with vortical structures

stretched along the rotation axis, and exhibits an asymmetry in the axis-parallel vorticity, with preferential cyclonic motion. Triadic statistical anisotropic EDQNM model simulations confirm this behaviour and underline the fact that no complete two-dimensionalization may occur without interference of boundary conditions, be they of periodic or non slip types. Moreover, the asymptotic limit of the EDQNM model, at vanishing Rossby number, recovers wave turbulence theory (see, e.g., the book by Zakharov *et al.* 1991, ref. in [24]), although for anisotropically dispersive waves in the case of rotating flows. The latter AQNM model, explicitly exploited with numerical simulations, confirms one is not to expect full two-dimensionalization of rotating homogeneous turbulence at large rotation rates and large time (Bellet et al., 2006) [1].

Non-standard results for detailed anisotropy were recently confirmed by an experimental approach, as discussed in the recent SIG 35 W2011-9 workshop. First experimental measurements of the anisotropic energy transfers in the physical space are presented. Large data sets of PIV (particule image velocimetry) have been obtained in grid-generated turbulence in the 'Gyroflow' rotating platform. The measured energy density and energy flux are consistent with a variant of Kármán-Howarth equation in which the third-order structure function is fully axisymmetric, with $S_3(r, \theta_r)$ [18]. It is observed that the small scales are more anisotropic than the large scales, as a first experimental confirmation of what we have shown for more than two decades, looking at the axisymmetric spectral transfer $T(k, \theta_k)$ (see [24] and references herein from Cambon & Jacquin, 1989.) More generally, Dynamical, structural and statistical aproaches are reconciled, with a first approach to a quantitative accurate linkage of third-order structure functions to spectral transfer terms mediated by cubic correlations as well [13].

3 Stratified turbulence

We study shearless buoyant turbulence in the presence of a vertical mean density gradient $\Gamma = \partial\langle\rho\rangle/\partial x_\parallel$ (stabilizing when $\Gamma < 0$, destabilizing otherwise). The vertical (axial) direction $x_\parallel$ sets the axis of symmetry for the flow statistics, and is antiparallel to the gravitational acceleration $\boldsymbol{g}$. Within the Boussinesq approximation, the coupled fluctuating fields of velocity and buoyancy are governed by the generalized Navier-Stokes equations including the buoyancy force, and the transport equation for the buoyancy scalar, or *active* scalar. In a first, simplified approach, we consider the dynamics of statistically quasi-homogeneous turbulence, in which the density gradient is uniform in space. It yields a Brunt-Väisälä frequency $N = (-g\Gamma/\rho_0)^{1/2}$ in the stabilizing case with $\Gamma < 0$, or its buoyancy-driving counterpart $N = \sqrt{g\Gamma/\rho_0}$ in the destabilizing case with $\Gamma > 0$ (ρ_0 is the reference density).

We propose to discuss the dynamics and statistics of the turbulent flow, in relation with the different structuration of the stabilizing and destabilizing cases. Our approach is based on theoretical and numerical models of increasing complexity, starting from quasi-analytical predictions of statistics when considering the linearized equations — *a.k.a.* the Rapid Distortion Theory (RDT) —, a statistical spectral model based on the multimodal axisymmetric EDQNM theory by [11], with nonlinear transfer terms for the cascade, and pseudo-spectral Direct Numerical Simulations, as a means of tackling the full, nonlinear problem.

3.1 Relevance of a poloidal-toroidal-potential decomposition in both stable and unstable cases

Navier Stokes equations with variable density fluctuation, within the Boussinesq approximation, write

$$\dot{\boldsymbol{u}} - \nu\nabla^2\boldsymbol{u} + \boldsymbol{\omega}\times\boldsymbol{u} + \boldsymbol{\nabla}p = b\boldsymbol{n}, \tag{1}$$

whereas the buoyancy "active" scalar b is governed by the following transport equation, in the presence of a mean density gradient of strength N^2:

$$\dot{b} - \kappa\nabla^2\boldsymbol{b} + \boldsymbol{u}\boldsymbol{\nabla}b = -N^2\boldsymbol{u}\cdot\boldsymbol{n}. \tag{2}$$

Here the buoyancy scalar is the product of gravitational acceleration g by density fluctuation ρ, but the same equations are valid for other stratifying agents (temperature, salinity). The axial vector $\boldsymbol{n}$ is antiparallel to the gravitational acceleration vector, or $\boldsymbol{g} = -g\boldsymbol{n}$. For the sake of simplicity, the Prandtl number will be chosen equal to 1, with the same diffusivity for velocity and temperature ($\nu = \kappa$). The pressure term p can include the kinetic energy if the nonlinearity is expressed in terms of the Lamb vector. This needs not be specified because $\boldsymbol{\nabla}p$ is determined only for ensuring the divergencefree condition of $\boldsymbol{u}$. One of the simplest way to do that is to Fourier-transform the equations and to project the velocity-equation on an orthonormal frame of reference, the so-called Craya-Herring frame $\boldsymbol{e}^{(1)}, \boldsymbol{e}^{(2)}, \boldsymbol{e}^{(3)} = \boldsymbol{k}/k$, which is attached to the direction of the wavevector $\boldsymbol{k}$ of modulus k. In this frame of reference, the velocity and vorticity vectors have only two components

$$\hat{\boldsymbol{u}} = u^{(1)}\boldsymbol{e}^{(1)} + u^{(2)}\boldsymbol{e}^{(2)}, \quad \text{and } \hat{\boldsymbol{\omega}} = \mathrm{i}k\left(u^{(1)}\boldsymbol{e}^{(2)} - u^{(2)}\boldsymbol{e}^{(1)}\right), \tag{3}$$

so that the divergence-free condition is automatically ensured and pressure fluctuation is removed from consideration. Choosing

$$\boldsymbol{e}^{(1)} = \frac{\boldsymbol{k}\times\boldsymbol{n}}{|\,\boldsymbol{k}\times\boldsymbol{n}\,|}, \tag{4}$$

(with $\boldsymbol{e}^{(2)} = \boldsymbol{e}^{(3)}\times\boldsymbol{e}^{(1)}$, $\boldsymbol{e}^{(3)} = \boldsymbol{k}/k$,) the two-components $u^{(1)}$ and $u^{(2)}$ inEq. (3) correspond to toroidal and poloidal modes in physical space. In the special case of vertical (axial) $\boldsymbol{k}$ ($\boldsymbol{k}$ aligned with $\boldsymbol{n}$,) the Craya-Herring frame can coincide with a fixed frame of reference, and $u^{(1)}, u^{(2)}$ generate the Vertically Sheared Horizontal (VSHF) mode very important 1D mode in the stable case. For mathematical convenience, the Fourier transform of b is scaled as a velocity defining $u^{(3)} = -\hat{\boldsymbol{b}}/N$ so that it corresponds to the density of potential energy. In terms of the variables $u^{(1)}$, $u^{(2)}$, $u^{(3)}$, the preceding system of equations is rewritten as

$$\dot{u}^{(1)} + \nu k^2 u^{(1)} = -\boldsymbol{e}^{(1)}\cdot\widehat{\boldsymbol{\omega}\times\boldsymbol{u}}, \tag{5}$$

$$\dot{u}^{(2)} + \nu k^2 u^{(2)} + N\sin\theta_k u^{(3)} = -\boldsymbol{e}^{(2)}\cdot\widehat{\boldsymbol{\omega}\times\boldsymbol{u}}, \tag{6}$$

and

$$\dot{u}^{(3)} + \nu k^2 u^{(3)} - N\sin\theta_k u^{(2)} = -\mathrm{i}\frac{k_i}{N}\widehat{u_i b}. \tag{7}$$

Implicit effects of fluctuating pressure and solenoidal property for $\boldsymbol{u}$ amount to modulate the N term by the

angle-dependent parameter $\sin\theta_k = k_\perp/k$. We have chosen to write the fully nonlinear equations in the stable case: In the unstable case, the sign of the factor $N\sin\theta_k$ must be changed in the last equation.

3.2 Inviscid RDT

This régime is found by discarding both the viscous term and the nonlinear one, in the right-hand-side of Eq. (5), Eq. (6), Eq. (7). Conservation of the toroidal mode comes from the fact that it is both horizontal, thus not affected by the explicit buoyancy term, and divergence-free, thus not affected by the pressure gradient, in basic Eq. (1). In the stable case, poloidal and potential components oscillate with opposite phase with the frequency $Nk_\perp/k$, which is the dispersion frequency of gravity waves. The simple toroidal/ poloidal decomposition, introduced as 'vortex/ wave' decomposition by [21], shows that only the poloidal and potential components must scale with a Froude number. Accordingly, in contrast with the results in Hanazaki and Hunt (1997), the RDT is not recovered in the limit of low Froude number, because this limit can let the toroidal mode survive with arbitrary nonlinear dynamics (full equation (Eq. (5)). Recall that conventional RDT is completely revisited in [11] but also embedded in a fully nonlinear theory. More generally, any global scaling for the equation of the velocity field in terms of Froude numbers is questionable, depending on the relative importance of toroidal and poloidal modes, even if they are possibly nonlinearly coupled. This also raises the question of the *a priori scaling* of $\boldsymbol{\nabla} p$ in physical space (e.g. Lindborg and coworkers), if its splitting in two different terms is not accounted for: the linear part, correcting the explicit buoyancy term, and the nonlinear contribution.

Looking at second order statistics, oscillations are damped, in agreement with the phase-mixing of gravity waves, and, for instance, toroidal and poloidal energies tend to equilibrate towards half their initial sum.

The RDT yields dramatic evolution in the unstable case. The toroidal mode is conserved again, but both poloidal and potential components are affected by exponential growth $\exp(Ntk_\perp/k)$. These tendencies are recovered in recent full DNS, with privileged amplification of the poloidal mode, affecting the vertical velocity, and relative concentration of the poloidal energy spectrum towards the mode $k_\parallel = 0$ (or maximum $k_\perp/k$,) as for a forced two-dimensionalization.

3.3 Stable case: Toroidal cascade in strongly stratified flows

This application is important in the atmosphere and the ocean, in which stable stratification limits vertical motions and renders the flow mainly horizontal. The problem of the direction of the cascade in such flows is still controversial, even if a global consensus is now emerging against the idea of a classical 2D inverse cascade. On the one hand, the analogy between quasi-geostrophic and 2D dynamics, with conservation of potential vorticity, was investigated by [**?**]. This analogy was revisited by Bartello (1995, ref. in [24]) with a refined analysis using the eigenmode decomposition. Regarding applications, Lilly (1983, ref. in [24]) proposed that the kinetic energy spectra observed in the atmosphere at mesoscales are a manifestation of this two-dimensional mechanism. Recently, Cho and Lindborg (2001) [6] deduced from analysis of third-order statistical moments that the energy cascade is in the direct sense. This observational evidence was further supported by a dimensional analysis related to the zig-zag instability by Billant and Chomaz (2001, ref. in [24]), showing that the vertical scale is necessary limited by a local buoyancy length scale $L_B = U/N$, where U is the horizontal velocity scale. Several DNS or LES with hyperviscosity were carried out by Lindborg and coworkers to investigate such a forward cascade. In these computations, only the two-dimensional and two-component modes (2D-2C) are randomly forced, and the horizontal lengthscales are a priori chosen much larger than the vertical ones, using vertically flattened boxes. Even if these studies present interest for atmospheric flows, their contribution to a better conceptual understanding of turbulence is limited by both geometric constraints and artificial forcing: No refined analysis of the anisotropy of the flow is performed, and no new mechanism of nonlinear cascade is derived from such simulations.

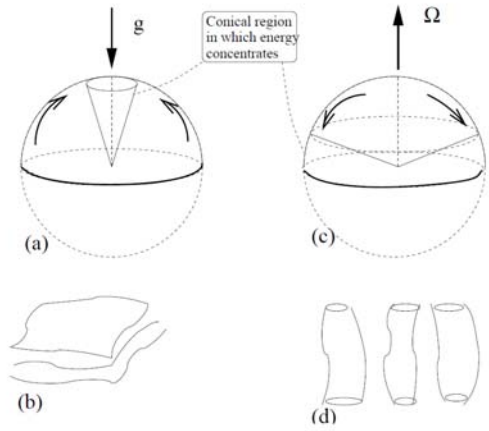

Figure 1: Sketch of anisotropic structure induced by nonlinearity: stratified (left), rotating (middle), spectral (top a-c) and physical (bottom b-d) space, from [11]

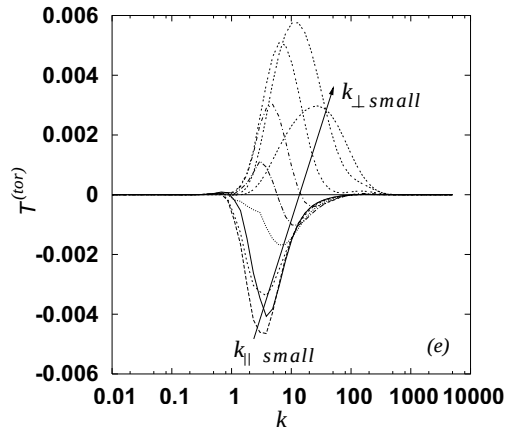

Figure 2: Recent anisotropic EDQNM result for toroidal energy transfer

We propose here to reinterpret the nature of the cascade in strongly stratified flows looking at the basic nonlinear mechanism, following the analyses by [23] and [11]. Even if the zig-zag instability is an efficient mechanism to break the vertical coherence of the flow and to illustrate the horizontal layering, it is only a modality of

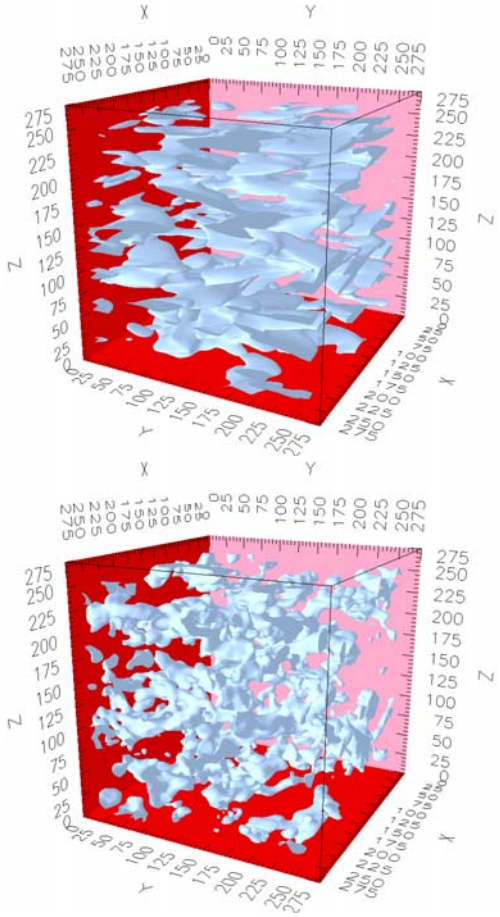

Figure 3: Isoenstrophy surfaces (snapshot of DNS of strongly stratified flows), using only the toroidal (top) and the poloidal (bottom) contributions from the velocity field. Courtesy of L. Liechtenstein.

a much more general nonlinear mechanism. Layering can be obtained without need of preexisting large coherent 2D vortical structures, and without randomly forcing such structures. For instance, it is shown in Figure (3) that layering is created in DNS from isotropic, unstructured initial data: This layering essentially affects the toroidal mode, whereas the poloidal mode remains quasi-isotropic. In addition, the stronly anisotropic description with angle-dependent spectra allows us to quantify the vertical layering in connection with a toroidal energy cascade, not only in DNS by [19]—with isotropic initial data, no forcing and no hyperviscosity— but also in statistical theory. For instance, the EDQNM$_2$ model by [11] firstly suggested the cartoon in Figure (1) (left and middle), confirmed by our recent studies, and showed that the cascade is essentially direct in terms of interacting spherical shells. In contrast with rotating turbulence, in which nonlinear interactions amount to draining the spectral energy from any wavevector direction towards the horizontal waveplane normal to the system angular velocity—this plane corresponds to the 2D manifold—, an inverse specific energy drain yields concentrating spectral energy towards vertical wavevectors in the stably-stratified case. The limit of vertical wavevectors corresponds to the Vertically Sheared Horizontal Flow mode and has nothing to do with the 2D mode; on the contrary, it characterizes horizontal layering with only vertical variability in physical space. Accordingly, this nonlinear mechanism illustrates a really *anti-2D* nonlinear trend, looking at *angle-to-angle* interactions in wave-space. Of course, this mechanism is not inconsistent with a direct energy cascade looking at *shell-to-shell* interactions. The fact that a cascade can be seen as inverse in terms of $k_\perp$ components, and as direct in terms of $k = |\boldsymbol{k}|$, demonstrates the importance of a detailed description of strongly anisotropic energy and transfer spectra (axisymmetric in our context), in terms of both vertical and horizontal wavevector components. Omitting viscosity, the toroidal velocity component is governed by the following exact equation

$$\dot{u}^{(1)} + \boldsymbol{e}^{(1)} \cdot \widehat{\boldsymbol{\omega} \times \boldsymbol{u}} = 0. \tag{8}$$

Attention is then restricted to a single triad, getting rid of nonlinear contributions such as $u^{(2)}u^{(1)}$ and $u^{(2)}u^{(2)}$, in dealing with 'weak' gravity wave turbulence. The system of equations

$$\dot{u}_k^{(1)} = (p_\perp^2 - q_\perp^2) G u_p^{(1)*} u_q^{(1)*}, \tag{9}$$

$$\dot{u}_p^{(1)} = (q_\perp^2 - k_\perp^2) G u_q^{(1)*} u_k^{(1)*}, \tag{10}$$

$$\dot{u}_q^{(1)} = (k_\perp^2 - p_\perp^2) G u_k^{(1)*} u_p^{(1)*}, \tag{11}$$

is almost the same as the one obtained by Kraichnan or Waleffe in pure 2D-2C turbulence. It conserves both energy and vertical enstrophy, and suggests than only 'reverse' (R) types of triadic interactions are involved. The latter result derives from Waleffe's instability principle [23], using the analogy of the former system of equations with Euler's problem for the angular momentum of a solid. Nevertheless, the fact that the completely symmetric factor G depends on both $k_\perp$ and $k_\parallel$ allows a different dynamics over more manifolds than the conventional 'dual' 2D-2C turbulent cascade, inverse for energy, direct for enstrophy. More precisely, the cartoon of Figure (1) is consistent with a drain of energy towards smaller and smaller $k_\perp$, as for the inverse cascade in 2D or in quasigeostrophic turbulence, but also towards larger and larger $k_\parallel$ as for a direct cascade.

We now need to compare the relative amounts of direct and inverse cascades, since the R-type triads allow both senses. Exact statistical Lin-type equations are

$$\left(\partial_t + 2\nu k^2\right) e^{(tor)} = T^{(tor)} \tag{12}$$

$$\left(\partial_t + 2\nu k^2\right) e^{(w)} = T^{(w)} \tag{13}$$

$$\left(\partial_t + 2\nu k^2 + 2\mathrm{i}N k_\perp/k\right) Z = T^{(z)} \tag{14}$$

in which $e^{(tor)}$ corresponds to $u^{(1)}u^{(1)*}/2$, and $e^{(pol)}$ and $e^{(pot)}$ to $u^{(2)}u^{(2)*}/2$ and $u^{(3)}u^{(3)*}/2$ respectively. $e^{(w)} = e^{(pol)} + e^{(pot)}$ is the total energy of gravity waves, and Z quantifies the unbalance between kinetic (poloidal) and potential (buoyancy) parts of the total wave energy. The real part of Z is $(1/2)(e^{(pol)} - e^{(pot)})$, and its imaginary part contains the poloidal-buoyancy flux (details in [11]). The closure of the transfer terms (rhs of 4–Eq. (17)) is found in terms of the above mentioned spectra, depending on both $k_\perp$ and $k_\parallel$, or equivalently on k and $\cos\theta = k_\parallel/k$, for the simplest statistical symmetry consistent with the dynamical basic equations which is axisymmetry with mirror symmetry. For instance, $T^{(tor)}$ is an integral of purely toroidal triple correlations $\langle u^{(1)}(\boldsymbol{k},t)u^{(1)}(\boldsymbol{p},t)u^{(1)}(\boldsymbol{q},t)\rangle$, and is modelled by terms such as $\theta_{kpq}e^{(tor)}(\boldsymbol{q},t)(a(\boldsymbol{k},\boldsymbol{p})e^{(tor)}(\boldsymbol{p},t) - b(\boldsymbol{k},\boldsymbol{p})e^{(tor)}(\boldsymbol{k},t))$ once closed by the anisotropic EDQNM procedure. Detailed equations and DNS/EDQNM comparisons, including the angle-dependent spectra, are given in [12]. Here, we simplify the EDQNM$_2$ procedure in order to focus on pure toroidal interactions and to reach ranges of very high

Reynolds numbers R_e, very low Froude numbers F_r, and long elapsed times, out of grasp of current DNS.

The simplest run is started with zero poloidal and zero potential energy. In this oversimplified configuration, the flow is purely horizontal but not 2D. Only equation (Eq. (5)) in the full system remain, and $U^{(tor)}$ is initially distributed as in isotropic turbulence, *i.e.* with no angular dependence.

4 Unstable case

Because there is an important buoyancy-driven production of energy, already shown by RDT, the detailed analysis of nonlinear dynamics is less important than in the stable case. Generalized Lin-type equations, however, are still useful in terms of the four spectra: The three kinds of energy density, $e^{(tor)}$, $e^{(pol)}$, $e^{(pot)}$ and the spectrum of the poloidal buoyancy flux F. is the same, with only an implicit buoyancy-driven effect in the nonlinear toroidal energy transfer. The system of equations (Eq. (15)–Eq. (17)) is modified as

$$\left(\partial_t + 2\nu k^2\right) e^{(pol)} + 2N\frac{k_\perp}{k}F = T^{(pol)} \quad (15)$$

$$\left(\partial_t + 2\nu k^2\right) e^{(pot)} + 2N\frac{k_\perp}{k}F = T^{(pot)} \quad (16)$$

$$\left(\partial_t + 2\nu k^2\right) F + N\frac{k_\perp}{k}\left(e^{(pol)} + e^{(pot)}\right) = T^{(F)}. \quad (17)$$

RDT for second-order statistics is recovered in the limit of zero spectral transfer terms in the right-hand-side. In this limit, both spectra of poloidal and potential energy are affected by the same exponential growth rate $\exp(2Ntk_\perp/k)$, so that their difference is only due to possible different initial data. This exponential growth affects the spectrum $F(k,\theta_k)$ of poloidal buoyancy flux as well.

Given the importance of linear dynamics, with forcing of both poloidal and potential energy, especially near the 2D waveplane, a too refined model of nonlinear interactions such as EDQNM_2 is not needed as in the stable case, so that an axisymmetric EDQNM_1 model, with no explicit N effect in the equations governing triads for cubic correlations, is in progress.

Finally, our study is to be extended towards Rayleigh-Taylor instability (RTI). Turbulent mixing zones geerated by RTI, when a heavy fluid and a lighter fluid mix together by effect of gravity, are classical examples of unsteady and inhomogeneous flows. At low Atwood number, however, the mean profile of concentration is quasi-linear, and the preceding approach to unstable stratification is still possible. More details on a common work in progress can be found in [4, 14, 15].

5 Applications to MHD turbulent flows

Classical MHD is governed by two coupled equations, as turbulence with an additional *active vector*. The magnetic field is governed by a transport equation (the induction equation), which is the same as the one for a material bipoint, or for the vorticity, up to a specific diffusion term. This vector is active, having feedback on the velocity field via the Lorentz force present in the Navier-Stokes equations.

$$\frac{\partial \boldsymbol{u}}{\partial t} + \boldsymbol{u}\cdot\nabla\boldsymbol{u} - \underbrace{(\boldsymbol{\nabla}\times\boldsymbol{b})}_{\boldsymbol{j}}\times\boldsymbol{b} = -\nabla p + \nu\nabla^2\boldsymbol{u} \quad (18)$$

$$\frac{\partial \boldsymbol{b}}{\partial t} - \boldsymbol{\nabla}\times(\boldsymbol{u}\times\boldsymbol{b}) = \eta\nabla^2\boldsymbol{b} \quad (19)$$

The generality of MHD equations is only restricted by the choice of a simplified equation for the current density $\boldsymbol{j}$. Except for kinematic, ν, and magnetic, η, diffusivities, the explicit inclusion of typical physical coefficients is avoided in the preceding equations by scaling $\boldsymbol{b}$ as a velocity ($\boldsymbol{b} \to \boldsymbol{b}/\sqrt{\mu_0\rho}$ where μ_0 is the magnetic permeability and ρ the density).

Emphasis is put on the dynamics and statistics of turbulent electrically conducting fluid in the presence of a strong magnetic field $\boldsymbol{V}_a$, without mean motion, for various applications such as geodynamo. In this case, $\boldsymbol{b}$ is replaced by $\boldsymbol{b}+\boldsymbol{V}_a$ in Eq. (18) and Eq. (19), so that additional linear terms $-(\nabla\times\boldsymbol{b})\times\boldsymbol{V}_a$ and $-(\nabla\times\boldsymbol{u})\times\boldsymbol{V}_a$, are called into play, respectively. Linearized equations allow us to identify important effects of waves and of ohmic dissipation. Linear solutions were investigated by Moffatt [20], with a classical removal of pressure in Fourier space, taking advantage of the solenoidal property of both velocity and magnetic field fluctuations. A slightly different method is used here, introducing the two solenoidal components of $\boldsymbol{b}$, $b^{(1)}$ and $b^{(2)}$, in the Craya-Herring frame of reference, as for the velocity vector. Not recalling the definition of this frame of reference, it is useful to retain that our general velocity-magnetic field is expressed in four variables, $u^{(1)}, u^{(2)}, b^{(1)}, b^{(2)}$, in which the superscripts $^{(1)}$ and $^{(2)}$ correspond to toroidal and poloidal contributions, respectively, in physical space [24].

5.1 The quasistatic limit, revisiting the nonlinear dynamics

In linearized equations, the magnitude of the magnetic field, scaled as a velocity, is the Alfvén velocity V_a. Without diffusivity, a non-dispersive wave-equation is obtained for $u^{(\alpha)} \pm ib^{(\alpha)}$, $\alpha = 1, 2$, corresponding to Elsasser's variables, with dispersion law $\sigma_a = V_a k_\parallel$. The differential diffusivity between velocity and magnetic fields is responsible for a very important effect: Alfvén waves are not only modulated by a diffusive effect, as they would if $\nu = \eta$, they are completely suppressed in a specific axisymmetric, around $\boldsymbol{V}_a$, spectral domain in term of $k_\perp$ and $k_\parallel$, at a given magnetic Prandtl number different from 1.

The important quasi-static régime [17] is permitted in a liquid metal by the very low value of the magnetic Prandtl number (e.g. 1.410^{-7} in mercury), and was the object of many studies, from pioneering experiments in Grenoble. In this regime of low magnetic Reynolds number (more precisely low Lundquist number), the induction equation is simple enough to be solved explicitely and to yield a close expression of the Lorentz force in term of the velocity. Contrasting results from nonlinear evolution with simple analytical results obtained in the purely linear régime, it appeared that the role of nonlinearity on various second-order statistics was not completely clarified. The nonlinearity is important because it is possible to consider a high Reynolds velocity flow in the low magnetic Reynolds limit, because of the very

small value of the magnetic Prandtl number. Our specific studies, starting from [25] with axisymmetric EDQNM, were recently resumed using high resolution DNS [26], then both DNS and EDQNM [27]. Analysis of second and third-order statistics were consistent with the following Lin equations for toroidal $e^{(tor)}$ and poloidal $e^{(pol)}$ energy spectra, with *the same linear operator* but with *different transfer terms* $T^{(tor)}$ and $T^{(pol)}$ mediated by nonlinear interactions:

$$\left(\frac{\partial}{\partial t} + 2\nu k^2 + 2M_0^2 \cos^2\theta_k\right) e^{(tor)}(k, \cos\theta_k, t) = T^{(tor)}(k, \cos\theta_k, t), \quad (20)$$

$$\left(\frac{\partial}{\partial t} + 2\nu k^2 + 2M_0^2 \cos^2\theta_k\right) e^{(pol)}(k, \cos\theta_k, t) = T^{(pol)}(k, \cos\theta_k, t), \quad (21)$$

where θ_k is the angle between the wave vector and the axial direction, and $M_0^2 = V_a^2/\eta$ gives the magnitude of the Lorentz force, reduced to an anisotropic ohmic dissipation. The angle-dependent term $\cos\theta_k = k_\parallel/k$ characterizes the anisotropy (axisymmetry) and means in the linear operator that axial Fourier modes, aligned with the imposed magnetic field, are rapidly dissipated whereas transverse ones remain unchanged.

If these equations, exact in homogeneous turbulence, are started with isotropic initial data, $e^{(tor)} = e^{(pol)} = E(k)/(4\pi k^2)$, the linear evolution yelds eventual two-dimensionalization, as a complete concentration of spectral energy in the transverse spectral plane $k_\parallel = 0$, or equivalently removal of the variability of velocity components in the axial direction in physical space. On the other hand, equipartition in terms of poloidal and toroidal components is preserved, so that two-dimensionalization, in the Taylor-Proudman sense, preserves both '2D-2C' (two-dimensional, two-component) vortical structures, with pure transverse velocity and axial vorticity, given by the 2D limit of toroidal modes, but also '2D-1C' jettal structures, with axial up-and-down velocity, given by the 2D limit of poloidal modes. In other words, the total energy distribution, or $e = (e^{(pol)} + e^{(tor)})/2$ becomes 2D, but polarization of this energy, or $Z = (e^{(pol)} - e^{(tor)})/2$ remains zero.

As a consequence, the typical ratio of Reynolds stress anisotropy, or $\langle u_\parallel^2\rangle/\langle u_\perp^2\rangle$, and of vorticity anisotropy $\langle \omega_\parallel^2\rangle/\langle \omega_\perp^2\rangle$, initially equal to 1 (3D-3C isotropy) tends to a factor 2 in the linear inviscid régime. Our main result is to confirm that the nonmonotonic evolution of the Reynolds stress anisotropy ratio, found in preceding DNS but attributed to a nonlinear 'return-to-isotropy' effect, results in fact from the rise of polarization anisotropy, fed by the development of polarization nonlinear transfer $T^{(tor)} - T^{(pol)}$ in Eq. (20),Eq. (21). Eventually, when both toroidal and poloidal energy components becomes almost 2D (2D-3C), axial contribution to the velocity field is rapidly decreasing versus its transverse counterpart, because Eq. (20) for $e^{(tor)}$ behaves as 2D (2D-2C) turbulence for purely vortical mode, with inverse cascade and therefore low dissipation, whereas Eq. (21) for $e^{(pol)}$ behaves as the one for a passive scalar in 2D turbulence, with direct cascade and therefore strong dissipation. This is illustrated in Figure (1) using both EDQNM and DNS, with spectral slope k^{-3} for $e^{(tor)}(k_\parallel \to 0)$ and spectral slope k^{-1} for $e^{(pol)}(k_\parallel \to 0)$.

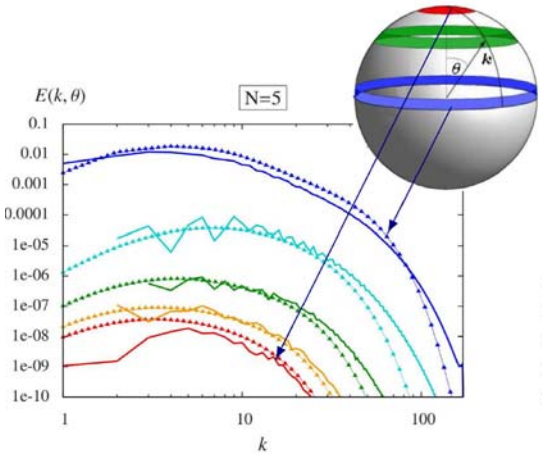

Figure 4: Angle-dependent energy spectra, DNS (full lines) and EDQNM$_2$ (dots)

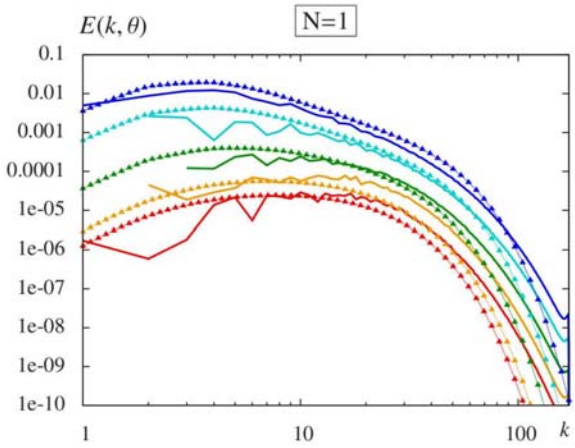

Figure 5: Same as Figure (4), with higher nonlinearity (smaller interaction parameter N

Many other statistical results, from angle-dependent spectra, in terms of both 'shell-to-shell' and (axisymmetric) 'ring-to-ring' distributions, to other averaged indicators, like Moreau or Shebalin angles, and integral length-scales, are provided by DNS and axisymmetric EDQNM in a completely consistent way.

5.2 Higher magnetic Reynolds number, introducing rotation

Without rotation, if we increase the magnetic Reynolds number, the role of induction equation is recovered, as the rise of Alfvén waves, and the kinetic and magnetic energies equilibrate after damped oscillations in the limit of large Lundquist number.

The superposition of rotation and an imposed magnetic field leads to a competition between Coriolis and Lorentz forces. The solutions of the linearized system can be found in term of the four variables $u^{(1)}, u^{(2)}, b^{(1)}, b^{(2)}$. It depends on the dispersion relation of magneto-inertial waves which is

$$\sigma_{mi} = \frac{1}{2}\mathrm{i}\left(\pm\sigma_i \pm \sqrt{\sigma_i^2 + 4\sigma_a^2}\right), \quad (22)$$

in which $\sigma_a = V_a k_\parallel$ and $\sigma_i = 2\Omega k_\parallel/k$ are the individ-

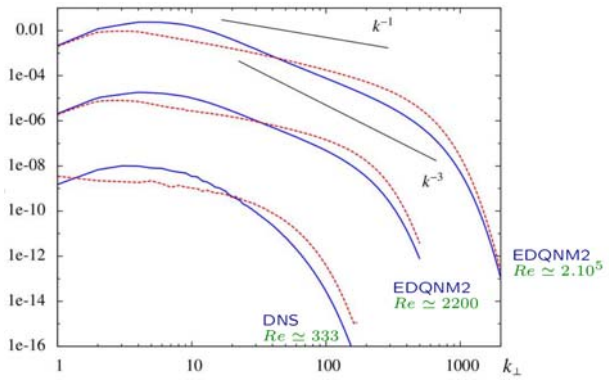

Figure 6: Equatorial ($k_\parallel = 0$) energy spectra, toroidal (blue) and poloidal (red). EDQNM$_2$ allows a dramatic increase for the Reynolds number vs. DNS

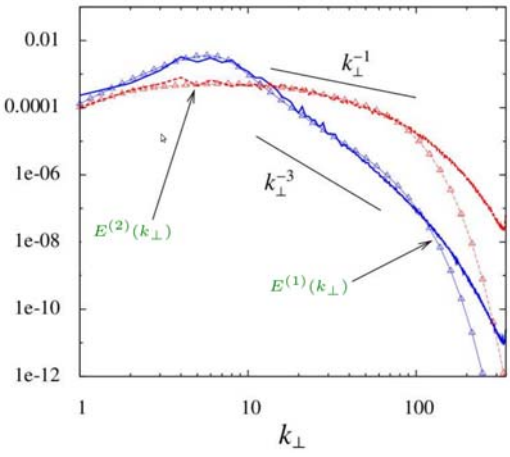

Figure 7: 2D-3C EDQNM (dots) and DNS (full lines). Poloidal (jettal in the 2D limit, red) mode and toroidal (vortical in the 2D limit, blue) mode

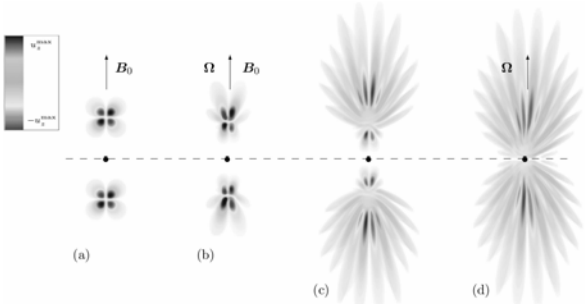

Figure 8: Visualizations of magneto-inertial wave packets. The vertical (axial, along $\boldsymbol{V}_a$ and $\boldsymbol{\Omega}$) component $u_\parallel$ of the velocity is presented in a vertical plan containing the initial impulse. $u_{\max}$ is the maximum value of the vertical velocity. The dots indicate the vertical position of the initial perturbation. (a) Pure Alfvén waves. (b) and (c) Magneto-inertial waves with increasing rotation rates. (d) Pure inertial waves.

ual dispersion laws for Alfvén and inertial waves, respectively, when the molecular and Joule dissipations are neglected. The important parameter for the interaction is the Elsasser number

$$\Lambda = V_a^2/(2\Omega\eta) = M_0^2/(2\Omega). \qquad (23)$$

Linear analysis, with visualizations of magneto-inertia wave packets given if Figure (2) is completed by an investigation by DNS of the role of rotation. It is shown how increasing rotation prevents more and more equipartition in terms of kinetic and magnetic energy, in inhibiting the rise of magnetic energy. In addition to various statistical results, the probability density function of the cross correlation between $\boldsymbol{u}$ and $\boldsymbol{b}$ is calculated in [28]. As rotation increases, we move from a quasi-alignment of $\boldsymbol{u}$ and $\boldsymbol{b}$ to a quasi orthogonality.

5.3 Achievements and perspectives

Our studies show the interest of an exact separation of linear and nonlinear terms in dynamical equations, using poloidal and toroidal Spatial Fourier Harmonics. This is in agreement with exact removal of pressure fluctuation in these equations and related treatment of solenoidal property for both velocity and magnetic fields. Exact generalized Lin equations are found and extensively used in the three cases: ($e, Z, \mathcal{H}$ (energy, including directional anisotropy or dimensionality, polarization and helicity spectra) equations in rotating turbulence (see Cambon & Jacquin, 1989, in [24]), Eqs. (12-14) for stably stratified turbulence, Eqs. (15-17) for the unstable case, and Eqs. (20-21) for QS MHD. Approach to the full spectral tensor of double velocity correlations is possible in anisotropic turbulence, in terms of a minimal number of angle dependent spectra, illustrating directional anisotropy and polarization anisotropy. All related two-point and one-point statistics are derived of the preceding spectra by exact quadratures (or summations using discretized DNS fields). Exploitation of 'shell-to-shell' as well as 'ring-to ring' distribution and multiscale interactions in Fourier space is illustrated by similar tools in DNS and anisotropic 'tradic' closure theory, EDQNM type here.

References

[1] F. Bellet, F. S. Godeferd, J. F. Scott, & C. Cambon (2006), Wave-turbulence in rapidly rotating flows, *J. Fluid Mech.* **562**, 83-121.

[2] G. Brethouwer, P. Billant, E. Lindborg, & J. M. Chomaz (2007), Scaling analysis and simulation of strongly stratified turbulent flows, *J. Fluid Mech.* **585**, 343-.

[3] C. Cambon (1990), 'Homogeneous MHD turbulence at weak magnetic Reynolds number; approach to angular-dependent spectra In Advances in Turbulence Studies (ed. H. Brannover and Y. Unger), AIAA Washington DC, **49**, 131–145

[4] C. Cambon, F. S. Godeferd, B. Favier, & B.- J. Gréa (2011), Axisymmetric turbulence subjected to stable and unstable density stratification, in *Proc. Seventh International Symposium on Strafified Flows*, Rome, August 15-18, 2011.

[5] J. G. Charney (1971), Geostrophic turbulence, *J. Fluid Mech.* **28**, 1087-1095.

[6] J. Y. N. Cho and E. Lindborg (2001), Horizontal velocity structure functions in the upper troposphere and lower stratosphere 1. Observations, *J. Geophys. Res.* **106** 10223-10232.

[7] P. A. Davidson (2011), Long-range interactions in turbulence and the energy decay problem, in *Dynamical barriers and interfaces in turbulent flows*, I. Eames and J. - B. Flor Ed., Phil. Trans. R. Soc., **369**, 701-832.

[8] B. Favier, f. S. Godeferd, C. Cambon & A. Delache (2010), On the two-dimensionalisation of quasi-static MHD turbulence, *Phys. fluids* **22**, 075104.

[9] B. Favier, F. S. Godeferd, & C. Cambon (2011), On the effect of rotation on MHD turbulence at high magnetic Reynolds number, *Geophys. and Astrophys. Fluid Dyn.*, under press, 1–23.

[10] B. Favier, f. S. Godeferd, C. Cambon, A. Delache & W. J. T. Bos (2011), Quasi-static MHD turbulence at high Reynolds number, *J. Fluid Mech.* **681**, 434–461.

[11] c F. S. Godeferd and C. Cambon (1994), Detailed investigation of energy transfers in homogeneous stratified turbulence, *Phys. Fluids* **6**, (6), 2084-

[12] F. S. Godeferd and C. Staquet (2003), Statistical modelling and DNS of decaying stably-stratified turbulence, *J. Fluid Mech.* **486**, 115-159.

[13] F. S. Godeferd (2011), Relating statistics to dynamics in axisymmetric homogeneous turbulence, *Physica D*, to appear.

[14] B.- J. Gréa, J. Griffond & O. Soulard (2010), One point structure tensors and spectral structure of Rayleigh - Taylor turbulence: From self-similar to rapidly distorted regimes, *IWPCTM Conference*, Moscow.

[15] B.- J. Gréa, J. Griffond, & O. Soulard (2011), Spectral anisotropy of Rayleigh-Taylor turbulence, *Report on W2011-9 SIG 35 workshop,* ERCOFTAC bulletin.

[16] H. Hanazaki and J. C. R. Hunt (1996), Linear processes in unsteady stably stratified turbulence, *J. Fluid Mech.* **318**, 303-337.

[17] B. Knaepen and R. Moreau (2008), MHD turbulence at low magnetic Reynolds number, *Annu. Rev. Fluid Mech.* **40**, 25–45.

[18] C. Lamriben, P.P. Cortet, F. Moisy, 2011, Direct measurements of anisotropic energy transfers in a rotating turbulence experiment, *Phys. Rev. Lett.*, submitted.

[19] L. Liechtenstein, F. S. Godeferd, & C. Cambon (2005), Nonlinear formation of structures in rotating stratified turbulence, *J. of Turb.* **6**, 1–18.

[20] H. K. Moffatt (1967), On the suppression of turbulence by a uniform magnetic field, *J. Fluid Mech.* **28**, 571–592

[21] J. J. Riley, R. W. Metcalfe, & M. A. Weissmann (1981), DNS of homogeneous turbulence in density-stratified fluids' in *AIP Conference Procs.*, 79-112.

[22] P. Sagaut & C. Cambon, Homogeneous Turbulence Dynamics, 2008, *Camb. U. Press* New York.

[23] F. Waleffe (1992), The nature of triad interactions in homogeneous turbulence, *Phys. Fluids* **4**, 350-

[24] Sagaut P. and Cambon C. (2008): Homogeneous Turbulence Dynamics. New York, *Camb. Univ. Press.*

[25] Cambon, C. (1990): Homogeneous MHD turbulence at weak magnetic Reynolds number; approach to angular-dependent spectra. In Advances in Turbulence Studies (ed. H. Brannover and Y. Unger), AIAA Washington DC, **49**, 131–145

[26] Favier, B., Godeferd, F. S., Cambon C., Delache, A. (2010): On the two-dimensionalization of quasistatic MHD turbulence. *Phys. Fluids* **22**, 075104

[27] Favier, B., Godeferd, F. S., Cambon, C., Delache, A., Bos W. (2011): Quasi-static MHD turbulence at high Reynolds number. *J. Fluid Mech.*, under press

[28] Favier, B., Godeferd, F. S., Cambon C. (2011): On the effect of rotation on MHD turbulence at high magnetic Reynolds number. *Geophys. and Astrophys. Fluid Dyn.*, under press, 1–23

[29] Plunan, F. and Stepanov, R. (2010): Cascades and disipation ratio in rotating MHD turbulence at low magnetic Prandtl number. *Phys. Rev. E* **82**, 046311

ERCOFTAC Special Interest Groups

1. Large Eddy Simulation

Geurts, B.J.
University of Twente, Holland.
Tel: +31 53 489 4125
Fax: +
b.j.geurts@math.utwente.nl

4. Turbulence in Compressible Flows

Comte, P.
University of Poitiers, France.
Tel: +33 5 49 36 60 11
Fax: +33 5 49 36 60 01
Pierre.comte@tea.univ-poitiers.fr

5. Environmental CFD

Morvan, H.
University of Nottingham, England.
Tel: +44 115 846 6374
Fax: +44 115 951 3898
herve.morvan@nottingham.ac.uk

10. Transition Modelling

Dick, E.,
University of Gent, Belgium.
Tel: +32 9 264 3301
Fax: +32 9 264 3586
erik.dick@ugent.be

12. Dispersed Turbulent Two Phase Flows

Sommerfeld, M.
Martin-Luther University, Germany.
Tel: +49 3461 462 879
Fax: +49 3461 462 878
martin.sommerfeld@iw.uni-halle.de

14. Stably Stratified and Rotating Flows

Redondo, J.M.
UPC, Spain.
Tel: +34 93 401 7984
Fax: +34 93 401 6090
Redondo@fa.upc.es

15. Turbulence Modelling

Jakirlic, S.
Darmstadt University of Technology, Germany.
Tel: +49 6151 16 3554
Fax: +49 6151 16 4754
s.jakirlic@sla.tu-darmstadt.de

20. Drag Reduction and Flow Control

Choi, K-S.
University of Nottingham, England.
Tel: +44 115 9513 792
Fax: +44 115 9513 800
kwing-so-choi@nottingham.ac.uk

24. Variable Density Turbulent Flows

Anselmet, F.
IMST, France.
Tel: +33 4 91 505 439
Fax: +33 4 91 081 637
fabian.anselmet@irphe.univ-mrs.fr

28. Reactive Flows

Tomboulides, A.
Aristotle University of Thessaloniki, Greece.
Tel: +30 2310 991 306
Fax: +30 2310 991 304
ananiast@enman.auth.gr

32. Particle Image Velocimetry

Stanislas, M.
Ecole Centrale de Lille, France.
Tel: +33 3 20 337 170
Fax: +33 3 20 337 169
stanislas@ec-lille.fr

33. Transition Mechanisms, Prediction and Control

Hanifi, A.
FOI, Sweden.
Tel: +46 8 5550 4334
Fax: +46 8 5550 3481
ardeshir.hanifi@foi.se

34. Design Optimisation

Giannakoglou, K.
NTUA, Greece.
Tel: +30 210 772 1636
Fax: +30 210 772 3789
kgianna@central.ntua.gr

35. Multipoint Turbulence Structure and Modelling

Cambon, C.
ECL Ecully, France.
Tel: +33 4 72 186 161
Fax: +33 4 78 647 145
claude.cambon@ec-lyon.fr

36. Swirling Flows

Braza, M.
IMFT, France.
Tel: +33 5 61 285 839
Fax: +33 5 61 285 899
braza@imft.fr

37. Bio-Fluid Mechanics

Van Steenhoven, A.A.
Eindhoven University of Technology, Holland.
Tel: +31 40 2472 722
Fax: +31 40 2433 445
a.a.v.steenhoven@wtb.tue.nl

38. Microfluids and Micro Heat Transfer

Tardu, S.
Laboratoire des Ecoulements Géophysiques et Industriels, France.
sedat.tardu@hmg.inpg.fr

39. Aeroacoustics

Bailly, C.
Ecole Centrale de Lyon, France.
Tel: +33 4 72 186 014
Fax: +33 4 72 189 143
christophe.bailly@ec-lyon.fr

40. Smoothed Particle Hydrodynamics

Le Touzé, D.
Ecole Centrale de Nantes, France.
Tel: +33 2 40 37 15 12
Fax:
david.letouze@ec-nantes.fr

41. Fluid Structure Interaction

Longatte, E.
EDF, France.
Tel: +33 1 30 87 80 87
Fax: +33 1 30 87 77 27
elisabeth.longatte@edf.fr

42. Synthetic Models in Turbulence

Nicolleau, F.
University of Sheffield, England.
Tel: +44 114 22 27867
Fax: +44 114 22 27890
f.nicolleau@sheffield.ac.uk

43. Fibre Suspension Flows

Hämäläinen, J.
Lappeenranta University of Technology, Finland.
Tel: +358 40 596 1999
jari.hamalainen@lut.fi

101. Quality and Trust in Industrial CFD

Hutton, A.G.
Airbus UK, England.
Tel: +44 117 936 7519
Fax:
anthony.hutton@airbus.com

102. ERCOFTAC Database Interests Group

Laurence, D.
UMIST, England.
Tel: +44 161 200 3704
Fax: +44 161 200 3723
dominique.laurence@manchester.ac.uk

ERCOFTAC Pilot Centres

Alpe – Danube – Adria

Reichl, C.
Austrian Institute of Technology,
Giefinggasse 2,
A-1210 Wien,
Austria.

Tel: +43 1 50550 6605
Fax: +43 1 50550 6439
christoph.reichl@arsenal.ac.at

Belgium

Geuzaine, P.
Cenaero,
CFD Multi-physics Group,
Rue des Frères Wright 29,
B-6041 Gosselies,
Belgium.

Tel: +32 71 919 334
philippe.geuzaine@cenaero.be

Czech Republic

Bodnar, T.
Institute of Thermomechanics AS CR,
5 Dolejskova,
CZ-18200 Praha 8,
Czech Republic.

Tel: +420 224 357 548
Fax: +420 224 920 677
bodnar@marian.fsik.cvut.cz

France – Henri Bénard

Cambon, C.
Ecole Centrale de Lyon.
LMFA,
B.P. 163,
F-69131 Ecully Cedex,
France.
Tel: +33 4 72 18 6161
Fax: +33 4 78 64 7145
claude.cambon@ec-lyon.fr

France South

Braza, M.
IMF Toulouse,
CNRS UMR – 5502,
Allée du Prof. Camille Soula 1,
F-31400 Toulouse Cedex,
France.
Tel: +33 5 61 28 5839
Fax: +33 5 61 28 5899
marianna.braza@imft.fr

France West

Bonnet, J-P.
Université de Poitiers,
Centre d'Etudes Aérodyn. et Thermiques,
43 Route de l'Aérodrome,
F-86036 Poitiers Cedex,
France.
Tel: +33 5 49 36 60 31
Fax: +33 5 49 45 60 01
jean-paul.bonnet@univ-poitiers.fr

Germany North

Gauger, N.
German Aerospace Center – DLR,
Institute of Aerodynamics,
Lilienthalplatz 7,
D-38108 Braunschweig,
Germany.
Tel: +49 531 295 3339
Fax: +49 531 295 2914
nicolas.gauger@dlr.de

Germany South

von Terzi, D.
Inst. Thermische Strömungsmaschinen,
Universität Karlsruhe (TH),
Kaiserstr. 12 (Geb. 10.91, Zi. 201)
D-76131 Karlsruhe,
Germany.

Tel: +49 721 608 6829
vonterzi@its.uni-karlsruhe.de

Germany West

Schröder, W.
RWTH – Aachen,
Institute of Aerodynamics,
D-52062 Aachen,
Germany.

Tel: +49 241 809 5410
Fax: +49 241 809 2257
ek@aia.rwth-aachen.de

Greece

Papailiou, K.D.
National Tech. University of Athens,
Laboratory of Thermal Turbomachines,
9 Iroon Polytechniou,
P.O. Box 64069,
Gr-15710 Athens, Greece.
Tel: +30 210 772 1634
Fax: +30 210 772 1658
kpapail@ltt.ntua.gr

Iberian East

Onate, E.
Universitat Politecnica de Catalunya,
Edificio C-1, Campus Norte,
Gran Capitan s/n,
E-08034 Barcelona,
Spain.
Tel: +34 93 401 6035
Fax: +34 93 401 6517
onate@cimne.upc.es

Iberian West

Theofilis, V.
Universidad Politécnica de Madrid,
Plaza Cardenal Cisneros 3,
E-28040 Madrid,
Spain.

Tel: +34 91 336 3291
Fax: +34 91 336 6371
vassilis@torroja.dmt.upm.es

Italy

Martelli, F.
University of Florence,
Department of Energy,
Via Santa Marta 3,
I-50139 Firenze,
Italy.
Tel: +39 055 479 6237
Fax: +39 055 479 6342
francesco.martelli@unifi.it

Nordic

Wallin, S.
Swedish Defence Research Agency FOI,
Computational Physics,
S-16490 Stockholm,
Sweden.

Tel: +46 8 5550 3184
Fax: +46 8 5550 3062
stefan.wallin@foi.se

Poland

Drobniak, S.
Technical University of Czestochowa,
Thermal Machinery Institute,
Al. A. Krajowej 21,
PL-42200 Czestochowa,
Poland.
Tel: +48 34 325 0507
Fax: +48 34 325 0555
drobniak@imc.pcz.czest.pl

Switzerland

Jenny, P.
ETH Zürich,
Institute of Fluid Dynamics,
Sonneggstrasse 3, ML H 38,
CH-8092 Zürich,
Switzerland.
Tel: +41 44 632 6987
Fax: +41 44 632 1147
jenny@ifd.mavt.ethz.ch

Netherlands

Ooms, G.
J.M. Burgerscentrum,
Research School for Fluid Mechanics,
Mekelweg 2,
NL-2628 CD Delft,
Netherlands.
Tel: +31 15 278 1176
Fax: +31 15 278 2979
g.ooms@wbmt.tudelft.nl

United Kingdom

Barton, I.
BAE Systems,
ATC – Sowerby, FPC 267,
P.O. Box 5,
Bristol BS34 7QW,
England.
Tel: +44 117 302 8251
Fax: +44 117 302 8007
iain.barton@baesystems.com

Best Practice Guidelines for Computational Fluid Dynamics of Dispersed Multi-Phase Flows

Editors

Martin Sommerfeld, Berend van Wachem
&
René Oliemans

The simultaneous presence of several different phases in external or internal flows such as gas, liquid and solid is found in daily life, environment and numerous industrial processes. These types of flows are termed multiphase flows, which may exist in different forms depending on the phase distribution. Examples are gas-liquid transportation, crude oil recovery, circulating fluidized beds, sediment transport in rivers, pollutant transport in the atmosphere, cloud formation, fuel injection in engines, bubble column reactors and spray driers for food processing, to name only a few. As a result of the interaction between the different phases such flows are rather complicated and very difficult to describe theoretically. For the design and optimisation of such multiphase systems a detailed understanding of the interfacial transport phenomena is essential. For single-phase flows Computational Fluid Dynamics (CFD) has already a long history and it is nowadays standard in the development of air-planes and cars using different commercially available CFD-tools.

Due to the complex physics involved in multiphase flow the application of CFD in this area is rather young. These guidelines give a survey of the different methods being used for the numerical calculation of turbulent dispersed multiphase flows. The Best Practice Guideline (BPG) on Computational Dispersed Multiphase Flows is a follow-up of the previous ERCOFTAC BPG for Industrial CFD and should be used in combination with it. The potential users are researchers and engineers involved in projects requiring CFD of (wall-bounded) turbulent dispersed multiphase flows with bubbles, drops or particles.

Table of Contents

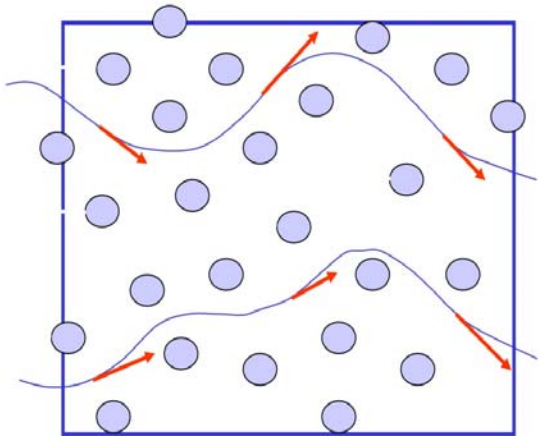

Copies of the Best Practice Guidelines can be acquired electronically from the ERCOFTAC website:

www.ercoftac.org

Or from:

ERCOFTAC ADO
Chaussée de la Hulpe 189 Terhulpsesteenweg
B-1170 Brussels
Belgium

Tel: +32 2 643 3572
Fax: +32 2 647 9398
Email: anne.laurent@ercoftac.be

The price per copy (not including postage) is:

ERCOFTAC members	
First copy	*Free*
Subsequent copies	45 Euros
Students	30 Euros
Non-ERCOFTAC academics	90 Euros
Non-ERCOFTAC industrial	180 Euros